MOSTAFA, A. 2020. *Laser induced fractures in porous media*. Robert Gordon University, PhD thesis. Hosted on OpenAIR [online]. Available from: https://doi.org/10.48526/rgu-wt-2271539

# Laser induced fractures in porous media.

MOSTAFA, A.

2020

# Laser induced fractures in porous media

Ayman Mostafa

A thesis submitted in partial fulfilment of the
requirements of the
Robert Gordon University
for the degree of Doctor of Philosophy

October 2020

ROBERT GORDON UNIVERSITY ABERDEEN

# ABSTRACT

Hydraulic fracturing is the most effective technique to enhance well productivity in oil and gas industry. There are many logistic, operational and environmental concerns associated with the existing techniques including the potential risk of underground water contamination and earthquakes which are the main reasons of the current debates regarding shale gas development in the UK. An alternative technique using clean energy source (laser) has been proposed and discussed in this research.

In order to evaluate the feasibility of using laser induced fractures as an alternative technique, an analytical model has been developed to calculate temperature distribution during the laser fracturing method. Novelty of the developed model lies in incorporating melting and vaporisation of rock materials during the laser fracturing process. The developed model has been validated against experimental data of cutting various materials by laser including rock and metals.

Further, a new waste power's correlation and methodology have been developed in this research in order to analytically calculate laser power requirements without the needs to develop complex numerical models. This correlation is developed from the verified numerical line-source model which showed good matching to experimental data of cutting metals and non-metals by melting.

Reservoir simulation model is also developed in this research in order to identify the potential flow improvement could be achieved due to laser induced fractures and the Heat Affected Zone (HAZ) around wellbore.

The results indicated that 100 kW average laser power is capable to cut a range of 5 – 15 m (average 10 m) of porous media depending on porosity and rock thermal properties and this can yield a significant improvement in well productivity during transient flow and a reasonable improvement during pseudo steady state flow (approx. 2 – 3 Fold of Increase, FOI).

The range of flow improvement indicated in this research is encouraging and equivalent to the potential improvement could be achieved, up to certain degree, by conventional matrix stimulation including acidizing and hydraulic fracturing techniques.

The range of power requirements indicated in this research is within the potential capacity of laser technology (could be higher than the available commercial range). However, further investigation is recommended regarding the challenges of using laser under downhole condition including footprint, cooling, cleaning, etc. and to identify any potential modifications to laser equipment could be required to achieve this target in future.

*keywords: laser cutting, material processing, porous media, heat transfer, finite difference, fractures.*

# DEDICATION

*I would like to dedicate this work to my beloved family for being patient and supportive throughout the duration of this research. My sincere gratitude to my wife Salma and my three lovely daughters Hams, Angy and Salma. I would not have been able to complete this work without them.*

*Last but not least, I would like to dedicate this achievement to my parents. They would have been very proud of this special moment in my life.*

# ACKNOWLEDGEMENT

*I would like to thank my principal supervisor Dr Mamdud Hossain for his continuous support and guidance during this research as well as Dr Faisal Nadimul.*

*I also want to thank Dr Firdaus Sukki and Dr Gbenga Oluyemi for their effort in facilitating the process of my research.*

# Contents

# List of Tables

# List of Figures

# Nomenclature

$A$ : Conductive loss function

$B$ : Radiative loss function

$b$ : Laser power transmitted without interacting with the cut front

$C$ : Convective loss function

$c_p$ : Specific heat capacity at constant pressure, J/kg.K

$c_t$ : Total compressibility, psi-1

$d$ : Material thickness, m

$E_{cut}$ : Specific energy needed to melt one unit of the material, J/m3

$FOI$ : Fold of Increase

$h$ : Reservoir thickness, ft

$HAZ$ : Heat Affected Zone

$k$ : Thermal conductivity, W/m.K

$k$ : Reservoir permeability, mD

$k_a$ : Altered permeability, mD

$L_h$ : latent heat, J/kg

$L_f$ : Latent heat of fusion, J/kg

$L_v$ : Latent heat of vaporization, J/kg

$P$ : Laser power, kW

$P_e$ : Peclet number

$p_i$ : Initial reservoir pressure, psi

$p_r$ : Average reservoir pressure, psi

$p_{wf}$ : Bottomhole flowing pressure, psi

$Q^*_{cond}$ : Dimensionless conduction heat loss rate

$Q_{cond}$ : Rate of conduction heat loss, watts

$Q_o$ : Oil flow rate, bbl/day

$r_f$ : Reflectivity of the cut zone

$r$ : Radius in radial coordinates, m

$r_a$ : Radius of altered zone around wellbore

$r_e$ : Reservoir drainage radius, ft

$r_w$ : Wellbore radius, ft

$S$ : Fluid saturation

$s$ : Skin factor

$T$ : Temperature, K

$T_c$ : Critical temperature, K

$T_i$ : Initial temperature, K

$T_m$ : Melting temperature, K

$T_v$ : Vaporization temperature, K

$t$ : Time, sec

$v$ : Cutting speed, m/s

$w$ : Kerf width, m

$WI$ : Well Index, bbl/day/psi

$x$ : Distance in axial coordinates, m

$x_f$ : Fracture half-length, m

$z$ : Gas deviation factor

## Greek Symbols

$\Delta$ : Delta, step of finite change (spatial, time or temperature)

$\rho$ : Density, kg/m3

$\alpha$ : Thermal diffusively, $m^2/sec$

$\gamma$ : Liquid (melt) fraction, dimensionless

$\phi$ : Porosity

$\mu$ : Viscosity, cp

$\beta_o$ : Oil formation volume factor, RB/STB

## Subscripts

$eff$: Effective

$g$ : Gas

$i$ : Spatial radial grid system

$j$ : Spatial axial grid system

$l$ : Liquid

$m$ : Melting

$n$ : Time level

$o$ : Oil

$r$ : Rock

$v$ : Vaporization

$w$ : Water

# Chapter 1: Introduction

## 1.1 Background

Hydraulic fracturing is the most effective technique to enhance oil and gas well productivity in oil and gas industry especially in low permeability reservoirs by creating fractures 'cracks' into hydrocarbon bearing formations around wellbore in order to increase the open area to flow and significantly improves reservoir recovery (Speight 2016).

Hydraulic fracturing operations require pumping a huge fracturing fluids (usually water-base fluids) into formations and very high hydraulic horse power in order to be able to breakdown the rock and create fractures. It is also associated with high degree of operational complexity and potential contamination to the environment including underground drinking water resources and the risk of earthquakes especially in shale gas development. According to this negative environmental impacts, shale gas development is currently halted in the UK (BBC 2019).

Hydraulic fracturing is the typical technique for sandstone formations while acid fracturing is the suitable technique to improve well productivity in carbonate formations such as limestone and chalk where permeability is very low and wells are usually not able to produce any fluids prior to acid fracturing operations. In principle, acid fracturing is similar to hydraulic fracturing technique except the use of acid instead of water-base fluids and also the manner by which fracture conductivity is created (Speight 2016).

Successful hydraulic fracturing operation would require good understanding of geomechanical property and reservoir characteristics including fluid rheology and leakoff rate into formation. Heterogeneity and uncertainty in rock and reservoir properties may jeopardize the performance of hydraulic fracturing operation and would also require complex geomechanical and reservoir modelling.

The above discussion has shed some lights on the potential gaps and complications associated with existing hydraulic fracturing technology and the needs for developing an alternative technique.

## 1.2 The future needs for an alternative technique

Hydraulic fracture was introduced by Stanolind Oil in 1949 (Montgomery and Smith 2010) and since that approximately 2.5 million fracture treatments have been performed worldwide. The first experimental fracturing was conducted in 1947 in the Hugoton field located in south western Kansas.

Hydraulic fracturing operation is typically achieved by applying high pressure into hydrocarbon bearing formation and fracture will be created and propagated into formation once the applied pressure exceeds formation in-situ stress. Crosslinked fluid is the typical fracturing fluid used to carry and transport proppant. Solid’s free fluid is pumped first to create the desired fracture geometry into formation then a mixture of fluid and proppant is pumped into the created fracture. Proppant will keep the fracture open and enhance gas and oil production due to the created high conductivity fracture.

Hydraulic fracturing operations require a significant amount of fracturing fluid, which considered as potential challenges from logistic and environmental point of views especially in shale gas fracturing where a large number of wells are required to extract economic quantities of shale gas. 200 – 250 wells are typically required to extract trillion cubic feet of gas (Rezaee 2015).

The demand in natural gas increases overtime and recently oil and gas industry gives more attention to unconventional resources such as shale gas reservoirs. Shale is ultra-low permeability formations and hydraulic fracturing is essential to enhance well productivity.

World natural gas production is expected to increase to 554 bcf/d by 2040 compared to 342 bcf/d in 2015 (EIA 2017). The largest component of this growth is natural gas production from shale resources, which grows from 42 bcf/d in 2015 to 168 bcf/d by 2040 as shown in Figure 1-1.

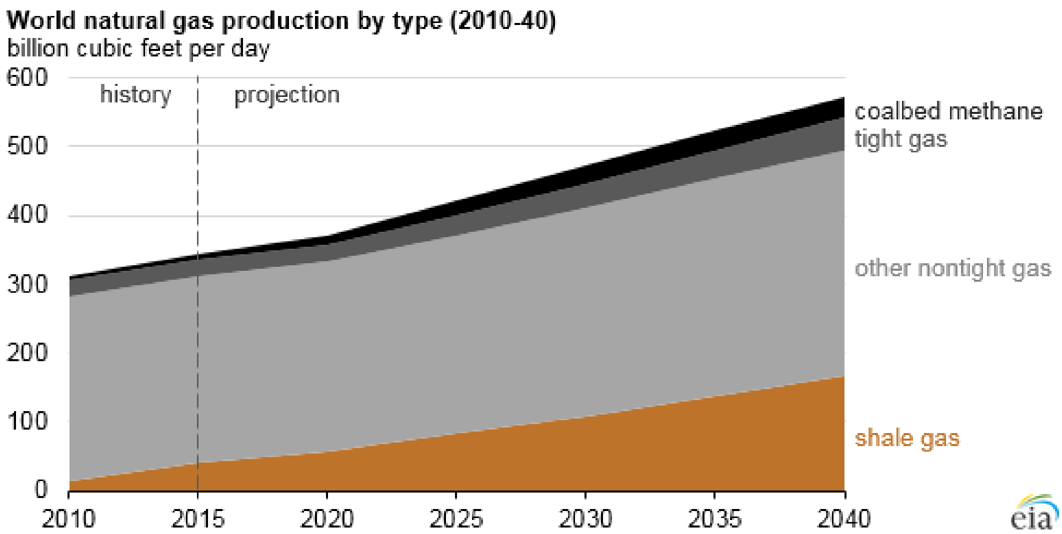


Figure 1-1: World natural gas production (EIA 2017)

Shale gas is expected to account for 30% of world natural gas production by the end of the forecasted period and this will significantly increase the future demand on hydraulic fracturing operations.

The main environmental issue in shale gas development is the requirement for disposal a huge amount of wastewater and the possibility that fracturing fluids can migrate into drinking water aquifers.

This research gives a potential solution to the traditional fracturing technique, developing an alternative fracturing technique using clean energy sources such as laser. Using laser in oil industry has been considered and suggested in the past mainly for perforation and drilling applications. Experimental tests showed the capability of laser to create holes and microfractures in rock samples but creating deep fractures has not been investigated neither experimentally nor by modelling. However, using laser to create deep fractures, as an alternative technique to the existing hydraulic fracturing technique, has been suggested and discussed in this research including the development of the appropriate mathematical models and methodology to simulate and investigate the using of laser to create deep fractures.

## 1.3 Research objectives

The aim of this research is to analyze the application of laser processing methods as an alternative fracturing technique. The objectives include the development of analytical methodology and numerical solution to analyze and discuss the possibility of using high power laser to induce fracture network around wellbore without the needs to pump any fluid into formation. The focus of this work will be on the selection of laser processing parameters for optimal feature quality and fracturing performance.

The objectives of this research can be divided into three main objectives (research stages) as the following:

**Objective-1:**

To develop the appropriate analytical and numerical solutions which can be used to calculate laser power requirements for creating fracture network into hydrocarbon bearing formations. To validate the developed models for both pulsed and continuous-wave laser modes and identify the optimum laser parameters required to create fractures under various conditions.

**Objective-2:**

To conduct sensitivity analyses for various laser processing parameters and rock properties including cutting speed, kerf width, material thickness, rock type, porosity and porous-media fluid saturations. To calculate laser power requirement under those parameters considering various cutting mechanism including melting and vaporization.

**Objective-3:**

To develop a reservoir simulation model in order to identify the potential improvement in well productivity could be achieved post laser interaction with hydrocarbon bearing formations. To conduct sensitivity analysis for reservoir properties in order to identify the optimum reservoir conditions which are suitable for the proposed technique and can yield maximum well productivity.

## 1.4 Research impact

The impact of this research can be significant in oil and gas industry and can be considered as a remarkable step in using clean energy source as an alternative fracturing technique.

The main concerns associated with shale gas development in the UK including underground water contamination and potential earthquakes could be mitigated by using the clean, effective and environmental friendly technique proposed in this research. The technically recoverable shale gas resources in the UK was estimated by 20 trillion cubic feet (Rezaee 2015) and laser induced fracture technique may support and encourage the UK in developing shale gas resources in future. Figure 1-2 shows the current local communities protesting against shale gas fracturing in the UK.


Figure 1-2: Local communities and environmental group protesting against fracking (BBC 2019)

As discussed above, the demand on gas increases overtime and hydraulic fracturing operations will be essential to develop and unlock unconventional resources in future.

The proposed fracturing technique using laser is effective and less operational complexity compared to the existing technique and will encourage the oil and gas industry to conduct more fracturing operations. Oil and gas production will increase accordingly and balance the expected increase in world gas demand. Also the potential contamination to environment will be minimized around the globe, which is of great interest and value.

# Chapter 2: Literature review

This chapter includes review and discussion regarding laser applications in oil industry, laser material processing modeling, laboratory experiments and laser technology screening. The aim of this chapter is to capture lesson learned and any useful outcomes from previous work which can be considered in this research.

## 2.1 Laser applications in oil industry

Laser was invented in 1958 and is widely used in manufacturing of various engineering and medical applications. However, laser applications in oil industry are very limited and few technical papers were published during the past decades regarding the possibility of using laser in perforation and drilling applications in future.

Using laser in drilling was studied by Gas Research Institute (GRI) and experimental tests were conducted to measure the rate of penetration by applying laser into rock samples using U.S. Army's facilities (StarWars laser technology). The results of GRI's project was presented by Graves and O'Brien (1998) and O'Brien, Graves and O'Brien (1999).

The project included two phases; in the first phase, Mid Infrared Advanced Chemical Laser (MIRCAL) of 900 kW CW average power was applied to thick sandstone slab and after 4.5 second, a hole of 2.5 inches was created and 5.5 pounds of material was removed (equivalent to 166 ft/hr rate of penetration in conventional drilling).

The test showed that high power lasers were very effective in drilling rock samples. Figure 2-1 shows sandstone sample following MIRACL laser interaction.

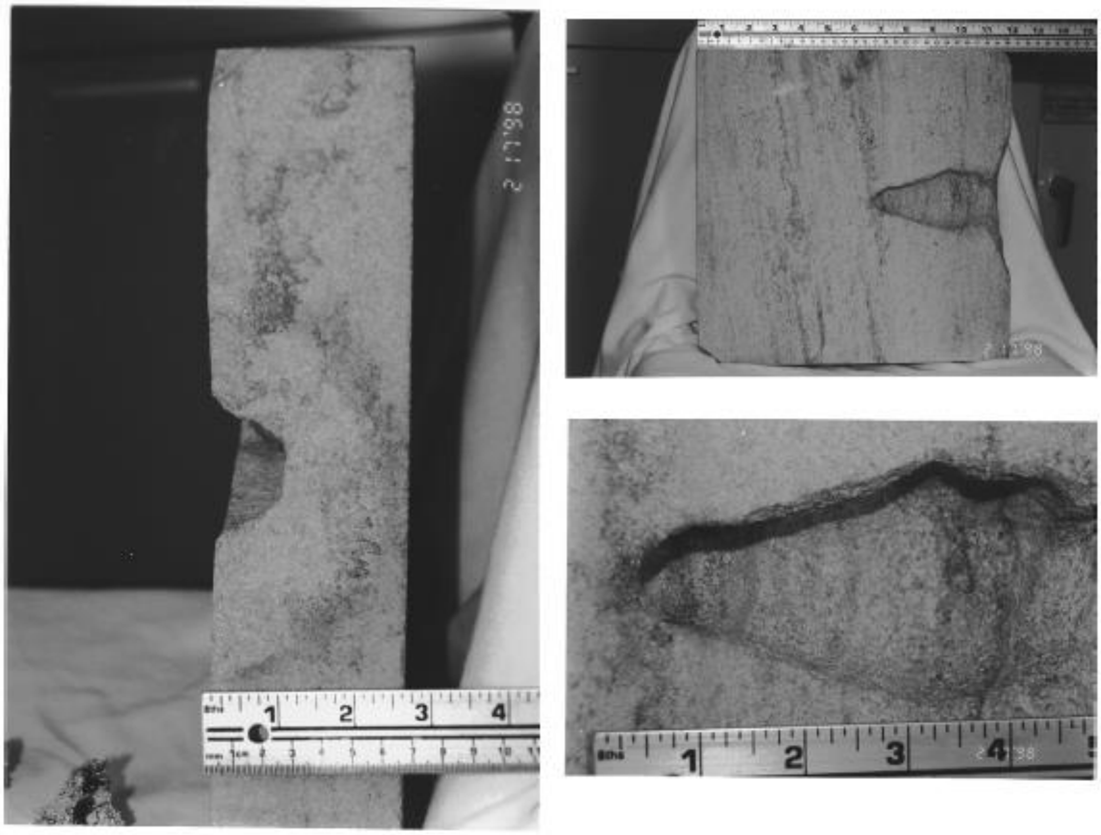

Figure 2-1: Sandstone sample following MIRACL high laser power (Graves and O'Brien 1998)

In the second phase, Chemical Oxygen Iodine Laser (COIL) 5 – 10 kW CW was applied to more than 100 of various rock samples and the results were encouraging as laser was able to penetrate all rock types with a range of 10 – 40 kJ/cm3 specific energy.

Graves et al. (2002a) continued the GRI research in order to support the proposed technology of drilling using high power lasers. Graves compared the specific energy required to cut Berea sandstone by using various laser types ($CO_2$, CO, COIL and Nd:YAG). 10 – 50% difference in specific energy was indicated due to different laser operating conditions and sample shapes. This could be considered as source of uncertainty when using experimental tests to verify mathematical models.

Gas Technology Institute (GTI) conducted a study to experimentally measure the possible benefit of using laser as an alternative to perforating technique (Batarseh et al. 2003). Two laser types were used at U.S Army facility; Mid-Infrared Advanced Chemical Laser (MIRACL) and Chemical Oxygen Iodine Laser (COIL). The results showed a clean perforation tunnels without debris and micro-fractures as shown in Figure 2-2.

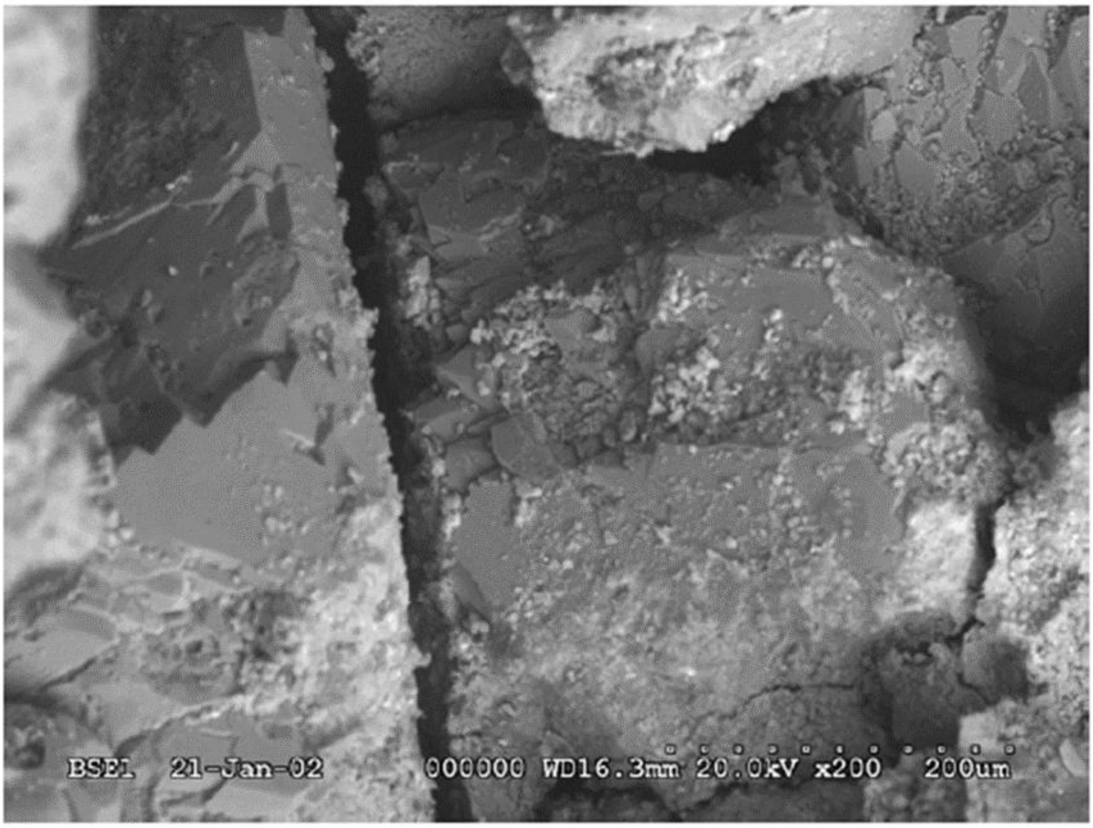


Figure 2-2: SEM image of quartz grain cracked after laser heat treatments in Berea Sandstone (Batarseh et al. 2003)

Gahan et al. (2004) conducted a laboratory experiment on Berea sandstone to determine the capability of fiber lasers in perforation and the possibility of minimizing specific energy by using purging gas to effectively remove cutting and avoid energy losses through thermal accumulations. The results indicated only 5.5 kJ/cc specific energy which represented a minimal value compared to previous laser rock interaction tests.

Gahan et al. (2005) and Batarseh, Gahan and Sharma (2005) conducted experimental tests to identify the effect of downhole condition on laser perforation. The results indicated that laser perforation system can significantly benefit from the high pressure condition downhole. Figure 2-3 shows significant reduction in specific energy when perforating under triaxial pressure. Limestone showed better results because it compresses and compacts more than sandstone when stress is applied to the rock.

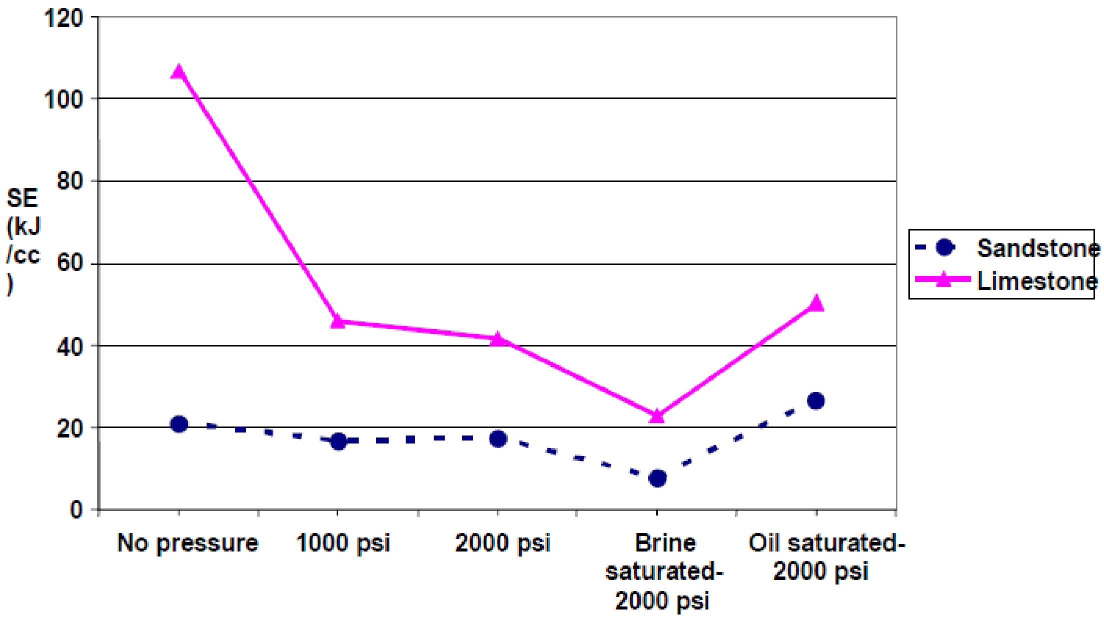


Figure 2-3: Laser perforation test under various triaxial pressure (Batarseh, Gahan and Sharma 2005)

Kobayashi et al. (2008) studied the effect of laser drilling underwater and the laboratory experiments showed that laser-irradiation into water induces mechanical forces in the forms of shock-waves, bubble formation and water jets. This laser-induced mechanical forces could be utilized for generating a cavity in the rock and increase the laser drilling efficiency. This findings could add benefit to laser processing under downhole conditions.

Laser can improve rock porosity and permeability. Rock spallation occurs at a temperature less than the melting point and microfractures can be developed with less specific energy compared to melting and vaporization (Sinha and Gour 2006). The lowest level of specific energy occurs just before the transition zone as shown in Figure 2-4 and this is the desired zone for laser to work.

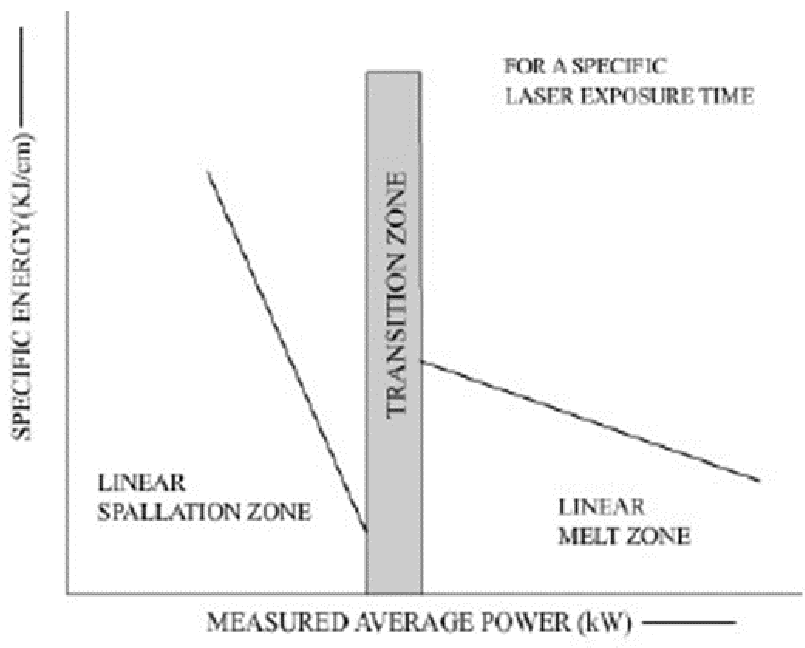


Figure 2-4: Comparison between SE for spallation and melting zones (Sinha and Gour 2006)

The microfractures created during laser perforation can facilitate hydraulic fracturing operation (Keshavarzi 2011).

Laser perforation can support hydraulic fracturing operation of horizontal wells by creating vertical holes to help initiate and propagate hydraulic fracture in the point of interest (Batarseh et al. 2012). Figure 2-5 shows different perforation hole geometry controlled by using different types of laser lenses which can be used to optimize hydraulic fracture propagation.

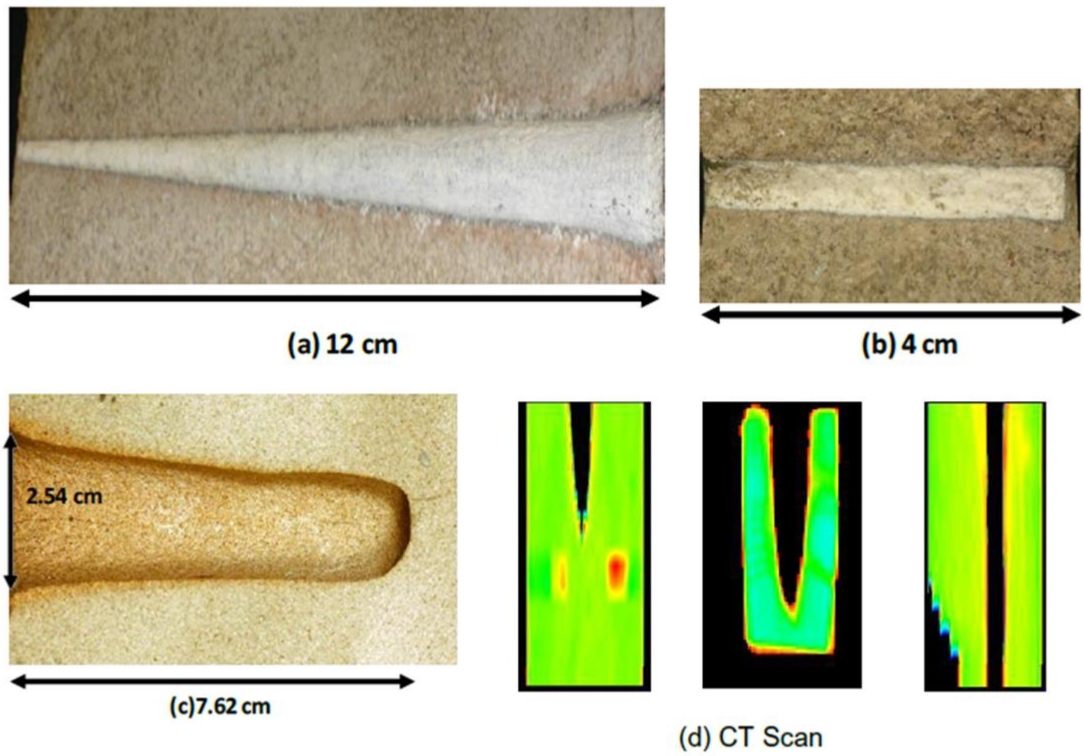


Figure 2-5: Different laser perforation hole geometry (Batarseh et al. 2012)

da Silva et al. (2017) conducted experimental tests to simulate laser perforation in cased and cemented wells. The results indicated the possibility of perforating steel-cement-carbonate samples with 1200 - 1500 watts laser power. Also microfractures were observed in the carbonate samples around the perforations created by laser as shown in Figure 2-6.

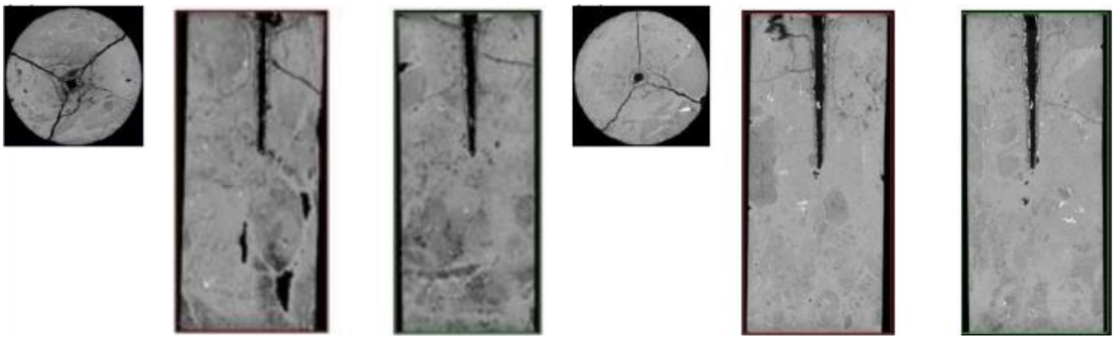

Figure 2-6: Microtomography images show perforation and microfractures in carbonate samples (da Silva et al. 2017)

Jamali et al. (2019) conducted experimental tests to support drilling application using laser by softening hard rocks. Jamali suggested a combination of laser and mechanical drilling technologies to facilitate the drilling operations.

The following is a brief summary of the main findings of this section:

1. Using laser in oil industry has been suggested for perforation and drilling applications only. However, it is still under researching phase and has not been implemented in oil industry. Note that the existing laser applications in oil industry is limited to fiber-optic for downhole temperature sensing and monitoring.

2. Experimental tests showed the capability of laser to penetrate and create microfractures in rock samples. The results also indicated that laser processing can significantly benefit from downhole conditions including high pressure.

3. Laser perforation was suggested to facilitate and support hydraulic fracturing operation of horizontal wells by creating vertical holes to help initiate and propagate hydraulic fracture in the point of interest.

However, using laser to create deep fractures as an alternative fracturing technique was not investigated.

## 2.2 Laser material processing modelling

The section includes a review for the analytical and numerical models used in the past to simulate laser material processing and some useful outcomes which have been used in this research regarding laser power modelling.

The energy balance theory during laser cutting including useful and waste energy was described by Powell et al. (1994). The waste energy was identified by experimental tests to measure the conductive heat losses as function of material thickness during laser cutting process. Equation 2.1 shows Powell's energy balance equation.

$$(P - b)\left[\frac{100-r_f}{100}\right] = (E_{cut}\, v\, d\, w) + [(0.5\, \pi\, d\, w)(A + B + C)] \text{-----}(2.1)$$

Powell's equation has been used in this research as the base equation to calculate the total laser power required to cut various material thickness. Detailed description about Powell's equation is provided in the analytical solution section (Chapter 3).

Prusa, Venkitachalam and Molian (1999) developed a model to calculate heat conduction losses during laser cutting of metals with oxygen jet in polar and cartesian coordinates. Prusa also developed a correlation to calculate heat losses as a function of Peclet number. Equation 2.2 shows Prusa's correlation.

$$Q^*_{cond} = 3.20\, P_e^{+0.868} \text{--------------------------------------------------}(2.2)$$

Prusa's correlation has been used in this research to analytically calculate the waste energy during laser cutting. Detailed description about Prusa's correlation is provided in the analytical solution section (Chapter 3).

Hossain, Acar and Malalasekera (2005) developed a mathematical model for airflow and heat transfer through fibrous webs. A melt fraction, $\gamma$, was considered in order to model the phase change in a volume element where solid and liquid may exist simultaneously within a small interval around fusion temperature. Figure 2-7 shows the variation of melt fraction with temperature.

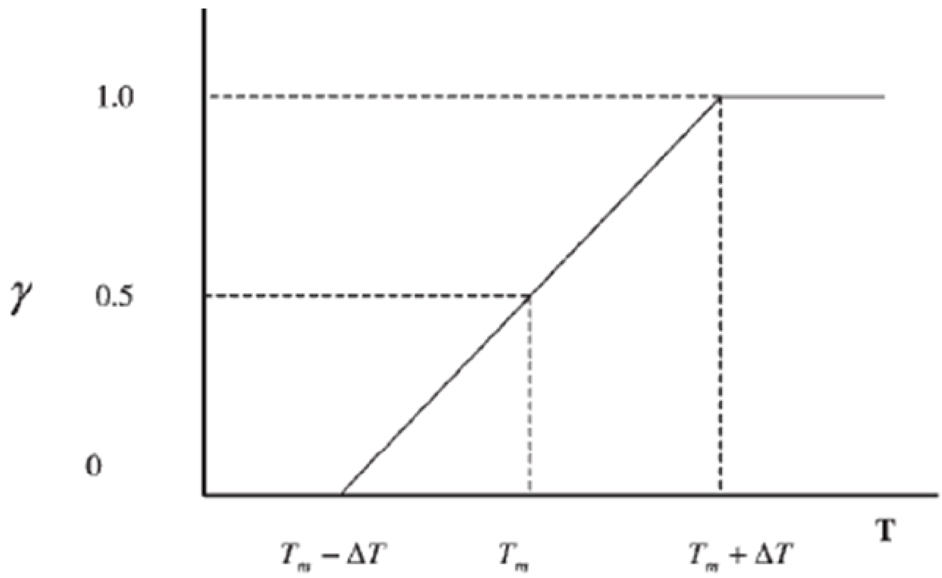


$$\gamma = \begin{cases} 1 & \text{if } T > T_\mathrm{m} + \Delta T \\ 0 & \text{if } T < T_\mathrm{m} - \Delta T \\ \dfrac{T - T_\mathrm{m} + \Delta T}{2\Delta T} & \text{if } T_\mathrm{m} - \Delta T < T < T_\mathrm{m} + \Delta T \end{cases}$$

Figure 2-7: Variation of melt fraction with temperature (Hossain, Acar and Malalasekera 2005)

Melting fraction concept has been considered and incorporated into the mathematical model developed in this research in order to model phase changing and melting progression in porous media during laser cutting. Detailed description about melting fraction concept is provided in the numerical solution section (Chapter 3).

Numerous numerical models were developed in the past to simulate temperature distribution during laser material processing for metals (non-porous material) using different coordinate systems in order to simulate various applications. Example of the models developed in the past is the 2D model developed by Sheng and Joshi (1995) to simulate Heat Affected Zone (HAZ) during laser cutting of stainless steel using finite element solution. Figure 2-8 shows the modelled HAZ propagation during laser cutting.

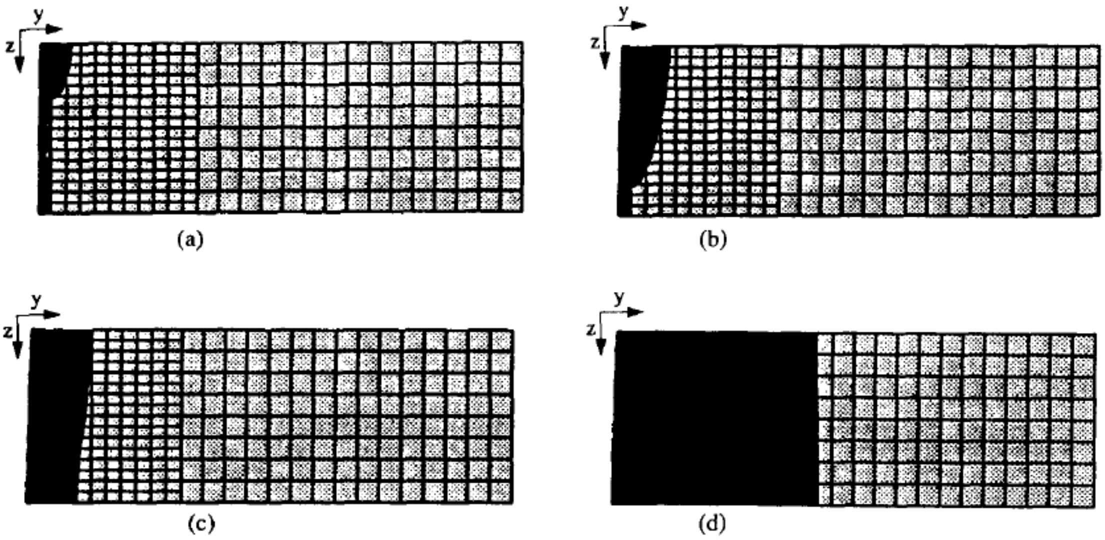


Figure 2-8: HAZ propagation during cutting, 2D finite element model (Sheng and Joshi 1995)

There are many other examples of the models developed in the past to simulate different laser applications for metals including the 3D finite difference model developed by Modest (1996) to simulate laser ablation, the 1D finite element model developed by Verhoeven et al. (2003) to simulate laser drilling, the 3D finite element model developed by Fu, Guo and Sealy (2014) to simulate laser cutting and the 1D finite volume model developed by Otto, Koch and Vazquez (2012) to simulate a wide range of laser material processing.

As shown above the models developed in the past are similar in principle where energy balance equations were numerically solved by finite element, finite difference or finite volume methods. However, each model was developed to simulate a particular application with specific coordinate system and boundary conditions suitable for the application and condition to be modelled. The results of these models could not be reinterpreted for different materials, thicknesses or boundary conditions and accordingly a simulation model which is more relevant to the application proposed in this research has been developed and discussed in the numerical solution section (Chapter 3).

Despite the numerous modelling conducted in the past, the majority of them focused on metals only and therefore there is a lack of literature regarding the modelling of laser material processing in porous media. However, the alloy powder beds used in Additive Layer Manufacturing (ALM) and Selective Laser Melting (SLM) could be treated as porous media with interconnected voids in heat transfer modelling.

Examples of the models treated powder beds as porous media are the model developed by Kundakcioglu, Lazoglu and Rawal (2016) to simulate transient temperature fields in ALM of 3D complex structures in powder bed systems using laser heat source and the 3D model developed by Pei et al. (2017) to simulate SLM of A1Si10Mg powder. Figure 2-9 shows Pei's model with the powder beds treated as porous media and the effect of laser scanning speed and hatch spacing on the molten pool behaviour.

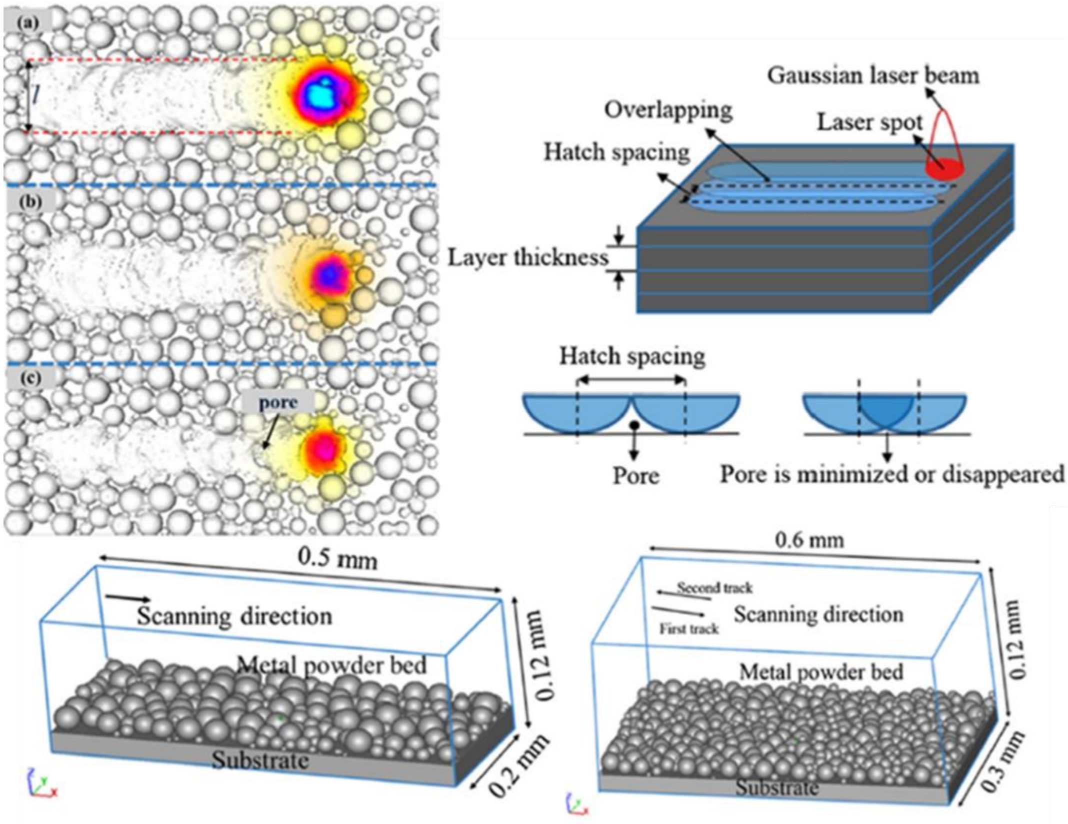


Figure 2-9: 3D model for Selective Laser Melting (SLM) of A1Si10Mg powder (Pei et al. 2017)

Li et al. (2018) developed a finite element model to simulate laser induced thermal stresses caused by temperature distribution in granite rock during laser perforation. The model showed that rock spallation occurs because the tensile stress generated by laser is significantly higher than the tensile strength of the granite sample. Figure 2-10 shows the stress distributions around perforation hole with different laser powers.

Modelling the induced stresses is not considered in this research. However, it has been recommended for future work.

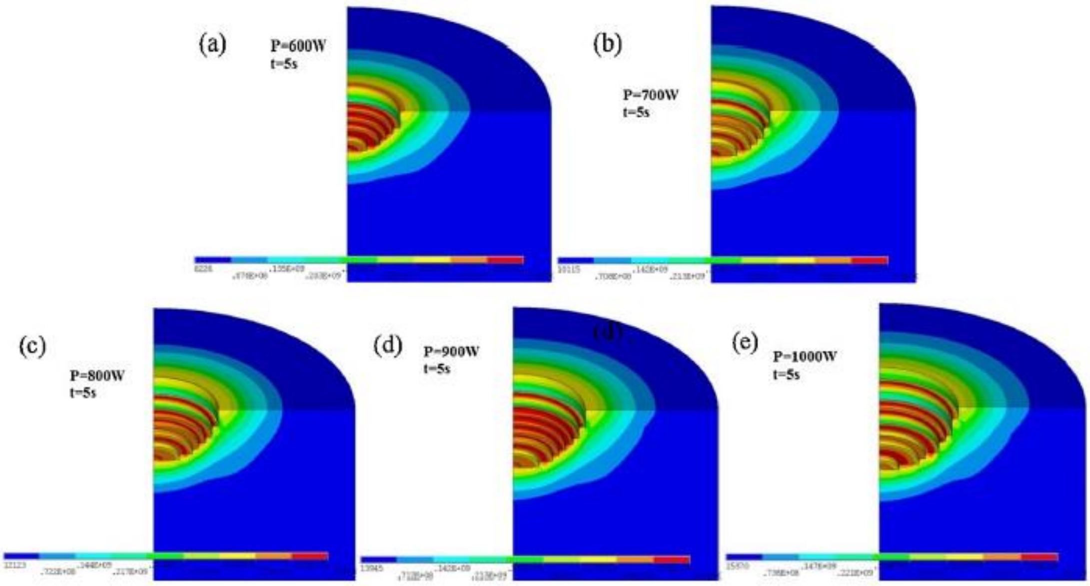


Figure 2-10: Stress distributions with different laser powers (Li et al. 2018)

The following is a brief summary of the main findings of this section:

1. Powell's energy balance equation has been used in this research as the base equation to calculate total laser power including useful and waste powers. Waste power due to heat transfer into surrounding is a transient process which is difficult to be calculated analytically and accordingly Powell conducted an experimental tests to measure the waste power during laser processing.

2. Prusa's correlation has been used in this research and incorporated into Powell's energy balance equation to analytically calculate the waste power during laser cutting as shown in the analytical solution section (Chapter 3).

3. Hossain's melting fraction has been incorporated into the mathematical model developed in this research in order to model

phase changing during laser cutting as shown in the numerical solution section (Chapter 3).

4. Numerous numerical models were developed in the past to simulate temperature distribution during laser material processing. The majority of them focused on metals (non-porous material) and therefore there is a lack of literature regarding the modelling of laser material processing in poupous media.

5. Each model developed in the past focused on simulating a particular application with relevant coordinate system and boundary conditions. The results of these models could not be reinterpreted for different conditions and accordingly a simulation model which is more relevant to the application proposed in this research has been developed and discussed in the numerical solution section (Chapter 3).

6. Latent heat was not considered (or not clearly presented) in many of the numerical models developed in the past to simulate temperature distribution during laser processing. However, latent heat of fusion and vaporizations has been incorporated into the analytical and numerical models and clearly presented in this research.

## 2.3 Laboratory experiments

The section includes a review for the laboratory experiments conducted in the past to various rock types in order to identify the potential improvement in rock porosity and permeability due to laser interaction. The results of these experimental tests has been used in the reservoir simulation modelling in this research.

Carstens and Brown (1971) performed intensive laboratory test for rock cutting by laser, it was probably the first time to measure the interaction of laser with rocks. The study was conducted in the united aircraft research laboratories to assist mechanical rock tunnelling. Various type of rocks including granite, basalt, limestone, dolomite and concrete were examined by laser with and without gas jet and penetration depth was measured for each rock type. Carstens and Brown pointed out that total laser power requirement can be estimated as 1 - 2 times the amount of power required simply to melt the kerf volume.

Gahan et al. (2001) conducted an experimental analysis to sandstone, limestone and shale samples in order to measure the specific energy required to remove a specific rock volume due to laser beam interaction. The created fractures depends on mineralogy, thermal properties of the rock and porosity, for examples clays contain water and by heating clays up to high temperature, the water will be evaporated, causes increase in the volume and pressure of the porous media and can cause fractures when this gases try to escape out into surrounding. Note that sandstones and shales have an appreciated amount of clays and fractures can be expected when applying laser beam into them.

Gahan pointed out that applying laser beam into sandstone sample can cause expansion in quartz grains. At 600$^{\circ}$C quartz grains expand by 1.75% of the original size, and in case of full grain contact (low porosity), grains have less space to expand and fractures can be developed.

The results of the experimental tests showed that high power laser can positively affect rock properties by increasing porosity and permeability around the lased hole.

Gahan investigated the interaction of high power pulsed laser with selected rock samples including breaking (spalling), melting and vaporizing. The work focused on laser variables affecting the specific energy calculations and it was limited to surface interaction by creating only shallow holes. Figure 2-11 shows the results of linear testing carried out by continuously moving of rock slabs under laser beam with various parameters. The results showed a significant alteration due to heating up the rock to spallation level even prior to reaching the melting point.

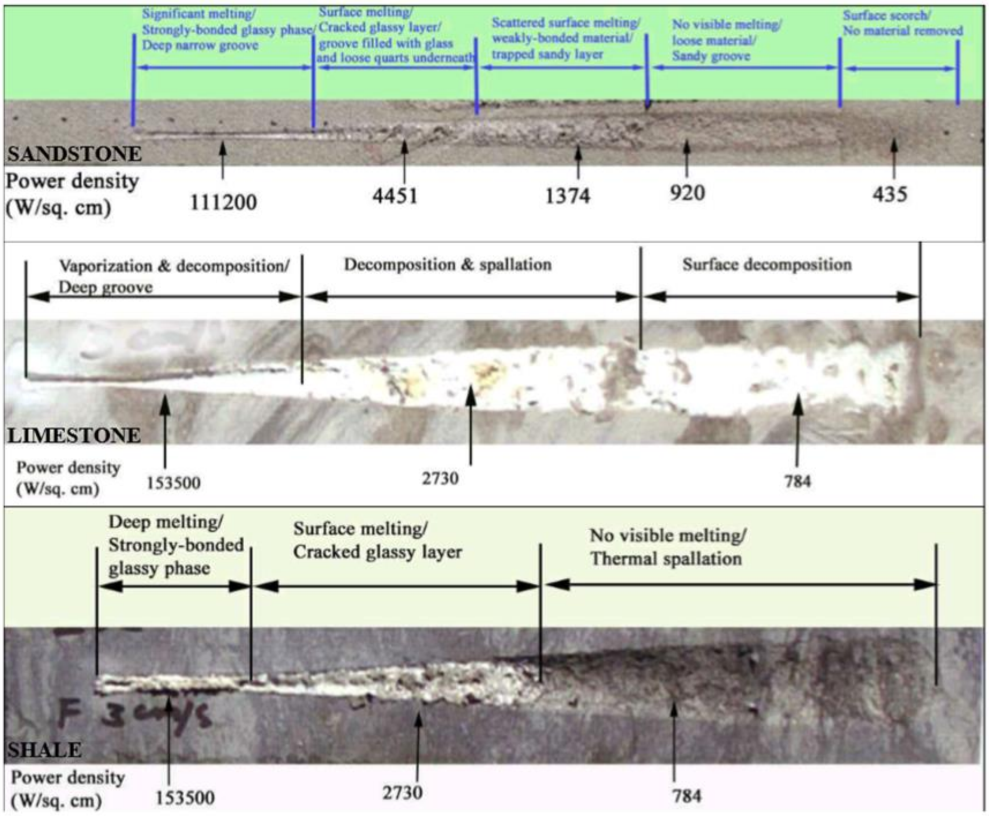


Figure 2-11: Various regions of laser interaction with rocks (Gahan et al. 2001)

Gahan also indicated that the time between pulses can cause cooling-down of the rock samples and increase the specific energy requirements accordingly. The findings in this research regarding the benefit of using continuous wave (CW) rather than pulsed laser is in line with Gahan's experimental work.

Figure 2-12 shows the relationship between repetition rate and specific energy where increasing repetition rate can significantly reduce the specific energy requirements due to the fact of decreasing the cooling-down time between pulses.

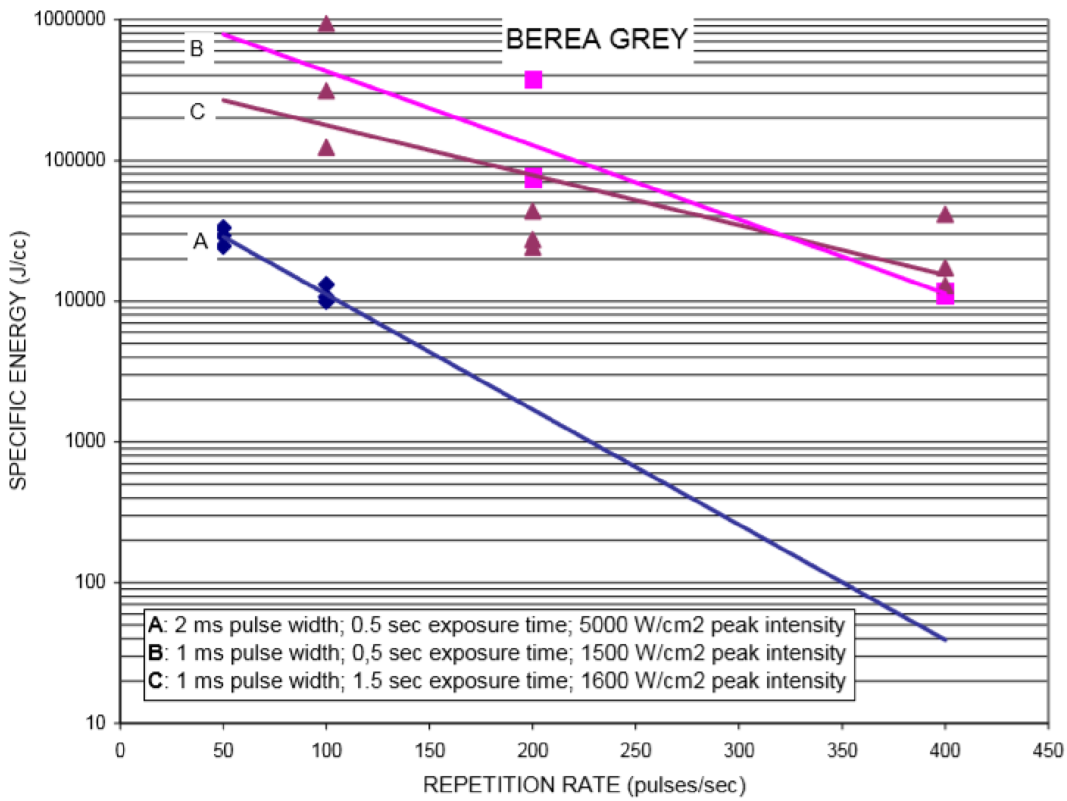


Figure 2-12: Effect of laser repetition rate on specific energy (Gahan et al. 2001)

The experimental tests conducted by Batarseh et al. (2012) showed a significant improvement in rock porosity and permeability due to laser interaction. Table 2-1 shows the effect of laser on rock permeability.

Table 2-1: Effect of laser on rock permeability, experimental tests (Batarseh et al. 2012)

| Sample | Permeability, mD | | Permeability increase, % |
|---|---|---|---|
| | Before | After | |
| Berea sandstone | 7754 | 7914 | 2 |
| | 554 | 674 | 22 |
| Limestone | 0.03 | 0.04 | 33 |
| Shaly sandstone | 111 | 301 | 171 |
| Shale | 0.43 | 0.55 | 28 |

It was also observed that when power increases, rock temperature reaches vaporization and a clean hole with no melt or damage will be created. The findings in this research regarding the benefit of cutting by vaporization is in line with Batarseh's observation. Cutting by vaporization is considered in this research in order to avoid the needs for melted rock removal using gas jetting which could be a challenge under downhole operating condition.

The results of all the tests showed that high power laser is capable of penetrating through casing, cementing into formations under all downhole conditions.

Graves et al. (2002b) presented the temperature effects of high power lasers on rock properties. The high temperature induced by lasers drilling through rock enhances porosity and permeability and reduces strength, also high temperature causes microcracks, vaporizes cementation, and dehydrates clays. At 550 °C smectite clay collapses and dehydrates resulting in increasing void space in the rock sample, also quartz grains expands by 1.75% at the same temperature and when grains cooled down, microcracks are created, which also increases the void space.

The results of the laboratory experimental tests showed that lasers improve porosity and permeability. Significant increase in high thermal conductivity sandstones was observed while insignificant increase in low thermal conductivity limestone. Rock strength of all rock types was reduced.

Sandstone porosity increased by 50% and shaly sandstone increased by 150% while limestone increased by only 20%. All rock types showed porosity increase near and away from the hole except limestone which didn't show change away from the lased hole due to the low thermal conductivity which causes less heat transfer and accordingly less heat induced porosity and permeability enhancement. The greatest permeability increase was 170% in shaly sandstone while limestone samples showed permeability increasing up to 35%.

Mineralogy plays an important role in how the rock can be changed during lasing, for example microfractures will develop in quartz, clays will dehydrate, and limestones will disassociate (low amount of quartz and clays) and can be vaporized or changed chemical composition and left a clean hole with a white lime powder (CaCO).

Figure 2-13 shows the microcracks created in shale sample after lasing due to thermal expansion and contraction.

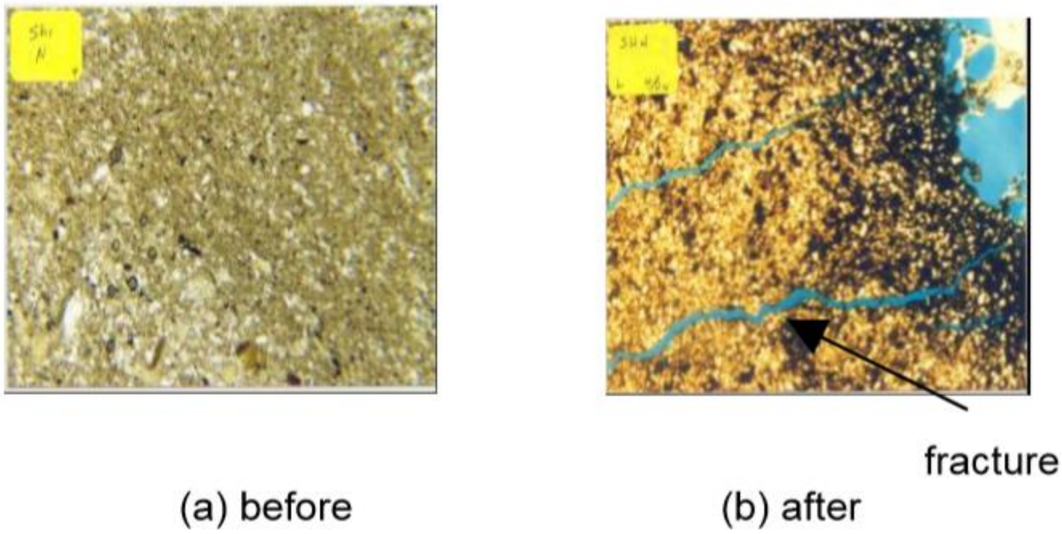


Figure 2-13: Microcracks created in shale sample after laser interaction (Graves et al. 2002b)

Figure 2-14 shows the dehydration of smectite clay sample due to laser interaction which increases void space.

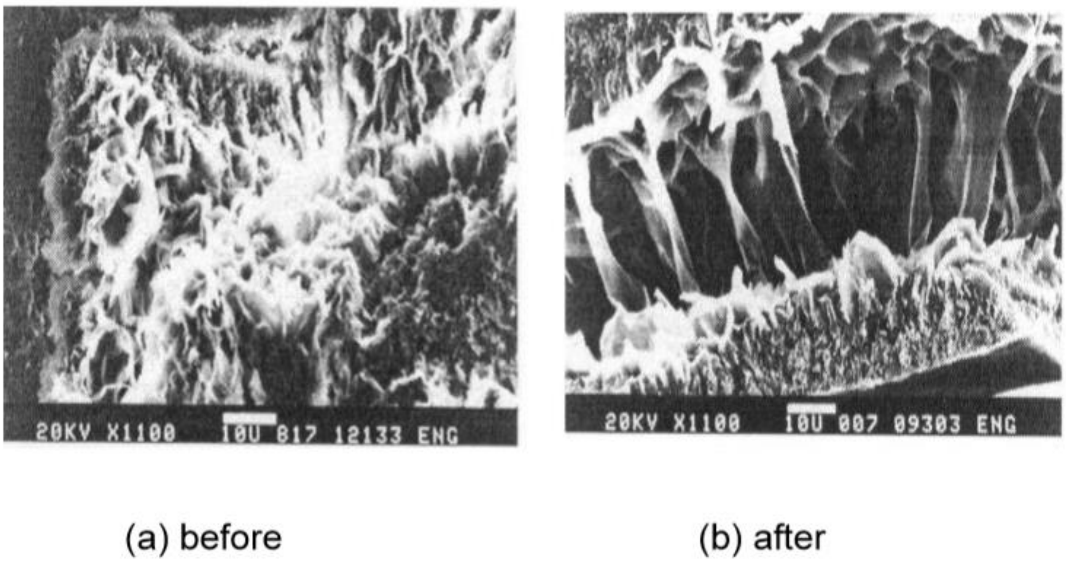


Figure 2-14: Smectite clay dehydration, increasing void space after lasing (Graves et al. 2002b)

Figure 2-15 shows the porosity improvement after lasing various rock types including Berea sandstone with 90% Quartz (BY), Berea sandstone with 85% Quartz (BG), shaly sandstone (Sst), limestone (LS) and shale (SH).

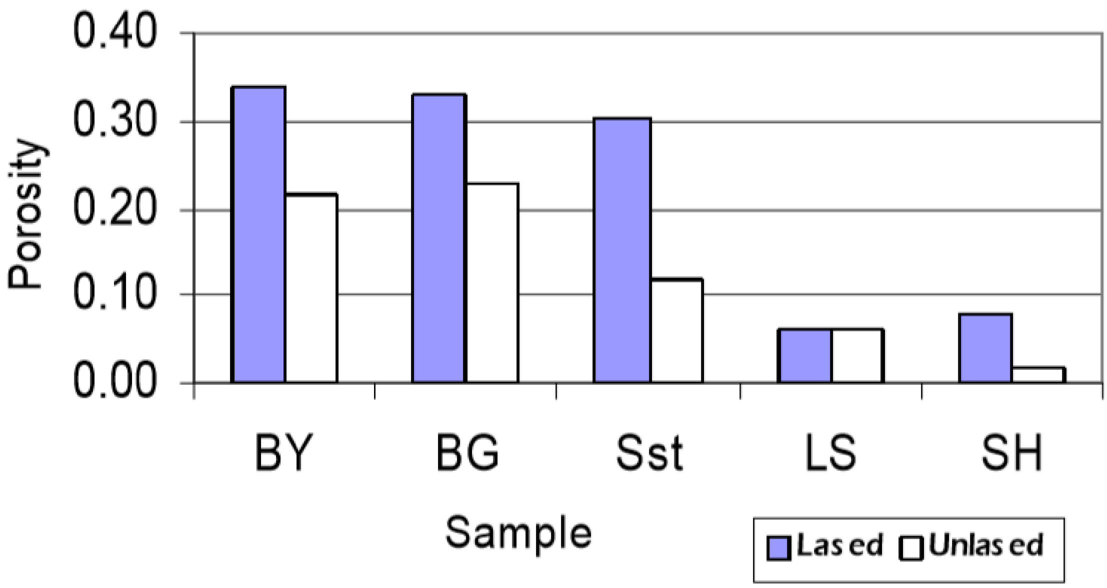


Figure 2-15: Porosity improvement after lasing various rock types (Graves et al. 2002b)

It is worth mentioning that also Young's Modulus, Shear Modulus and Bulk Modulus are significantly reduced after laser interaction specially in sandstone and shaly sand samples. Decreasing rock strength can increase the risk of sand production after lasing especially for unconsolidated sand, this point should be considered in shallow formation and unconsolidated sandstone.

Graves and Bailo (2004) presented a method to calculate the change in porosity and permeability of porous medium due to laser interaction and calibrated the results with measured data. Graves and Bailo pointed out that permeability and porosity increase, in the vicinity of the lased hole, by more than 50% due to microfractures.

Keshavarzi et al. (2010) pointed out that considerable permeability increases and high rate production can be achieved by using laser perforation technique instead of the conventional explosive charges. The tunnel during laser perforation in limestone is created by the thermal dissociation of $CaCO_3$ into CaO and $CO_2$ at about 825 °C, also experimental studies of GTI have proven that at in-situ pressure condition penetration depth increases and specific energy decreases significantly to 88% lower than the basecase of limestone.

Erfan et al. (2010) conducted an experimental analysis using Nd:YAG laser in carbonate rocks to investigate laser drilling applications. The rate of penetration (ROP) and the specific energy (SE) required to remove the rock were measured for dry, water and oil saturated formations. The results indicated an inverse relationship between ROP and SE regardless the porous fluid content type as shown in Figure 2-16. The findings in this research regarding increasing waste power with decreasing cutting speed and also the effect of fluid type in porous media is in line with Erfan's findings.

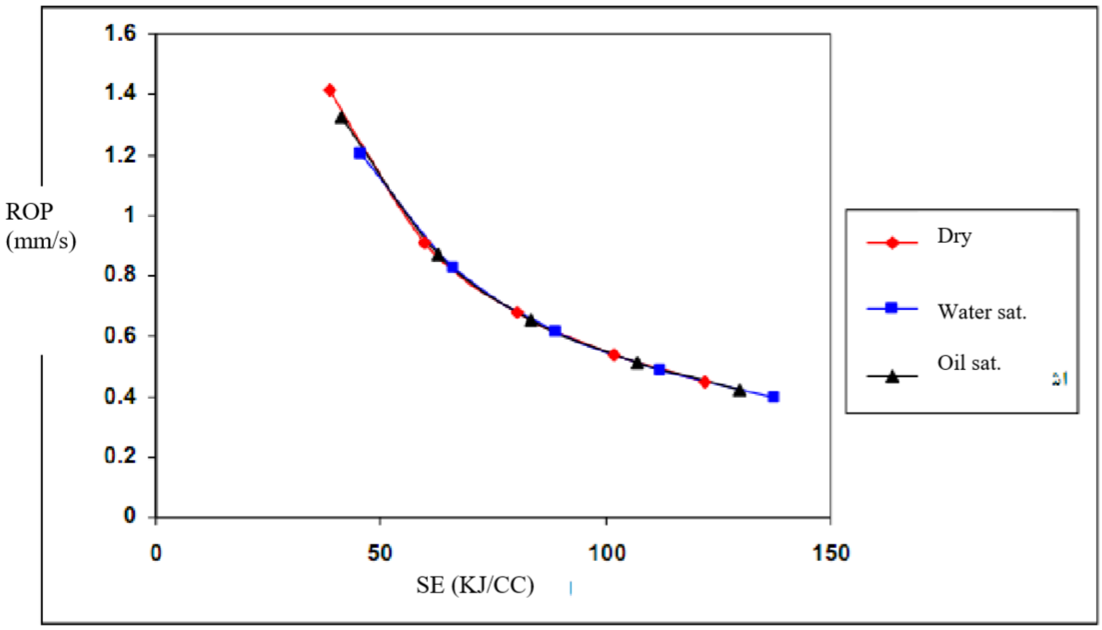


Figure 2-16: Relationship between ROP and SE (Erfan et al. 2010)

The results also indicated that SE increases with increasing drilling depth, and water saturated rock requires higher specific energy than the oil and dry rocks due to the difference in boiling point and heat capacity between water and oil as shown in Figure 2-17.

Erfan also pointed out that specific energy increases with depth (secondary effect) and this can be removed if the laser nozzle moves down to the sample with a velocity equivalent to ROP. This secondary effects has made laser technology still unviable for drilling while it is more attractive to perforation. In order to avoid this effect in the alternative fracturing technique proposed in this research, a proper kerf cleaning has to be considered. Note that moving laser source inside formation during cutting is not possible under downhole condition.

Increasing SE with hole depth can be interpreted in a similar way to the increasing of power requirement with increasing material depth, due to the fact of increasing waste energy, as indicated in the power calculation section in this research. Figure 2-17 shows a significant increasing in SE with hole depth where more than circa 10 mm was impossible to be achieved, this could be due to the limitation of the pulsed laser power used in this test.

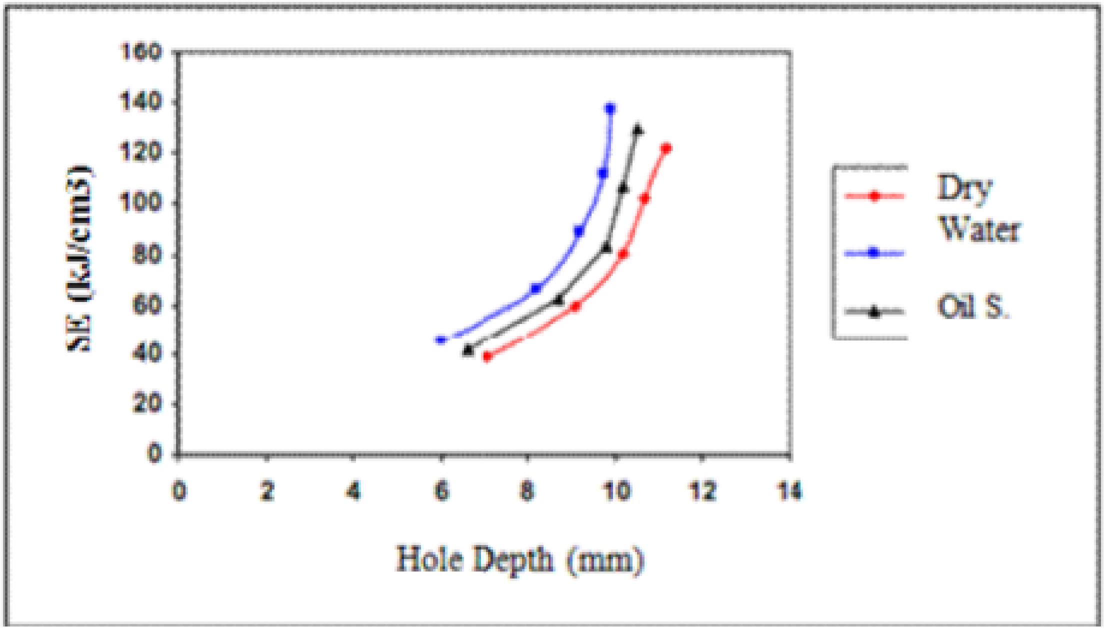


Figure 2-17: Effect of hole depth on SE (Erfan et al. 2010)

Bazargan et al. (2012) conducted laboratory experiments and the results showed that lasers improve porosity and effective permeability due to creating micro-fractures and dehydration or expansion of some minerals. It was also observed that the increasing of permeability in oil saturated limestone may be above the washed sample (water saturated).

Li et al. (2019) conducted laser perforation experiment on sandstone samples with 1600 W laser power. Complex crack net structure was formed around every hole as shown Figure 2-18.

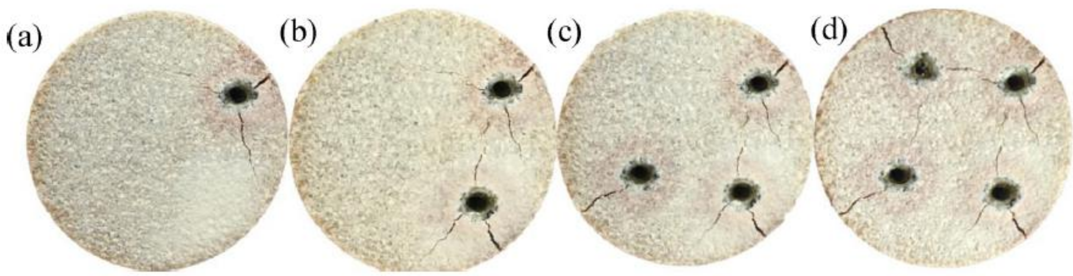


Figure 2-18: Morphologies of sandstone laser perforating test (Li et al. 2019)

The following is a brief summary of the main findings of this section:

1. Intensive laboratory experiment work was conducted to various rock types and significant improvement in rock porosity and permeability due to laser interaction was observed and identified. Microfractures were also observed in the heat affected zone due to quartz expansion, clay dehydration and limestone dissociation.

2. There are other important findings from these experimental tests regarding the benefit of using continuous wave laser mode, material thickness impacts on power requirement and cutting by evaporation. The results of this research are in line with those findings. The risk of reducing rock strength after laser interaction was also discussed in this section.

## 2.4 Laser technology screening

This section includes a review for the laser technology available in the market and the potential laser types could be suitable for the laser induced fracture technique proposed in this research and capable to provide high laser power.

The majority of existing laser can be classified into two main categories; low density including gas lasers and high density including solid-state lasers. Gas laser represents approximately half of the existing commercial lasers.

$CO_2$ gas laser is one of the most well-known and widely used laser in the market. It can produce a continuous wave power greater than 100 KW and pulsed mode energy up to 10 KJ (Silfvast 2004). CO2 laser is the highest average power gas laser and it has many applications but it best known for its use in laser material processing due to high power, efficiency and reliability (Webb and Jones 2004). This laser type could be suitable for the laser induced fracture technique proposed in this research.

Copper Vapor Laser (CVL) operates at pulsed mode with average output power of 100 W and up to 1 MW per pulse (Silfvast 2004). One megawatt is quite high power but pulse duration is very short, within nanoseconds.

Chemical laser have been developed primarily for military application and can produce power up to several megawatts for antimissile defines and high power weapons (Silfvast 2004). Chemical laser could be a challenge in the laser induced fracture technique proposed in this research due to the size required for chemical storage in addition to safety and environmental concerns.

Free electron laser has not been developed yet, but various applications including material processing have been suggested. It can produce up to 1 GW power per pulse for a 60 nanosecond pulse duration (Silfvast 2004). It could be one of the future candidate for the laser induced fracture technique proposed in this research.

Neodymium-YAG is one of the solid state laser types and can produce energy of approximately 80 KJ with a peak power of $8 \times 10^{13}$ watts (Silfvast 2004). Optical fibers can be used to transport Nd:YAG laser to the workpiece by hundreds of meters (Webb and Jones 2004). Using optical fibers to transport high power laser thousands of meters in oil and gas wells might not be suitable and will not provide a sufficient power based on the technology available at present. However, it could be considered in future when technology permits.

There are other laser types which has not been discussed in this section due to low power capability including gas, metal vapor lasers, X-Ray plasma and solid state lasers.

# Chapter 3: Methodology and mathematical models

This chapter discusses the analytical and numerical models developed in this research in order to simulate the actual physics during laser interaction and calculate the total laser power requirement to induce fractures into hydrocarbon bearing rocks under various laser parameters and rock properties.

## 3.1 Concept of creating fracture network using laser

The concept of creating fractures into hydrocarbon bearing formations using laser energy is different than conventional hydraulic fracturing. In conventional technique, water-base fluid is pumped into formation and pressure must exceed formation minimum in situ stress in order to create and propagate fractures. This technique requires high hydraulic horse power equipment. There are cases where, with as much as 15,000 hhp available, more than 10,000 hhp was actually used (Speight 2016).

The concept of using laser is quite different, the aim is to use the thermal energy generated by laser interaction to melt the rock and create fracture network around wellbore.

Conventional hydraulic fracturing can typically create a single fracture perpendicular to minimum in situ stress direction while the proposed laser induced fractures is independent of stress directions and multiple fractures (network) can be created around wellbore and significant improvement in well productivity can be achieved accordingly.

In conventional hydraulic fracturing, proppant (high permeability sand) is pumped into formation in order to keep the created fracture open while laser induced fractures will kept open by the uneven and rough cutting surface created by laser, similar to acid fracturing technique in carbonate rock where acid react with carbonate formations and create etched flow paths to keep the fracture open.

High quality cutting edge (smooth and clean cutting surface) is not required in the proposed laser induced fracture technique but rough cutting surface would be ideal to keep fractures open, unlike the standard requirement of laser material processing where high quality cutting is essential.

Laser energy must be high enough to melt the rock considering the energy losses into surrounding during processing in the form of heat transfer into surrounding.

The following sections show the analytical and numerical models developed in this research in order to calculate the total laser power requirement including useful and waste energy during laser interaction.

## 3.2 Analytical solution

Conservation of energy is the basis of laser power calculations. Webb and Jones (2004) described the laser cutting energy balance theory and this work was initially developed by Powell et al. (1994).

### 3.2.1 Energy balance equation

The energy balance equation was described by Webb and Jones as following:

Laser energy supplied to the cut zone = useful energy used in material cutting + waste energy which doesn't contribute into the process.

$$(P - b)\left[\frac{100 - r_f}{100}\right] = (E_{cut}\, v\, d\, w) + [(0.5\, \pi\, d\, w)(A + B + C)] \text{ ----(3.1)}$$

Where;

$P$ = total laser power, watts

$b$ = laser power transmitted without interacting with the cut front, watts

$r_f$ = reflectivity of the cut zone, %

$E_{cut}$ = specific energy needed to melt one unit of the material, J/m$^3$

$v$ = cutting speed, m/s

$d$ = material thickness, m

$w$ = kerf width, m

$A$ = conductive loss function, W/m$^2$

$B$ = radiative loss function, W/m$^2$

$C$ = convective loss function, W/m$^2$

The left hand side of the equation describes the primary losses which is the energy losses before laser interaction with the material ($b$ and $r_f$) while the right hand side describes the secondary losses which is the energy losses after thermal transformation and these include heat transfer into surrounding by conduction, convection and radiation ($A + B + C$).

Secondary losses are function of cutting front temperature and its surface area in contact with surrounding. Figure 3-1 shows a schematic of the cut front geometry assumed in the energy balance equation.

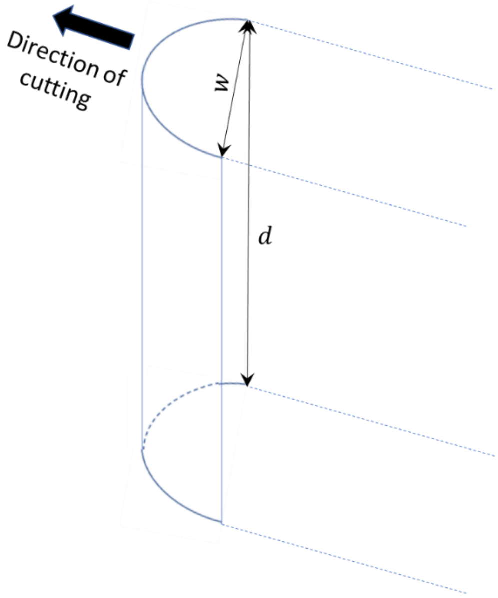


Figure 3-1: Schematic of a simplified cut front geometry (Webb and Jones 2004)

The conductive losses comes from the convex face in contact with surrounding material and convective and radiative losses comes from the concave face in contact with surrounding atmosphere. Powell et al. (1994) pointed out that convective and radiative losses are negligible but conductive losses are considerable also the proportional of the useful to wasted energy will change if the cutting speed is changed in order to cut different material thickness.

Powell did not develop mathematical calculations for the waste energy including conductive, radiative and convective functions (A, B and C) but conducted experimental work instead. For the purpose of this experiment, 50 mm diameter circle discs were cut in mild and stainless steel with various thickness, all cuts were carried out at maximum possible speed for each material thickness. Immediately after cutting, the discs were placed in an insulated water bath and the absorbed heat was measured by calorimeter. Figure 3-2 shows the experiment conductive losses.

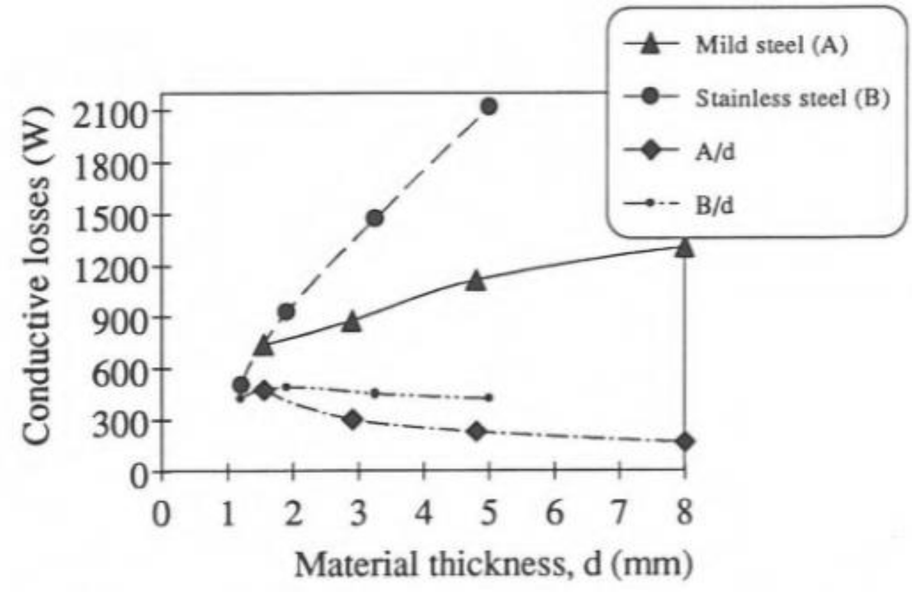


Figure 3-2: Experiment conductive losses as function of material thickness (Powell et al. 1994)

The conclusion of Powell's experiments is that heat losses by conduction increases in an approximately linear manner with material thickness.

### 3.2.2 Waste power correlation

The aim of this section in the research is to develop a simple and appropriate mathematical equation which can be used to analytically calculate the potential laser power required to cut oil bearing rock with various thickness.

Useful power is a straightforward calculation based on the volume of material to be melted while waste power due to transient heat transfer into surrounding is complex to be calculated analytically.

Prusa, Venkitachalam and Molian (1999) developed a correlation to calculate conduction heat loss rate during laser cutting using Peclet number (Pe) and it showed a good matching with experimental results. This correlation has been used in this research to calculate the waste power.

The major source of heat losses during laser cutting is conduction while the contribution of convection and radiation are very small and can be neglected.

Peclet number is a dimensionless cutting speed which represent a relationship between cutting speed and kerf width based on thermal properties of the material.

$$P_e = \frac{w}{2}\, v\, /\alpha \text{ ---------------------------------------------------------(3.2)}$$

Where;

$\alpha$ is thermal diffusivity = $k/\rho c_p$

$P_e$ = Peclet number

$w$ = kerf width, m

$v$ = cutting speed, m/s

$k$ = thermal conductivity, W/m.K

$\rho$ = density, kg/m3

$c_p$ = specific heat capacity at constant pressure, J/kg.K

The correlation developed by Prusa is shown below:

$$Q^*_{cond} = 3.20\, P_e^{+0.868} \text{ ----------------------------------------------------(3.3)}$$

Where $Q^*_{cond}$ is dimensionless conduction heat loss rate, and

$$Q^*_{cond} = \frac{Q_{cond}}{k\ d\ \Delta T} \text{ -------------------------------------------------------------(3.4)}$$

Where:

$Q_{cond}$ = rate of conduction heat loss, W

$k$ = thermal conductivity, W/m.K

$d$ = material thickness, m

$\Delta T$ = temperature rise, K and = $(T_m - T_i)$

$T_m$ = melting temperature, K

$T_i$ = initial temperature, K (ambient in case of cutting at surface)

Note that the validity of using this correlation is limited to Peclet number $\left(\frac{w\ v\ \rho\ c_p}{2\ k}\right)$ range of $0.2 \leq P_e \leq 10$

From the above equations, waste power due to conduction can be written as following:

$$Q_{cond} = 3.20\ P_e^{+0.868}\ k\ d\ \Delta T \text{ -------------------------------------------(3.5)}$$

$$Q_{cond} = 3.20\ k\ d\ \Delta T\ \left(\frac{w\ v\ \rho\ c_p}{2\ k}\right)^{+0.868} \text{ ---------------------------------(3.6)}$$

### 3.2.3 Proposed equation including useful and waste powers

As indicated in Powell's energy balance equation, total laser power = useful power + waste power.

$$(P - b)\left[\frac{100 - r_f}{100}\right] = \left( E_{cut}\, v\, d\, w\right) + \left[ (0.5\, \pi\, d\, w)(A + B + C) \right] \text{ ----(3.7)}$$

Assumptions made to simplify Powell's equation:

1. No light will be transmitted without interacting with material due to the fact that this process will take place downhole, not the same case as conventional laser cutting at surface where portion of light can pass into atmosphere without interaction, $b$ = zero accordingly.

2. For simplicity, it is assumed that material will fully absorb laser light, $r_f$ = zero accordingly.

3. Neglect radiative loss function, $B$ and convective loss function, $C$.

Based on the above assumptions, the left hand side of the energy balance equation can be simply replaced by laser power, $P$.

$$Total\ laser\ power = (P - b)\left[\frac{100 - r_f}{100}\right] = P \text{ -------------------------(3.8)}$$

The right hand side of the energy balance equation consists of useful power and waste power as following:

$$useful\ power = \left( E_{cut}\, v\, d\, w\right) \text{ ---------------------------------------(3.9)}$$

Where;

$$E_{cut} = c_p\, \rho\, \Delta T + \rho\, L_h = \rho\, (c_p\, \Delta T + L_h) \text{ --------------------------(3.10)}$$

Note that latent heat, $L_h$, is added to the specific energy required to melt one unit of the material. This energy will be absorbed by material during melting process (phase changing).

So, $useful\ power = \rho\ v\ d\ w\ \left(c_p\ \Delta T + L_h\right)$ ----------------------(3.11)

And replacing the waste power by the rate of conduction heat loss as a function of Peclet number correlation.

$$Waste\ power = [(0.5\ \pi\ d\ w)(A + B + C)] \cong Q_{cond} =$$

$$3.20\ k\ d\ \Delta T\ \left(\frac{w\ v\ \rho\ c_p}{2\ k}\right)^{+0.868}$$ ------------------------------------------(3.12)

So the total laser power equation including useful and waste powers can be written as following:

$$P = \rho\ v\ d\ w\ \left(c_p\ \Delta T + L_h\right) + 3.20\ k\ d\ \Delta T\ \left(\frac{w\ v\ \rho\ c_p}{2\ k}\right)^{+0.868}$$ ---------(3.13)

Where;

$P$ = laser power, watts

$c_p$ = specific heat capacity at constant pressure, J/kg.K

$\rho$ = density, kg/m3

$v$ = cutting speed, m/s

$d$ = material thickness, m

$w$ = kerf width, m

$\Delta T$ = temperature rise, K

$k$ = thermal conductivity, W/m.K

$L_h$= latent heat, J/kg

Note that Equation 3.13 doesn't include the effect of porosity and fluid saturations. Porosity and fluid saturations has been incorporated into the equation and discussed in the subsequent sections.

### 3.2.4 Proposed equation including Porosity and fluid saturation

In order to incorporate the effect of porosity and fluid saturation exist in the porous media including water, oil and gas phases into the base equation, the thermal properties shown in the above equation will be replaced by the effective thermal properties using volumetric average as following:

$$useful\ power = v\, d\, w\, \left(\rho\, c_p\, \Delta T +\ \rho\, L_h\right)$$

$$= v\, d\, w\, \left(\overline{\rho c_p}_{eff1} \Delta T_1 + \overline{\rho c_p}_{eff2} \Delta T_2 + \overline{\rho L_h}_{eff}\right) \text{-------------(3.14)}$$

$$waste\ power = 3.20\ k\ d\ \Delta T\ P_e^{+0.868}$$

$$= 3.20\ k\ d\ \Delta T \left(\frac{w\,v}{2\,\alpha}\right)^{+0.868}$$

$$= 3.20\ k\ d\ \Delta T \left(\frac{w\,v}{2}\right)^{+0.868} \quad \left(\frac{1}{\alpha}\right)^{+0.868}$$

$$= 3.20\ d\ \left(\frac{w\,v}{2}\right)^{+0.868} \quad \left[\overline{k\left(\frac{1}{\alpha}\right)^{+0.868}_{eff1}}\ \Delta T_1\ +\ \overline{k\left(\frac{1}{\alpha}\right)^{+0.868}_{eff2}}\ \Delta T_2\right] \text{-------------------------------------------------------------------------------(3.15)}$$

$Total\ laser\ power\ =\ useful\ power\ +\ waste\ power$

$$= v\,d\,w\,\left(\overline{\rho c_p}_{eff1}\Delta T_1 + \overline{\rho c_p}_{eff2}\Delta T_2 + \overline{\rho L_h}_{eff}\right)$$

$$+ 3.20\,d\,\left(\frac{w\,v}{2}\right)^{+0.868}\ \left[\overline{k\left(\frac{1}{\alpha}\right)^{+0.868}_{eff1}}\ \Delta T_1\ +\ \overline{k\left(\frac{1}{\alpha}\right)^{+0.868}_{eff2}}\ \Delta T_2\right]$$

---------------------------------------------------------------------------(3.16)

Effective thermal properties can be described as following:

$$\overline{\rho c_p}_{eff} = \phi\,\left(\overline{\rho c_p}_w\,S_w + \overline{\rho c_p}_o\,S_o + \overline{\rho c_p}_g\,S_g\right) + (1\ -\ \phi)\,\overline{\rho c_p}_{rock}$$ -----------(3.17)

$$\overline{\rho L_h}_{eff} = \phi\,\left(\overline{\rho L_v}_w\,S_w + \overline{\rho L_v}_o\,S_o\right) + (1\ -\ \phi)\,\overline{\rho L_h}_{rock}$$ --------------------(3.18)

$$\overline{k\left(\frac{1}{\alpha}\right)^{+0.868}_{eff}}\ =\ \phi\,\left(\overline{k\left(\frac{1}{\alpha}\right)^{+0.868}_{w}}S_w\ +\ \overline{k\left(\frac{1}{\alpha}\right)^{+0.868}_{o}}\ S_o\ +\ \overline{k\left(\frac{1}{\alpha}\right)^{+0.868}_{g}}\ S_g\right)\ +\ (1\ -\ \phi)\ \overline{k\left(\frac{1}{\alpha}\right)^{+0.868}_{rock}}$$

---------------------------------------------------------------------------(3.19)

Where;

$\Delta T_1$ = temperature difference from initial temperature to the temperature of vaporization of the liquid in porous media.

$\Delta T_2$ = temperature difference from temperature of vaporization of the liquid in porous media to the final temperature (rock melting or vaporization).

$\overline{\rho c_p}_{eff1}$ = effective $\rho c_p$ for the system below the temperature of vaporization of the liquid in the porous media.

$\overline{\rho c_p}_{eff2}$ = effective $\rho c_p$ for the system above the temperature of vaporization of the liquid in the porous media.

$\overline{\rho L_h}_{eff}$ = effective $\rho L_h$ for the system.

$\overline{k\left(\frac{1}{\alpha}\right)^{+0.868}}_{eff1}$ = effective $k\left(\frac{1}{\alpha}\right)^{+0.868}$ for the system below the temperature of vaporization of the liquid in the porous media.

$\overline{k\left(\frac{1}{\alpha}\right)^{+0.868}}_{eff2}$ = effective $k\left(\frac{1}{\alpha}\right)^{+0.868}$ for the system above the temperature of vaporization of the liquid in the porous media.

$\phi$ = porosity

$S_{w,} S_{o,} S_g$ = water, oil and gas saturation initially exist in the porous media.

$L_{v_w}$ = water latent heat of vaporization.

$L_{v_o}$ = oil latent heat of vaporization.

$L_{h_r}$ = rock latent heat of fusion (for cutting by melting) or latent heat of fusion + latent heat of vaporization (for cutting by vaporization).

### 3.2.5 Fluid phase changing in porous media

Fluid phase changes in the porous media will be occurred on stages as a function of temperature increases and can be described as following:

Stage-1: $T \le T_{v_o}$ $(T_i \overset{to}{\rightarrow} T_{v_o})$: this stage takes place below the temperature of vaporization of oil (from initial temperature to the temperature of vaporization of oil), assuming that temperature of vaporization of oil is less than that of water. There is no fluid phase changes until temperature of vaporization of oil is reached.

It is assumed that three phases (water, oil and gas) are initially exist in the porous media during this stage.

Stage-2: $T_{v_o} \leq T \leq T_{v_w}$ $(T_{v_o} \overset{to}{\rightarrow} T_{v_w})$: this stage takes place between the temperature of vaporizations of oil and water respectively. When the temperature of vaporization of oil is reached, oil phase will be changed to oil-vapor phase.

Water, oil-vapor and gas will be exist in the porous media during this stage.

Stage-3: $T \geq T_{v_w}$ $(T_{v_w} \overset{to}{\rightarrow} T_{m_r})$: this stage takes place above the temperature of vaporization of water (between the temperature of vaporizations of water and the melting temperature of rock). When the temperature of vaporization of water is reached, water phase will be changed to water-vapor phase.

Water-vapor, oil-vapor and gas will be exist in the porous media during this stage.

Note that water-vapor, oil-vapor and gas are all at gaseous state but it is important to distinguish between them in laser power calculations due to the different thermal properties and fluid compositions of each phase.

### 3.2.6 Phase diagrams and temperature of vaporization

Phase diagram for each liquid phase including water and oil is essential to identify the temperature of vaporization for each phase. These temperatures are required in the laser power calculations in order to accurately represent the phase change in the porous media during temperature rising due to laser interaction.

Also the temperature of vaporization is required in order to determine the latent heat of vaporization. There is indirect relationship between latent heat of vaporization and temperature, as temperature increases the latent heat of vaporization decreases and accordingly the temperature of vaporization is required and can be identify from phase diagram under reservoir pressure.

Figure 3-3 shows the typical water phase diagram where water is boiled at 100°C (at room pressure of 1 bar) and critical point at 374.15 °C (647.3 K) and 221.3 bar (3210 psi). Under downhole condition, reservoir pressure is definitely much higher and the temperature of vaporization for water under downhole condition can be identify from the phase diagram.

Example of how to identify the temperature of vaporization of water under downhole condition is illustrated in the figure using red lines. Assuming reservoir pressure of 100 bar and reservoir temperature of 100 °C, under this downhole condition water is in liquid phase (point-1) and with increasing temperature due to laser interaction, liquid phase will be changed into vapor phase at point-2 (circa 325 °C). Point-2 is vaporization temperature of water under this downhole condition.

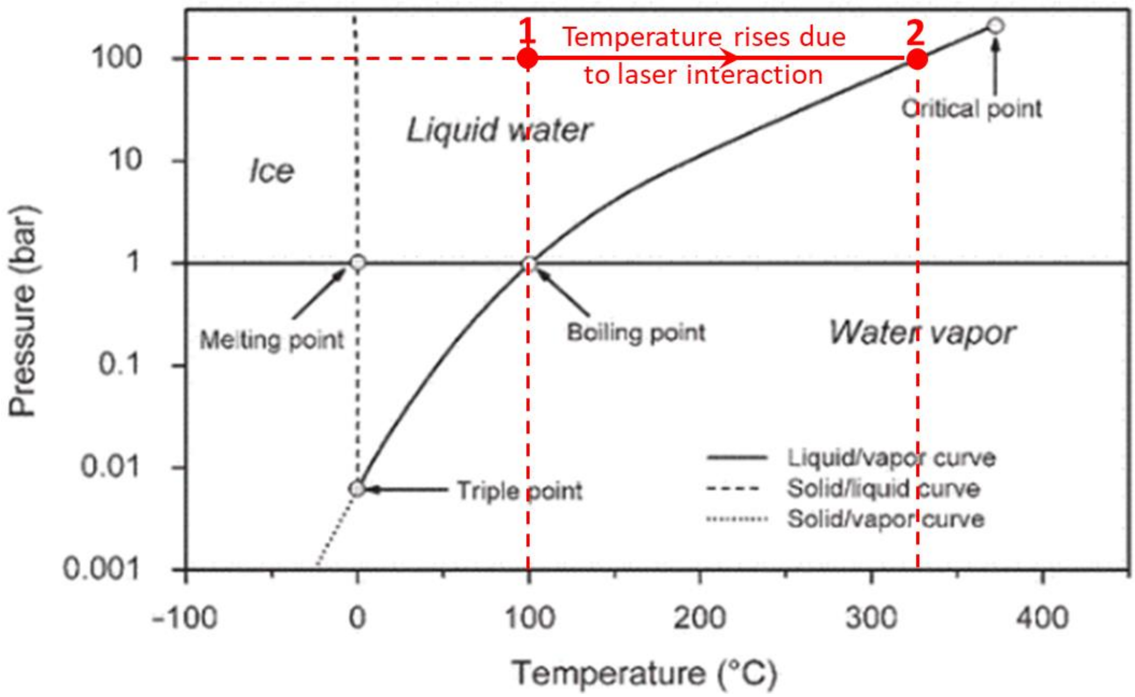


Figure 3-3: Water phase diagram (Worch 2015), modified by red lines to illustrate laser interaction

For reservoirs with pore pressure above the critical pressure of water (above 3210 psi), increasing temperature, due to laser interaction, above the critical temperature (above 374.15 °C) will cause water phase to be changed directly to the supercritical fluid phase. Due to the complexity of identifying the thermal properties of the supercritical fluid, it has been assumed that reservoir pressure is below the critical pressure of the water so the temperature of vaporization at downhole condition can be identify as shown above. If reservoir pressure is above the critical pressure, the thermal properties of supercritical fluid will be assumed as gaseous state properties.

Note that during laser interaction, the fluid is heated up but pressure is constant, even gas expansion during interaction will escape and dissipate into surrounding (open system) and create micro-fractures but wouldn’t cause any increasing in reservoir pressure.

Oil phase diagram is much more complex than water phase diagram because oil consists of multi-component mixture. Figure 3-4 shows the difference between the phase diagram shapes of single (pure) component where vapor-pressure line separates liquid from gas and multi-component mixture where two-phase envelop exists between the complete liquid and gas phases.

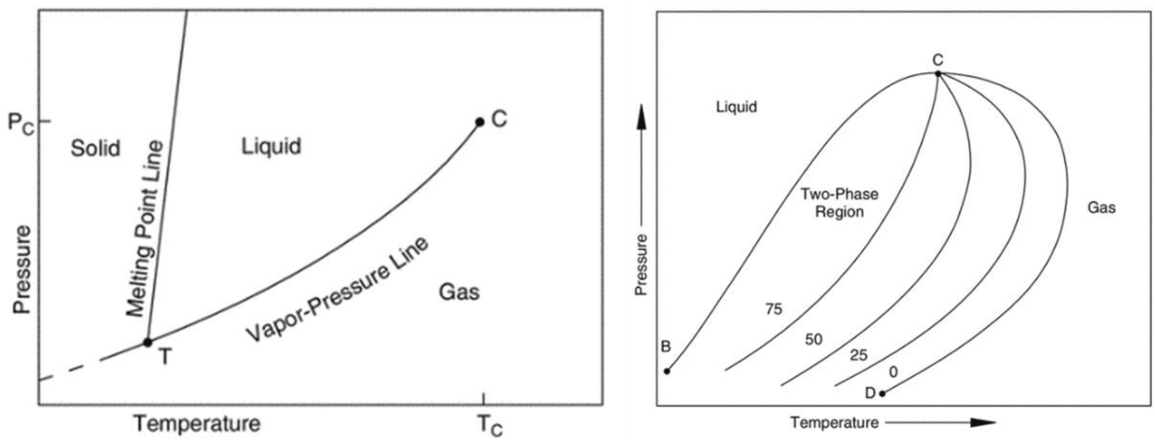


Figure 3-4: Phase diagram for single component on the left, and multi-component mixture on the right (Arnold and Stewart 2008)

Reservoir fluids contain various hydrocarbon mixture including light and heavy components. Phase diagram shape and critical point location depend on reservoir fluid composition as shown in Figure 3-5.

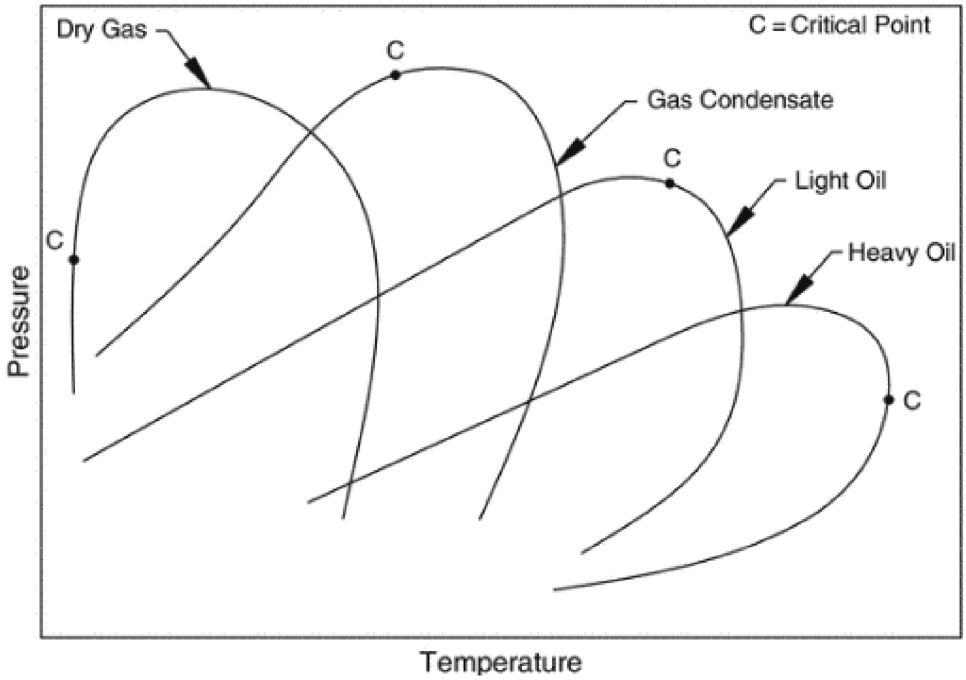


Figure 3-5: Phase diagrams for various reservoir fluids (Arnold and Stewart 2008)

There are five typical reservoir types classified according to fluid compositions including black oil, volatile oil, retrograde gas (also called gas condensate), wet gas and dry gas reservoirs as shown in Figure 3-6.

Black oil reservoir contains more heaver components (C7+) than the light ones. Note that light components increase towards gas reservoir types where they are mainly contain the lightest component (C1 Methane). Table 3-1 shows an example of the typical hydrocarbon fluid compositions of each reservoir type.

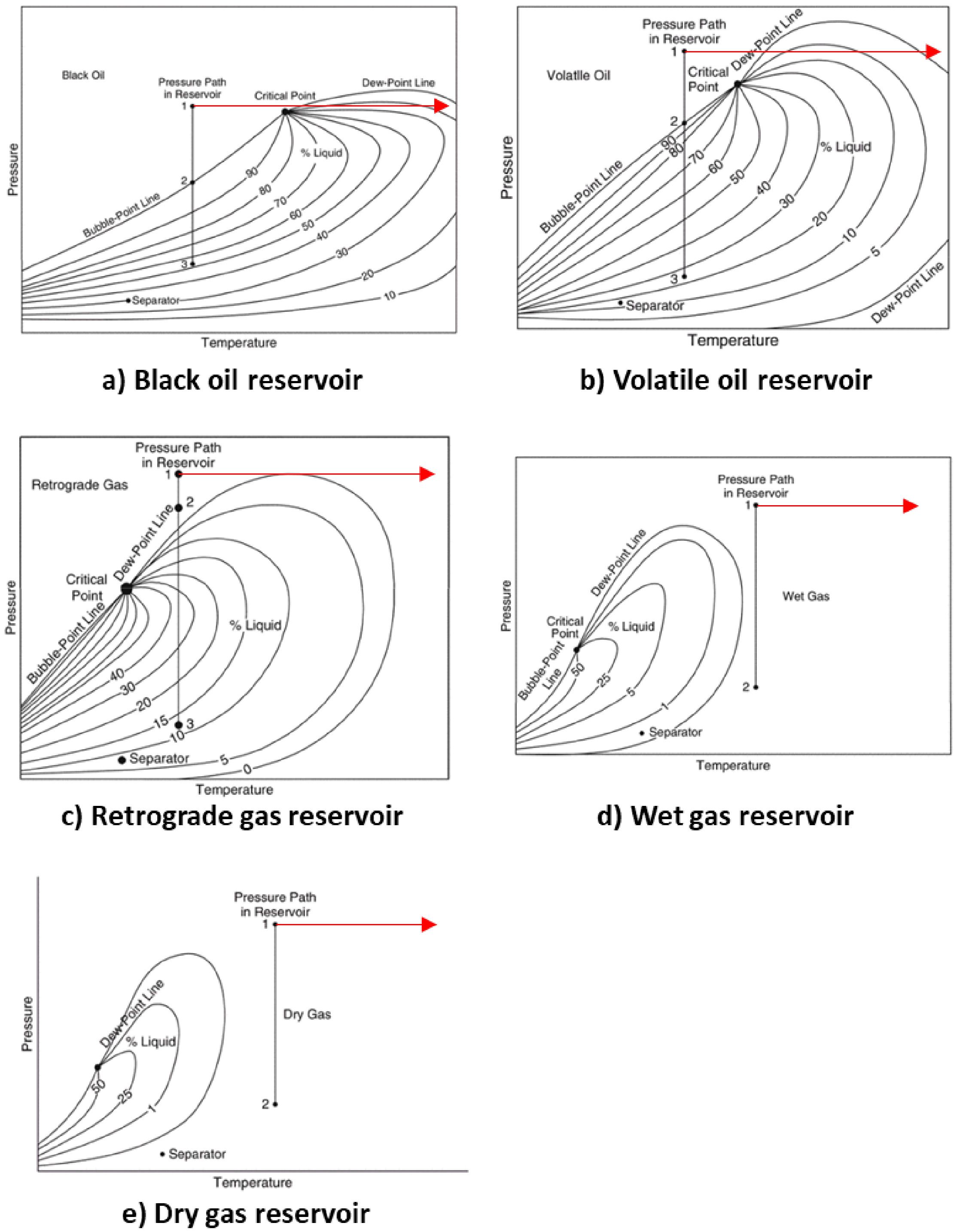


Figure 3-6: Typical reservoir fluid types (Arnold and Stewart 2008), modified by red lines to illustrate laser interaction

Table 3-1: Typical hydrocarbon fluid compositions of various reservoir types, mol% (Jahn, Cook and Graham 1998)

| Reservoir Type | | Black oil | Volatile oil | Gas-Condensate | Wet gas | Dry gas |
|---|---|---|---|---|---|---|
| $C_1$ | Methane | 52.60 | 66.70 | 72.7 | 88.7 | 96.30 |
| $C_2$ | Ethane | 5.00 | 9.00 | 10.0 | 6.0 | 3.00 |
| $C_3$ | Propane | 3.50 | 6.00 | 6.0 | 3.0 | 0.40 |
| $C_4$ | Butanes | 1.80 | 3.30 | 2.5 | 1.3 | 0.17 |
| $C_5$ | Pentanes | 0.80 | 2.00 | 1.8 | 0.6 | 0.04 |
| $C_6$ | Hexanes | 0.90 | 2.00 | 2.0 | 0.2 | 0.02 |
| $C_{7+}$ | Heptanes | 27.90 | 11.00 | 5.0 | 0.2 | 0.00 |

The aim of this section is not to provide detailed descriptions for reservoir fluid types but to shed some lights into the change of reservoir fluid phases during increasing temperature due to laser interaction. The vertical lines shown in the figure represent the isothermal reduction of reservoir pressure during production from initial condition (point-1) to reservoir abandonment pressure (point-3) which is important to identify fluid phase changes inside reservoir due to pressure depletion.

As shown, the location of the initial reservoir condition (point-1) relative to the critical point is important to identify the fluid phase at initial condition as well as at higher temperatures. The initial condition of black oil (a) and volatile oil (b) reservoirs is liquid phase and if reservoir pressure is higher enough than the critical point, liquid phase can be completely changed into gas phase once the critical temperature is exceeded. The initial condition of retrograde (c), wet (d) and dry (e) gas reservoirs is gas phase and will not be changed during heating up by laser.

For reservoirs already on production prior to laser processing, reservoir pressure might be depleted and located inside the two phase envelop and in this case the concentration of each phase (oil and gas) must be identified in order to accurately calculate the laser power requirement. It is very complex to accurately determine the concentration of each phase inside the two phase envelop because sometimes gas segregate into the top of reservoir and create secondary gas-cap while oil segregate into the bottom by gravity, if fluid segregation time permitted.

Knowledge of oil phase diagram is very important in order to identify the fluid phase (liquid or gas) exists in the porous media, the critical point and the temperature of vaporization under downhole condition. This information is essential in laser power calculations.

### 3.2.7 Latent heat of vaporization

There is indirect relationship between temperature of vaporization and latent heat of vaporization. As temperature of vaporization increases towards the critical point, the latent heat of vaporization decreases. In other words, if the temperature is high and close to the critical point, less energy will be required to change the liquid phase into gas phase than the energy required at lower temperature.

Modified Watson equation can be used to calculate the latent heat of vaporization as a function of temperature (Coker 2007):

$$L_v = A\left(1 - \frac{T}{T_c}\right)^n \quad \text{--------------------------------------------------(3.20)}$$

Where;

$L_v$ = Latent heat of vaporization, kJ/mol

$A \; and \; n$ = Regression coefficients

$T_c$ = Critical temperature, K

$T$ = Temperature, K

Table 3-2 shows the data required to calculate the latent heat of vaporization as function of temperature for some relevant fluids. $T_{min}$ and $T_{max}$ are the minimum and maximum temperature where the above correlation is applicable within this range. Minimum and maximum temperatures correspond to the melting (freezing) and critical points respectively.

Table 3-2: Regression coefficients for latent heat of vaporization (Coker 2007)

| Substance | Formula | A | $T_c$ | n | $T_{min}$, K | $T_{max}$, K |
|---|---|---|---|---|---|---|
| n-Pentane | ($C_5$) C5H12 | 39.854 | 469.65 | 0.398 | 143.42 | 469.65 |
| n-Heptane | ($C_7$) C7H16 | 49.730 | 540.26 | 0.386 | 182.56 | 540.26 |
| n-Decane | ($C_{10}$) C10H22 | 71.428 | 618.45 | 0.451 | 243.49 | 618.45 |
| Water | H2O | 52.053 | 647.13 | 0.321 | 273.16 | 647.13 |

The above correlation is used in this research to calculate the latent heat of vaporization for $C_5$, $C_7$, $C_{10}$ and water. The results are shown in Figure 3-7.

$C_5$, $C_7$ and $C_{10}$ are selected in order to compare between the latent heat of vaporization for various hydrocarbon compositions, as shown heaver hydrocarbon ($C_{10}$) requires higher latent heat of vaporization than the relatively lighter hydrocarbon ($C_5$). Also note that latent heat of vaporization for all fluids decreases with increasing temperature and drops to zero at critical temperature.

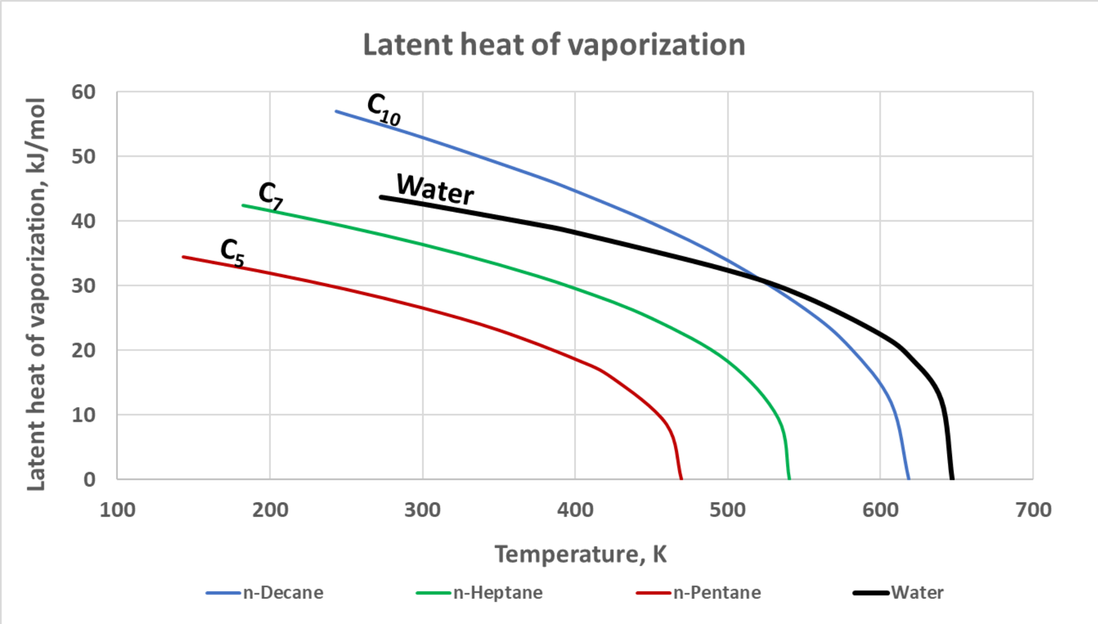


Figure 3-7: Latent heat of vaporization for water and various hydrocarbon compounds as a function of temperature

It is important to identify the temperature of vaporization for water and oil from phase diagrams as shown in the previous section, then to use those temperatures to calculate the latent heat of vaporization as shown above.

$C_7$ will be assumed as an average composition for black oil and will be used in the laser power calculations.

### 3.2.8 The effect of temperature and pressure on thermal properties

The previous section shows that latent heat changes with temperature, also other thermal properties including thermal conductivity and heat capacity change with temperature. Coker (2007) described some experimental correlations which were developed to calculate the change in thermal properties as a function of temperature. Summary of the correlations and regression coefficients are presented in Appendix-1.

It is observed that heat capacity of gas and liquid increases with increasing temperature, also thermal conductivity of low pressure gas increases with increasing temperature. Thermal conductivity of liquid and solids is generally much higher than gases. However, thermal conductivity of liquid and solids decreases with increasing temperature.

The change in the thermal properties of solids, the dominating material in heat transfer into surrounding during laser cutting, is not significant and accordingly changes of rock thermal properties with temperature has been ignored for simplicity.

The effect of pressure was not considered on the experimental correlations presented by Coker. The correlations developed for liquid are valid for temperatures up to approximately the critical temperature of each liquid compound which means they are valid for pressures up to the critical pressure of each compound, also pressure has to be above the pressure-vapor line in order to keep the compounds in liquid states (for example above 3,200 psi for water at critical temperature). This means that the effect of pressure is implicitly included, to some extent, in the experimental correlations for liquid states.

The experimental correlations for gas are different than liquid. Gas compounds must exist at low pressure (below the pressure-vapor line) in order to keep the compounds in gaseous states and accordingly the effect of pressure is not considered in these gas experimental correlations.

Generally, the effect of pressure on the physical and thermal properties of liquids are expected to be minimal compared to gases.

## 3.3 Numerical solution

### 3.3.1 Partial Differential Equation

Unsteady-state (transient) conduction heat transfer in cylindrical and axial coordinates can be described by the following partial differential equation (Bennett and Myers 1983):

$$\frac{\partial T}{\partial t} = \alpha \left( \frac{\partial^2 T}{\partial r^2} + \frac{1}{r} \frac{\partial T}{\partial r} + \frac{\partial^2 T}{\partial x^2} \right) \text{------------------------------------}(3.21)$$

Where $T$ is temperature in Kelvin, $t$ is time in second, $r$ is radius in cylindrical coordinates in meter, $x$ is distance in axial coordinates in meter and $\alpha$ is thermal diffusively in $m^2/sec$ and equal $k/\rho\, c_p$ where $k$ is thermal conductivity in $W/m\ K$ , $\rho$ is density in $kg/m^3$ and $c_p$ is specific heat capacity at constant pressure in $J/kg\ K$.

It is assumed that there is no variation on temperature with angular position and accordingly the angular term, $\frac{1}{r^2}\frac{\partial^2 T}{\partial \theta^2}$, is already omitted from the above equation.

### 3.3.2 Latent heat and melting fraction

In order to model the effect of melting progression of the rock on heat transfer into surrounding during laser interaction, a modification is made to the partial differential equation by adding melt fraction and latent heat of melting as proposed by Hossain, Acar and Malalasekera (2005).

Hossain, Acar and Malalasekera described the transient heat transfer and melting process of nonwoven fibers by adding latent heat of fusion $L_f$ (J/kg) and liquid (melt) fraction $\gamma$ (dimensionless) into the energy equation where $\gamma$ is a function of temperature as following:

$$\gamma = \begin{cases} 1 & if\ T > T_m + \Delta T\ (complete\ liquid\ state) \\ 0 & if\ T < T_m - \Delta T\ (complete\ solid\ state) \\ \frac{T - T_m + \Delta T}{2\Delta T} & if\ T_m - \Delta T < T < T_m + \Delta T\ (phase\ changing\ 0 < \gamma < 1) \end{cases}$$ ----

-------------------------------------------------------------------------(3.22)

Where $T$ is the mean temperature in Kelvin, $T_m$ is melting temperature in Kelvin and $\Delta T$ is a small temperature interval around the melting temperature as solid and liquid may exist simultaneously in a volume element if temperature is within a small interval $2\Delta T$ around the melting temperature as shown in Figure 3-8.

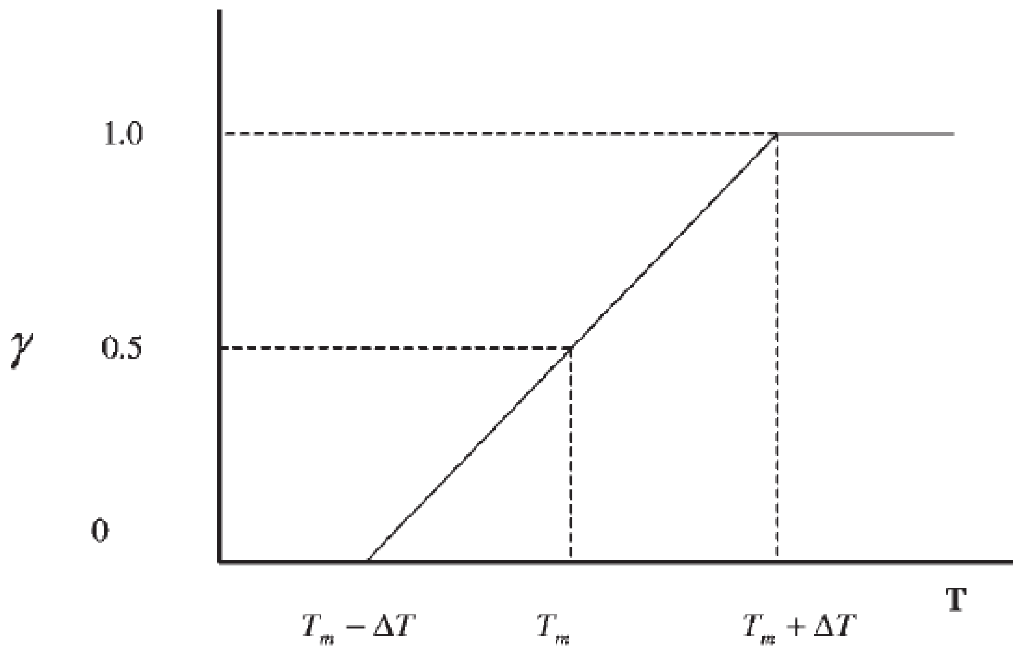


Figure 3-8: Variation of melt fraction with temperature (Hossain, Acar and Malalasekera 2005)

The modified partial differential equation after adding the latent heat of fusion and melt fraction (will be defined here as $\gamma_m$) is shown below:

$$\frac{\partial T}{\partial t} = \alpha \left( \frac{\partial^2 T}{\partial r^2} + \frac{1}{r} \frac{\partial T}{\partial r} + \frac{\partial^2 T}{\partial x^2} \right) - \frac{L_f}{c_{p_r}} \frac{\partial \gamma_m}{\partial t} \text{------------------------(3.23)}$$

Where $L_f$ is latent heat of fusion, $c_{p_r}$ is specific heat capacity at constant pressure for the rock and $\gamma_m$ is melt fraction. For simplicity, same thermal properties will be assumed for both solid and melt states of the rock.

### 3.3.3 Porosity and fluid saturation

Porosity and fluid saturation exist in porous media have been incorporated into the partial differential equation by considering effective thermal diffusivity and also modeling the vaporization progression for the liquid exists in porous media using the same concept of melting fraction described above.

The modified partial differential equation after adding porosity and fluid saturation can be written as following:

$$\frac{\partial T}{\partial t} = \alpha_{eff} \left( \frac{\partial^2 T}{\partial r^2} + \frac{1}{r} \frac{\partial T}{\partial r} + \frac{\partial^2 T}{\partial x^2} \right) - (1-\phi) \frac{L_f}{c_{p_r}} \frac{\partial \gamma_m}{\partial t} - \phi \frac{L_v}{c_{p_l}} \frac{\partial \gamma_v}{\partial t} \text{-(3.24)}$$

Where;

$\alpha_{eff}$ is effective thermal diffusivity.

$$\alpha_{eff} = \phi\left(\alpha_w S_w + \alpha_o S_o + \alpha_g S_g\right) + (1 - \phi)\, \alpha_{rock} \text{-----------------------(3.25)}$$

$\phi$ is porosity, $S$ is fluid saturation in porous media and subscripts $w, o\ and\ g$ refer to water, oil and gas respectively.

$L_f$ and $c_{p_r}$ are latent heat of fusion and specific heat capacity of the rock.

$L_v$ and $c_{p_l}$ are latent heat of vaporization and specific heat capacity of the liquid exists in porous media.

$\gamma_m$ is melting fraction of the rock

$\gamma_v$ is vaporization fraction of the liquid exists in porous media

Note that the term $(1-\phi)\frac{L_f}{c_{p_r}}\ \frac{\partial \gamma_m}{\partial t}$ represents the melting progression of the rock and the term $\phi\ \frac{L_v}{c_{p_l}}\ \frac{\partial \gamma_v}{\partial t}$ represents the vaporization progression of the liquid exists in porous media.

### 3.3.4 Finite difference solution

Figure 3-9 shows a schematic of laser interacts with one rock element in cylindrical coordinates where finite difference method can be used to solve the partial differential equation and model the unsteady-state heat transfer into surrounding in both radial and axial directions during laser interaction with porous media. $i\ and\ j$ are the spatial grid system in radial and axial coordinates respectively.

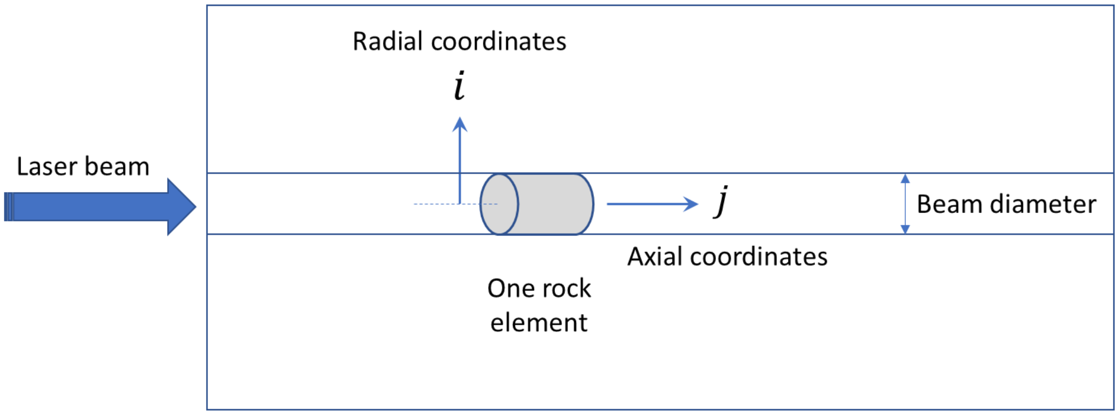


Figure 3-9: Schematic shows heat transfer coordinate systems

Figure 3-10 shows cross-sections of the cylindrical element (heat source) and describes the explicit finite difference solution for radial heat transfer into surrounding in cylindrical coordinates where $T$ at time level $n+1$ can be calculated using the values of the previous time level $n$.

$T_i^{n+1}$ can be calculated at all time levels as long as the initial and boundary conditions are known. Note that $i$ represents the spatial radial grid system, $\Delta t$ is time step and $\Delta r$ is spatial step in radial coordinates.

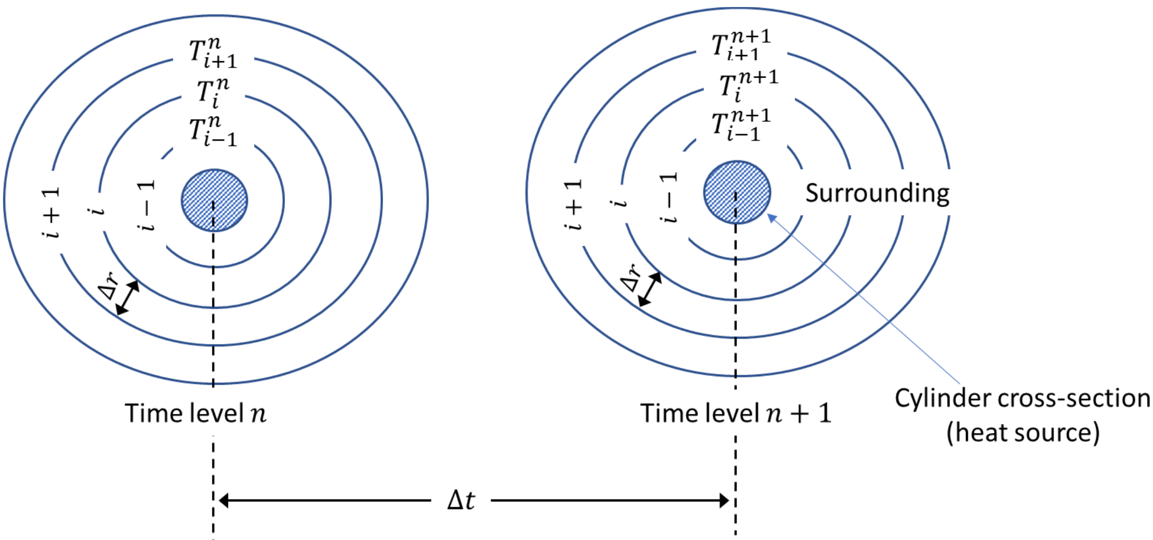


Figure 3-10: Radial heat transfer into surrounding (cross-section perpendicular to laser beam)

Figure 3-11 shows cross-sections in the direction of laser cutting and describes the explicit finite difference solution for axial heat transfer into surrounding in the same direction of the laser beam. Note that $j$ represents the spatial grid system in $x$ direction, $\Delta t$ is time step and $\Delta x$ is spatial step in axial coordinates.

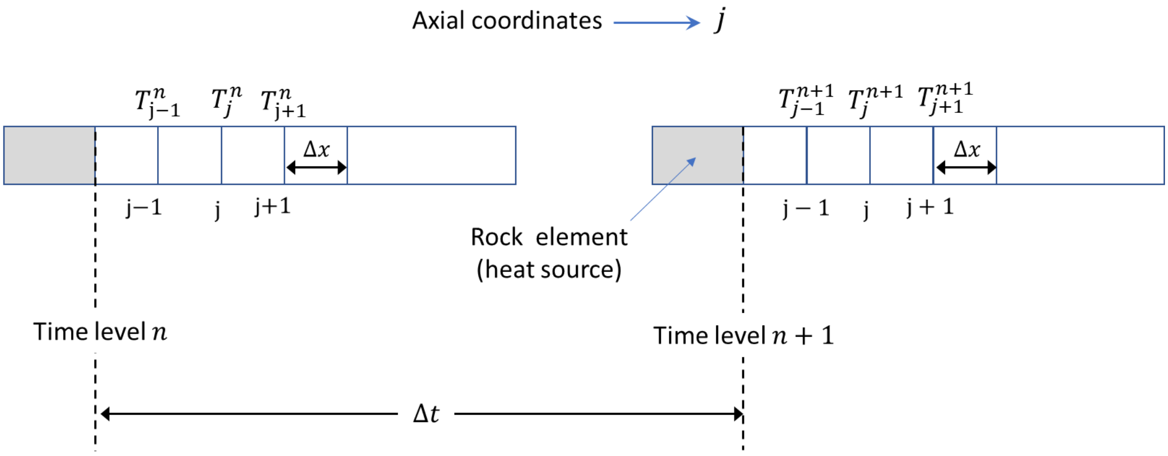


Figure 3-11: Axial heat transfer into surrounding (cross-section in the direction of laser cutting)

Finite difference solution for each derivative is shown below:

The 1st time derivative in both radial and axial coordinates:

$$\left[\frac{\partial T}{\partial t}\right]_{i,j} = \frac{T^{n+1}_{i,j} - T^n_{i,j}}{\Delta t} \text{ ------------------------------------------------------(3.26)}$$

The 2nd spatial derivative in radial coordinates:

$$\left[\frac{\partial^2 T}{\partial r^2}\right]_{i} = \frac{T^n_{i+1} + T^n_{i-1} - 2T^n_i}{\Delta r^2} \text{ -------------------------------------------------(3.27)}$$

The 1st spatial derivative in radial coordinates:

$$\left[\frac{\partial T}{\partial r}\right]_i = \frac{T_i^{n+1} - T_i^n}{\Delta r} \quad \text{-----(3.28)}$$

The 2nd spatial derivative in axial coordinates:

$$\left[\frac{\partial^2 T}{\partial x^2}\right]_j = \frac{T_{j+1}^n + T_{j-1}^n - 2T_j^n}{\Delta x^2} \quad \text{-----(3.29)}$$

The 1st time derivative, for $\gamma_m \; and \; \gamma_v$ fractions, in both coordinates:

$$\left[\frac{\partial \gamma}{\partial t}\right]_{i,j} = \frac{\gamma_{i,j}^{n+1} - \gamma_{i,j}^n}{\Delta t} \quad \text{-----(3.30)}$$

After substituting the derivatives in the partial differential equation by the above finite difference solution and rearranging the equation to keep $T_{i,j}^{n+1}$ in one side, the equation can be written as following:

$$T_{i,j}^{n+1} = \left[\begin{array}{c} \frac{\alpha_{eff}\,\Delta t}{\Delta r^2}\left(T_{i+1,j}^n + T_{i-1,j}^n\right) + \frac{\alpha_{eff}\,\Delta t}{\Delta x^2}\left(T_{i,j+1}^n + T_{i,j-1}^n\right) \\ + T_{i,j}^n\left(1 - \frac{2\,\alpha_{eff}\,\Delta t}{\Delta r^2} - \frac{\alpha_{eff}\,\Delta t}{r\Delta r} - \frac{2\,\alpha_{eff}\,\Delta t}{\Delta x^2}\right) \\ -(1-\phi)\frac{L_f}{c_{p_r}}\left(\gamma_{m}{}_{i,j}^{n+1} - \gamma_{m}{}_{i,j}^{n}\right) - \phi\,\frac{L_v}{c_{p_l}}\left(\gamma_{v}{}_{i,j}^{n+1} - \gamma_{v}{}_{i,j}^{n}\right) \end{array}\right] \Bigg/ 1 - \frac{\alpha_{eff}\,\Delta t}{r\Delta r} \quad \text{-----(3.31)}$$

This is the final equation to calculate rock melting progression and heat transfer into surrounding during laser interaction process.

### 3.3.5 Initial and boundary conditions

Initial condition of the grid system in radial and axial coordinates is straightforward as it simply represents the initial temperature of the system prior to laser interaction with material. Initial reservoir temperature is used as initial condition when modelling laser interaction with rock under downhole condition while ambient temperature is used when modelling laser material processing at surface (standard condition).

The boundary condition of the heating source generated by laser due to interaction with material is a complex matter and can be predicted and modelled in different ways based on material thickness and cutting method (melting or vaporization). Boundary condition is a dynamic source of heat during laser interaction and can be considered as one of key parameter, and also source of uncertainty, in modelling heat transfer into surrounding (waste energy) during laser material processing.

Two potential boundary conditions have been considered in this research and can be described as following:

1. Line source boundary condition; where source of heat is considered as a moving line, expanding with melting progression. In other words, during melting any element, laser beam will always be in contact with the internal wall of the hole (kerf circumference) for the elements which already melted and cleaned, so laser beam will be considered as a moving line (heating source) during melting progression.

2. Point source boundary condition; where source of heat is considered as only the point of interaction with material at laser beam tip while laser beam is not in contact with the hole already melted, so heating source is like a moving point during melting progression.

## 3.4 Summary

The following is a brief summary of the analytical solution:

1. The energy balance equation proposed by Powell et al. (1994) and the waste power correlation proposed by Prusa, Venkitachalam and Molian (1999) have been used to develop an analytical model for laser power calculations in this research.

2. Porosity and fluid saturation exist in porous media have been incorporated into the analytical model using effective thermal property concept.

3. Fluid phase changes in porous media during laser interaction has been discussed.

4. A methodology to identify the temperature of vaporization for water and oil, under downhole condition during laser interaction with porous media, using phase diagrams, has been developed and discussed.

5. Changing of latent heat of vaporization, for water and oil, with temperature of vaporization has been calculated and discussed.

6. The effect of temperature and pressure on thermal properties during laser interaction has been discussed.

7. Cutting by vaporization is suggested in order to avoid the complex kerf cleaning under downhole condition.

The following is a brief summary of the numerical solution:

1. Partial differential equation for transient heat transfer in cylindrical and axial coordinates has been used to numerically calculate the waste energy during laser cutting. The equation is solved using finite difference solution.

2. Porosity and fluid saturations have been incorporated into the models using effective thermal properties (volumetric average).

3. Melting fraction concept is considered to represent the melting progression of the rock during heat transfer.

4. In similar manner, vaporization fraction is considered to represent the vaporization progression of the liquid exists in porous media during heat transfer.

5. One of the key parameters, and also source of uncertainty, in modeling heat transfer is boundary condition. Boundary condition represents the dynamic source of heat during laser interaction. Two scenarios including line-source and point-source boundary conditions have been suggested and considered in this research in order to identify the optimum scenario for various laser processing parameters including cutting by melting and vaporization techniques.

# Chapter 4: Modelling results and discussion

Laser power modelling has been conducted for various rock types including the main hydrocarbon bearing formations (sandstone and limestone) with sensitivity analyses for rock porosity, fluid type and saturations exist in the porous media including water, oil and gas. The results are discussed in this chapter.

## 4.1 Thermal properties used in laser power modelling

Ideally, physical and thermal properties of liquids and gases exist in porous media to be cut by laser should be accurately measured at reservoir pressure and various temperatures starting from reservoir temperature (initial condition) up to rock melting temperature in order to represent the change in liquid and gas properties during laser interaction with rock. This laboratory work might be expensive and time consuming and accordingly some approximations and assumptions can be considered.

The change of solid's thermal properties with temperature is not significant and it will be ignored for simplicity. Thermal properties measured at standard condition and shown in Table 4-1 are used in the laser power modelling in this research.

Table 4-1: Thermal properties of liquids and gases at standard condition (ASHRAE 2017)

| Substance | Specific heat capacity at constant pressure, (J / kg. K) | Thermal conductivity, (W / m . K) | Latent heat of vaporization ($L_v$), kJ/kg |
|---|---|---|---|
| Water (liquid) | 4180 | 0.602 | 2257 |
| Petroleum (liquid) | 2000 – 3000 (Average 2500) | 0.15 (n-Decane C10) | 230 – 384 (Average 307) |
| Methane gas (C1) | 2180 | 0.031 | -- |
| Water vapor | 2050 | 0.0247 | -- |

Also the following data and conditions are assumed in laser power modelling:

1. Average densities of gas, oil and water under reservoir pressure are 150, 800 and 1000 kg/m3 respectively.

2. Temperature of vaporization is 500 K for both oil and water which is below the critical temperatures of both liquids (Tc is 647.3 K for water and 618.5 for C10). The exact values can be identified from phase diagrams as described in the phase diagram section.

3. All gaseous states including water-vapor, oil-vapor and gas will be represented by average thermal properties (2115 J/kg.K specific heat and 0.028 W/m.K thermal conductivity). However, it is recommended to accurately measure the thermal properties of each phase under reservoir pressure and temperature.

4. Initial reservoir temperature is 100°C (373 K)

Table 4-2 shows the thermal properties of sandstone and limestone rocks used in laser power modelling in this research.

Table 4-2: Thermal properties of sandstone and limestone rocks (Fuchs 1996)

| Substance | Specific heat capacity at constant pressure, (J / kg . K) | Thermal conductivity, (W / m . K) | Density, (kg/m$^3$) |
|---|---|---|---|
| Sandstone (at 40 C) | 710 | 1.83 | 2200 |
| Limestone (at 100 – 300 C) | 900 | 1.30 | 2500 |

Table 4-3 shows the melting and vaporization temperatures and the latent heat of fusion and vaporization for sandstone and limestone rocks.

Table 4-3: Latent heats for sandstone and limestone rocks (Khan and Islam 2007)

| Rock type | Temperature of melting ($T_m$), °C | Temperature of vaporization ($T_v$), °C | Latent heat of fusion ($L_f$), J/kg | Latent heat of vaporization ($L_v$), J/kg |
|---|---|---|---|---|
| Sandstone | 1540 (1813 K) | 2200 (2473 K) | 2 x $10^6$ | 13.6 x $10^6$ |
| Limestone | 1260 (1533 K) | 2000 (2273 K) | 1.8 x $10^6$ | 12 x $10^6$ |

## 4.2 Analytical model results

### 4.2.1 Peclet number and temperature of vaporization

Peclet numbers are different at each stage (below and above the temperature of vaporization of the liquid exist in the porous media) due to the different effective thermal properties of each stage. Peclet number for the stage below the temperature of vaporization is higher than the Peclet number above because heat capacity and density of liquid are much higher than that of gas.

However, the overall process is dominated by the stage above the temperature of vaporization because this stage is longer and requires much more power compared to the stage below the temperature of vaporization. For example, according to the assumptions made in this calculations, stage-1 represents the power required to rise the temperature by only 127 K (from the initial temperature of 373 K to fluid temperature of vaporization of 500 K) while stage-2 represents the power required to rise the temperature by 1313 K (from fluid temperature of vaporization of 500 K to sandstone melting temperature of 1813 K). The average Peclet number of the two stages (based on the temperature ratio of each stage) is very close to the Peclet number of the dominated stage above the temperature of vaporization (stage-2).

The Peclet numbers reported in this section represent the stage above the temperature of vaporization of the liquid exists in the porous media.

### 4.2.2 Kerf width and cutting speed relationship

There is indirect relationship between kerf width and cutting speed for each Peclet number. Figure 4-1 shows the results of Peclet number calculations as a function of cutting speed and kerf width for sandstone rock, 20% porosity and 100% water saturation.

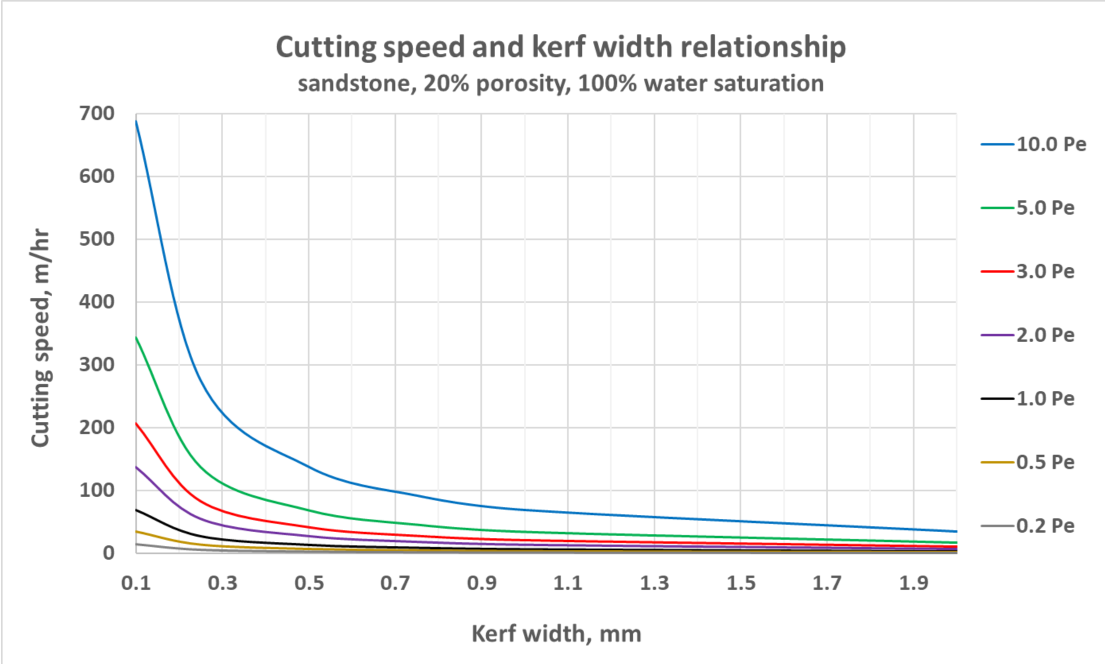


Figure 4-1: Cutting speed and kerf width relationship (sandstone, 20% porosity, 100% water saturation)

This result is in line with Yilbas, Shaukat and Ashraf (2017) study, where kerf width size variation due to laser power and cutting speed was examined and the results showed that increasing laser power or reducing cutting speed results in increasing the kerf width size.

Table 4-4 shows the combination of kerf width and cutting speed that represent each Peclet number. A practical range of kerf width is assumed, then the equivalent cutting speed for each Peclet number is calculated.

Each Peclet number can represent numerous combinations of kerf width and cutting speed, however the product of kerf width x cutting speed is always constant for each Peclet number.

Table 4-4: Cutting speed and kerf width for each Peclet number (sandstone, 20% porosity and 100% water saturation)

| kerf width, mm | Cutting speed, m/hr | | | | | | |
|---|---|---|---|---|---|---|---|
| | 0.2 Pe | 0.5 Pe | 1.0 Pe | 2.0 Pe | 3.0 Pe | 5.0 Pe | 10.0 Pe |
| 0.10 | 13.8 | 34.4 | 68.8 | 137.5 | 206.3 | 343.8 | 687.5 |
| 0.25 | 5.5 | 13.8 | 27.5 | 55.0 | 82.5 | 137.5 | 275.0 |
| 0.50 | 2.8 | 6.9 | 13.8 | 27.5 | 41.3 | 68.8 | 137.5 |
| 0.75 | 1.8 | 4.6 | 9.2 | 18.3 | 27.5 | 45.8 | 91.7 |
| 1.00 | 1.4 | 3.4 | 6.9 | 13.8 | 20.6 | 34.4 | 68.8 |
| 2.00 | 0.7 | 1.7 | 3.4 | 6.9 | 10.3 | 17.2 | 34.4 |

### 4.2.3 Peclet number and laser power

There is a particular power required to cut a particular material thickness for each Peclet number. High laser power would be required for high Peclet number (high cutting speed or kerf width). Figure 4-2 shows an example of cutting sandstone by melting, 20% porosity and 100 water saturation. As shown, higher laser power would be required to cut the same material thickness with higher Peclet number.

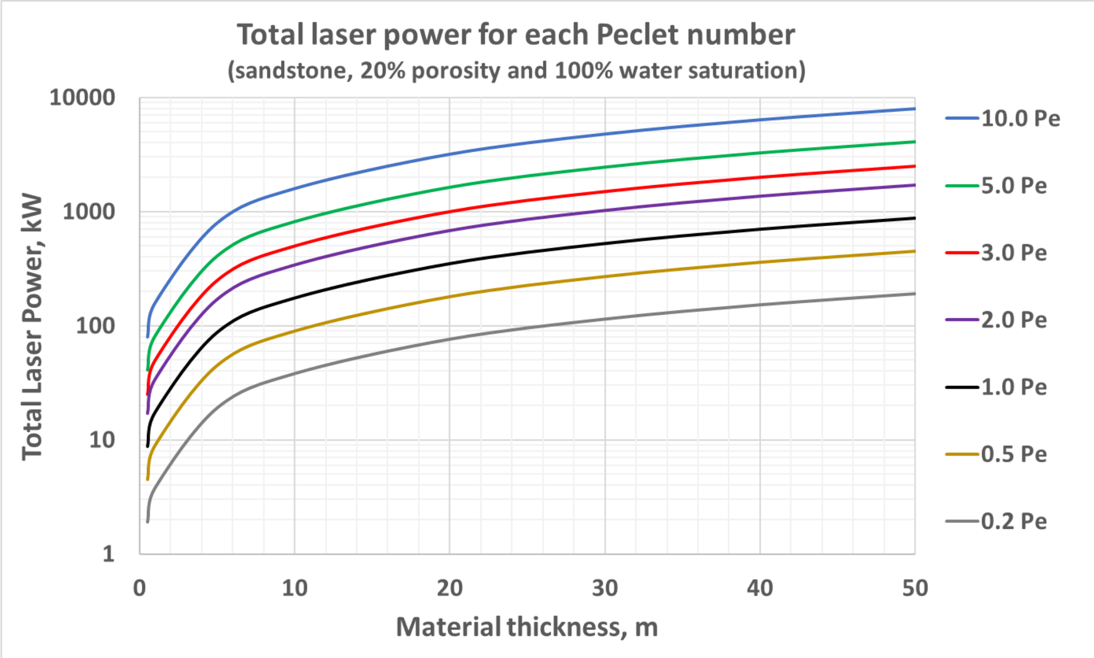


Figure 4-2: Total laser power and Peclet number (sandstone, 20% porosity, 100% water saturation)

### 4.2.4 Cutting by melting - sandstone

Laser power required to cut various thickness of sandstone rock was calculated considering various porosity and fluid saturation. The main observation is that total laser power required to cut particular thickness decreases with increasing porosity due to the fact that the volume of the rock to be melted (or vaporized) decreases with increasing porosity and accordingly the useful power decreases.

Also waste power decreases with increasing porosity because the thermal conductivity of fluids is much lower than that of rock and accordingly the heat transfer into surrounding decreases with increasing porosity.

Figure 4-3, Figure 4-4 and Figure 4-5 show porosity sensitivity analysis for sandstone, cutting by melting, 100% water saturation and 0.2 Peclet number (1.0 mm kerf width with 1.0 m/hr cutting speed) for total, useful and waste laser power respectively. As shown, the total laser power (including useful and waste powers) decreases with increasing porosity and this finding was also observed for any Peclet number and any fluid type exists in the porous media.

It is worth mentioning that zero porosity has been considered in all sensitivity analyses conducted in this research because the developed models may also be used for non-porous materials such as metals.

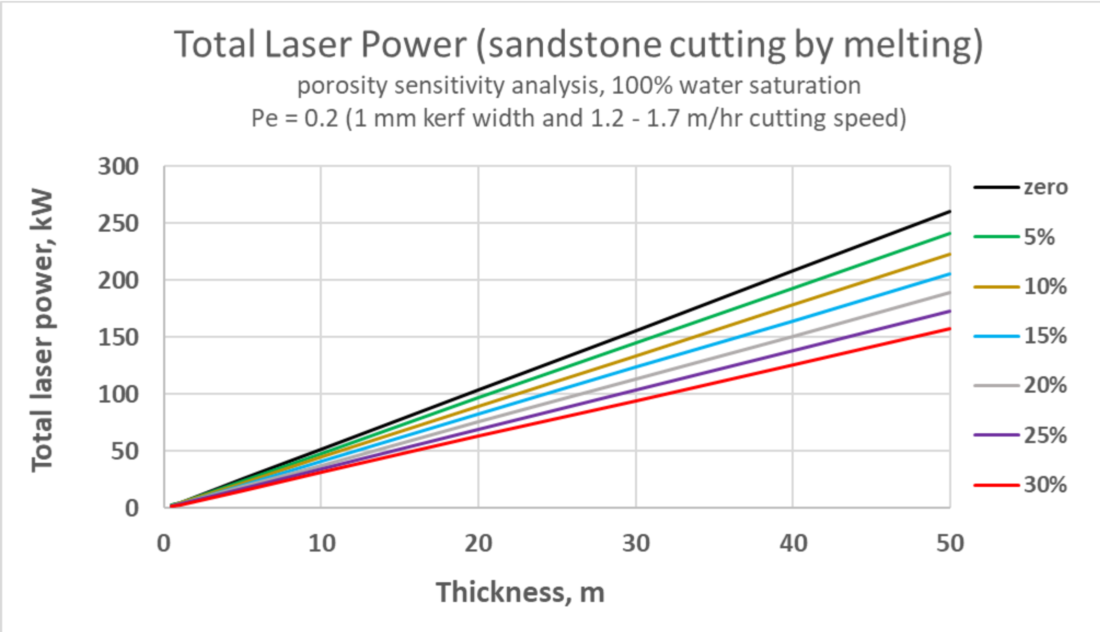


Figure 4-3: Total laser power with porosity sensitivity analysis for sandstone, cutting by melting, 100% water saturation, 0.2 Peclet number

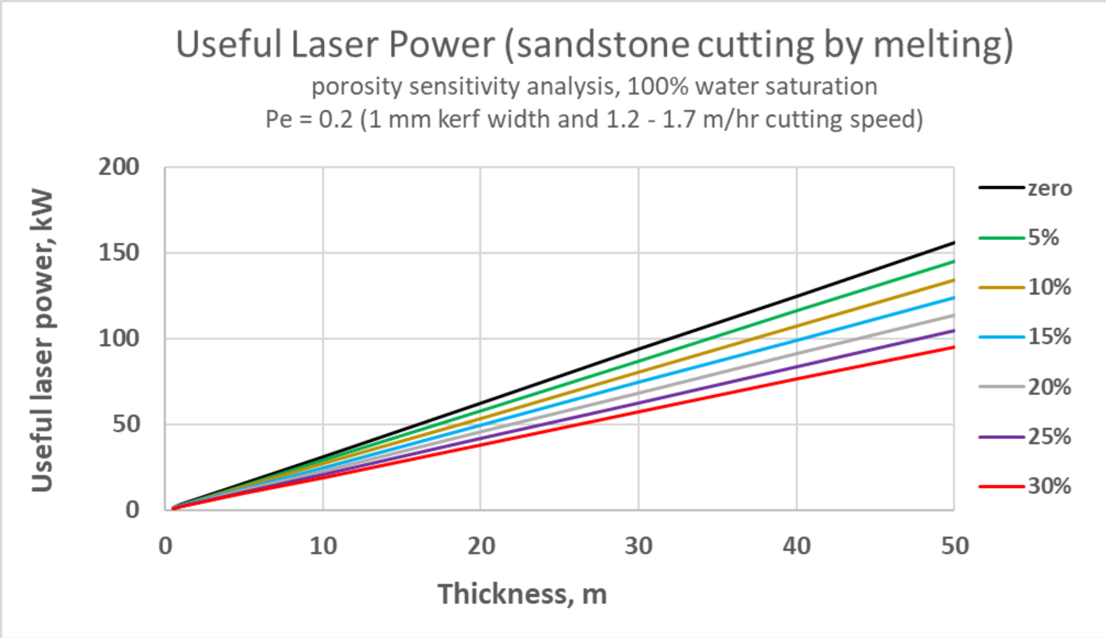


Figure 4-4: Useful laser power with porosity sensitivity analysis for sandstone, cutting by melting, 100% water saturation, 0.2 Peclet number


Figure 4-5: Waste laser power with porosity sensitivity analysis for sandstone, cutting by melting, 100% water saturation, 0.2 Peclet number

It is also observed that for any particular porosity, the waste power ratio (waste power / total power) decreases with increasing Peclet number due to the fact that higher Peclet number is associated with higher cutting speed and accordingly less heat transfer (waste energy) into surrounding and also due to the significant increase in useful power. This finding is also observed for any fluid type exists in the porous media. Figure 4-6 shows the waste power ratio for cutting sandstone by melting, 20% porosity and 100% water saturation.

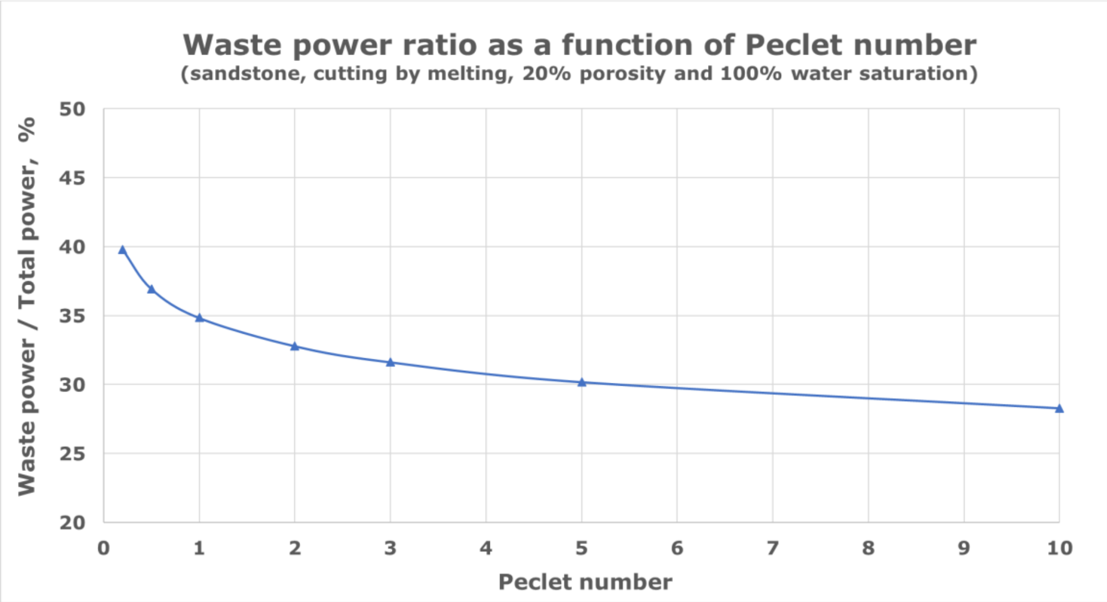


Figure 4-6: Waste power ratio (sandstone, cutting by melting, 20% porosity and 100% water saturation)

Figure 4-7 shows the effect of various fluid types on the total laser power required to cut a fixed rock thickness of 5 meters at 0.2 Peclet number (sandstone, cutting by melting). As shown, water require more power compared to oil and gas and this is mainly due to the high latent heat of vaporization for water, while oil and gas are close to each other because the latent heat of vaporization for oil is low. This finding is similar for any Peclet number and any rock thickness.

The analysis indicated that the main property which can cause difference between various fluid types is the latent heat of vaporization while the effect of other thermal properties including heat capacity, thermal conductivity and density of fluids can cause minor difference in laser power requirement. However, the analysis showed that water is always the highest power under all cutting conditions followed by oil then gas.

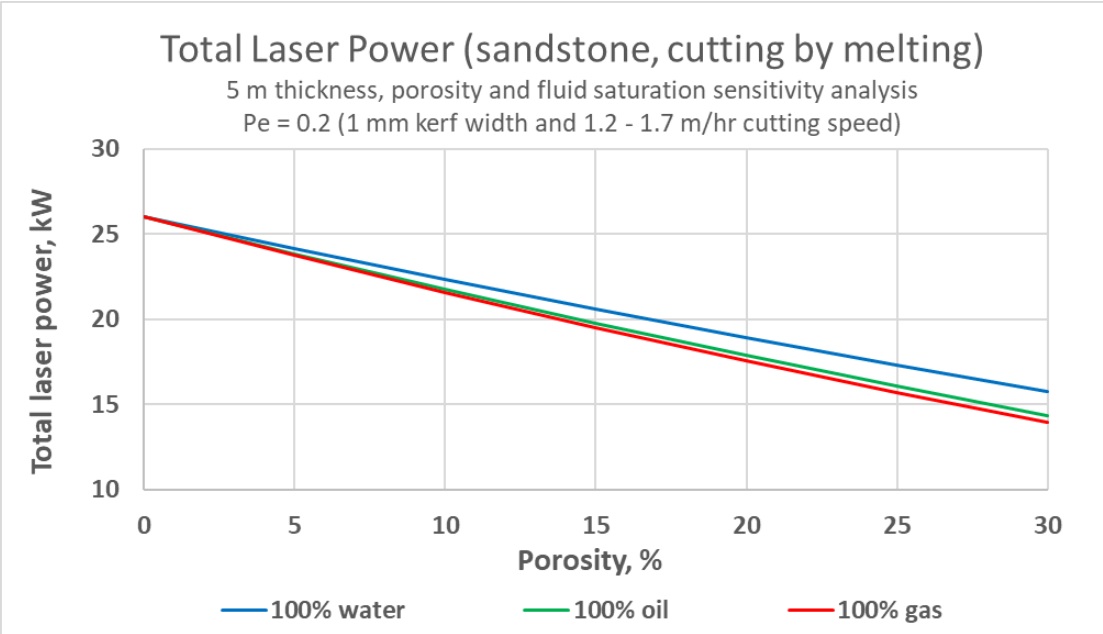


Figure 4-7: Fluid type sensitivity analysis (sandstone, cutting by melting, 5 m thickness and 0.2 Peclet number)

### 4.2.5 Cutting by melting vs vaporization - sandstone

Cutting by melting requires a continuous cutting kerf cleaning from the molten material during laser processing. Cutting kerf cleaning is a standard process for laser cutting operation at surface but it can be a challenge under downhole condition specially when deep cut (high rock thickness) is required. Cutting by vaporization is suggested and considered in this research in order to avoid the needs for the complex cutting kerf cleaning.

The analysis indicated that cutting by vaporization would require significantly higher laser power compared to that required for cutting by melting mainly due to the significant increase in useful power.

Useful power significantly increases for cutting by vaporization due to the significant energy absorbed during phase changing of the rock from molten material to vapor (latent heat of vaporization), while waste power relatively increases due to the increasing of final temperature from 1813 K (temperature of melting for sandstone) to 2473 K (temperature of vaporization for sandstone) and accordingly more heat transfer into surrounding.

Figure 4-8, Figure 4-9 and Figure 4-10 show comparisons between cutting by melting and vaporization for total, useful and waste power respectively for sandstone, 100% water, 0.2 Peclet number with various porosity. As shown, the increasing in total power is dominated by the increasing in useful power due to latent heat of vaporization, while the increasing in waste power is relatively very low compared to that of useful power. The same effect of porosity was also observed as laser power requirement significantly decreases with increasing porosity. This effect was also observed for all Peclet numbers and fluid types.

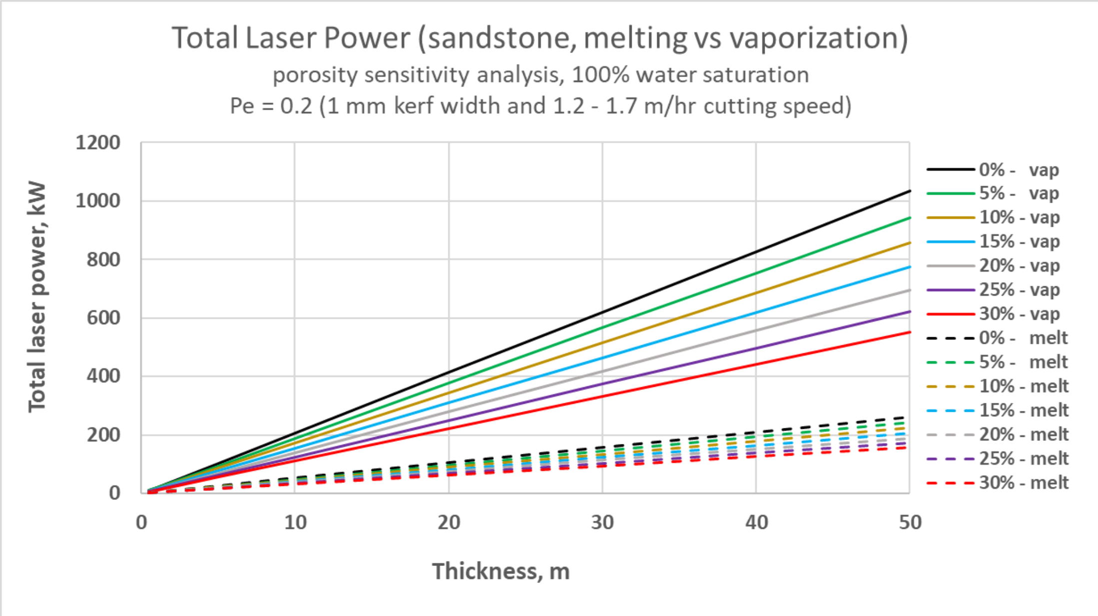


Figure 4-8: Comparison between cutting by melting and vaporization (total laser power, sandstone, 100% water saturation, 0.2 Peclet number and porosity sensitivity analysis)

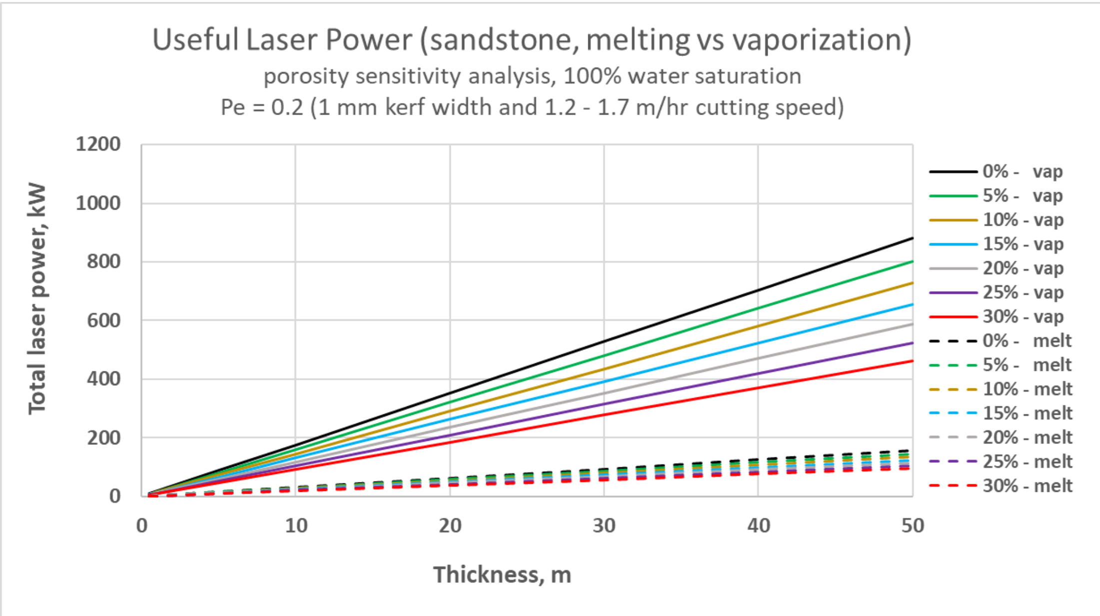


Figure 4-9: Comparison between cutting by melting and vaporization (useful laser power, sandstone, 100% water saturation, 0.2 Peclet number and porosity sensitivity analysis)

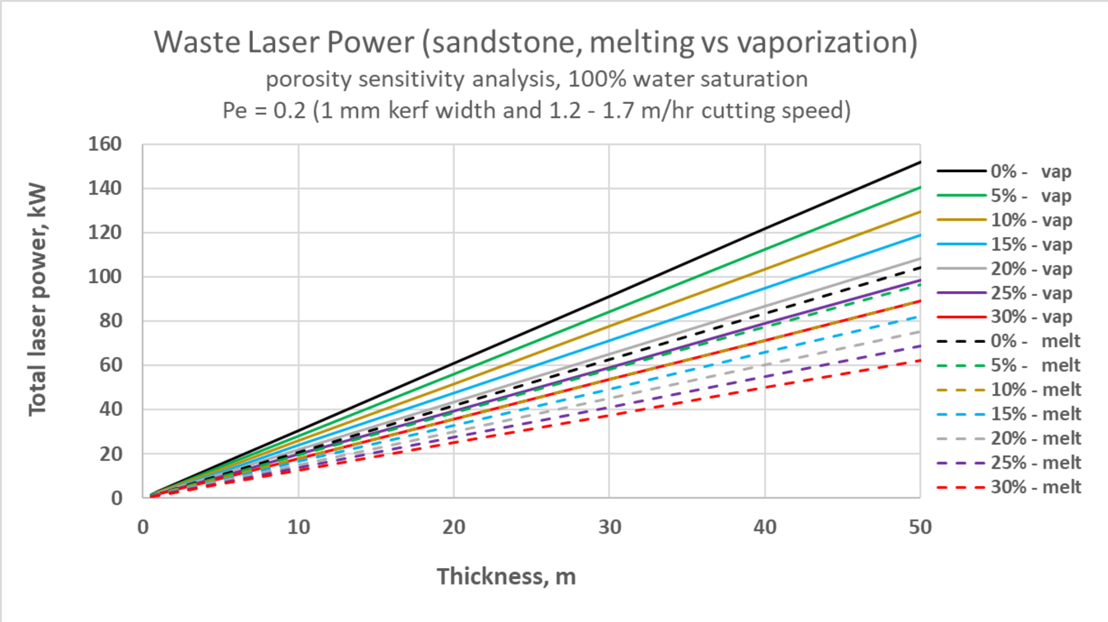


Figure 4-10: Comparison between cutting by melting and vaporization (waste laser power, sandstone, 100% water saturation, 0.2 Peclet number and porosity sensitivity analysis)

Figure 4-11 shows comparison between the waste power ratio for cutting by melting and cutting by vaporization for sandstone, 20% porosity and 100% water saturation. The increasing in useful power for cutting by vaporization is much higher than the increasing in waste power, and accordingly the waste power ratio for cutting by vaporization is significantly lower than that of cutting by melting. This finding was also observed for all fluid types exist in porous media.

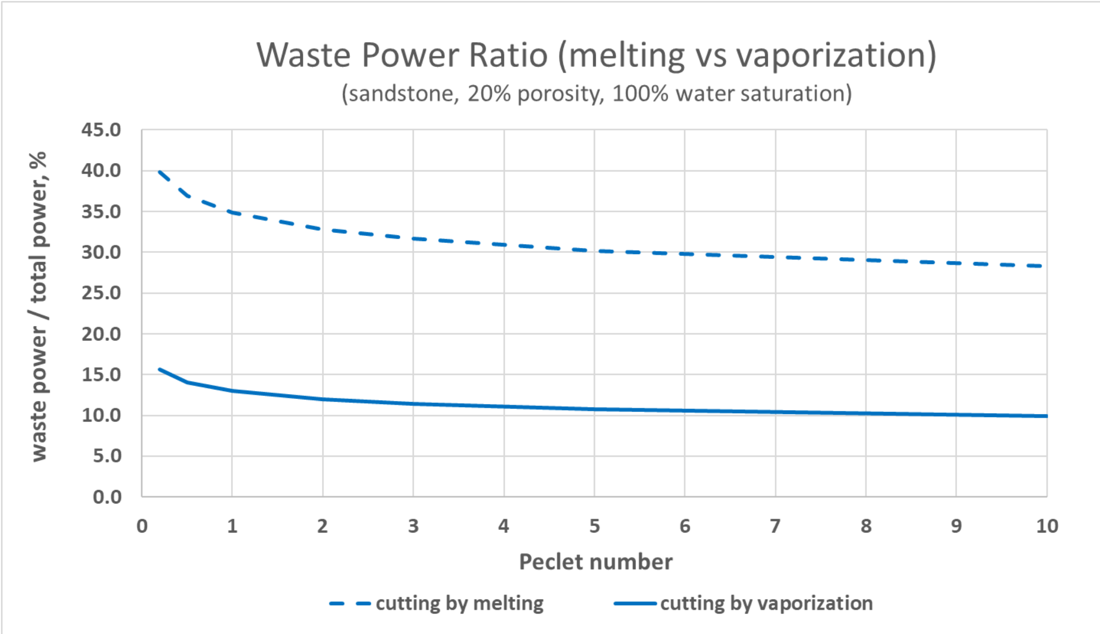


Figure 4-11: Waste power ratio for cutting by melting and vaporization (sandstone, 20% porosity, 100% water saturation)

Figure 4-12 shows comparison between cutting by melting and vaporization for 5 meters sandstone thickness at 0.2 Peclet number with porosity and fluid saturation sensitivity analyses.

The same finding was observed for both cutting methods where water requires slightly more power compared to oil and gas. This finding is similar for any Peclet number and any rock thickness. However, the effect of porosity in reducing laser power is significant compared to the effect of fluid type exist in porous media.

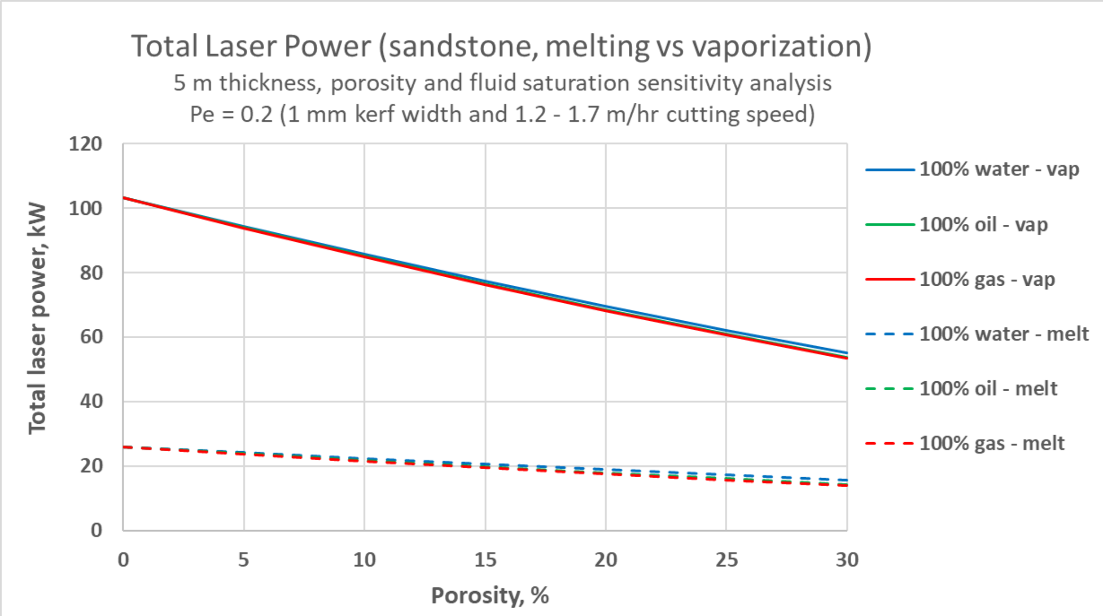


Figure 4-12: Comparison between cutting by melting and vaporization for various fluid types to cut 5 m sandstone thickness at 0.2 Peclet number

As a conclusion, useful power for cutting by vaporization is approximately 5 times higher than that for cutting by melting due to the high energy required to heat the rock up to vaporization temperature in addition to the high latent heat of vaporization, while waste power is higher by only 1.5 times which represents the increasing in heat transfer into surrounding associated with the incremental heat added to the rock in order to reach vaporization temperature. However, total laser power is higher by approximately 4 times in case of cutting by vaporization.

### 4.2.6 Comparison between cutting sandstone and limestone

The same findings concluded in the sandstone power calculations are observed in the limestone calculations. The only difference is that limestone rock requires significantly lower power than sandstone rock. Useful power is lower due to the lower temperature of melting and vaporization and latent heats while waste power is lower due to the lower thermal diffusivity of limestone compared to sandstone.

Figure 4-13 shows comparison between the total laser power required to cut 5 meters thickness of sandstone and limestone rocks, by melting and vaporization, 0.2 Peclet number, porosity and fluid saturation sensitivity analyses. As shown sandstone requires higher power compared to limestone and cutting by vaporization requires significantly higher power compared to cutting by melting. Also, power significantly decreases with increasing porosity while the effect of fluid saturation is minor (water is slightly higher than oil and gas).

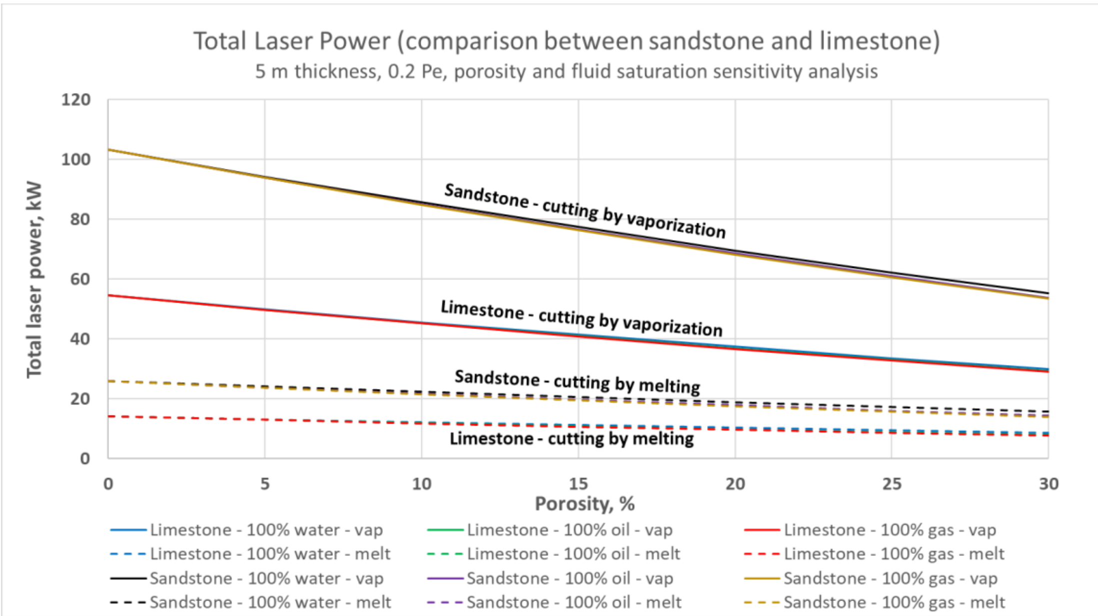


Figure 4-13: Comparison between sandstone and limestone, cutting by melting and vaporization (5 m thickness, 0.2 Peclet number, porosity and fluid saturation sensitivity analyses)

As a conclusion, the range of total laser power required to cut 10 – 20 m of rock by melting at 0.2 Pe is 50 – 100 kW and 25 – 50 kW (half power) for sandstone and limestone respectively. This range of laser power is within the capacity of the available laser technology as described in the laser technology screening section. $CO_2$ gas laser can produce a continuous wave power greater that 100 kW, but the challenges of using such technology under downhole condition must be considered. However, laser interaction with 10 – 20 meters of rock around wellbore can significantly enhance well productivity as described in the reservoir simulation section.

## 4.3 Numerical model results

The results of the numerical model are discussed in this section including the effect of boundary conditions, comparison with the analytical model's results and model verifications.

### 4.3.1 Thermal properties of metals

Thermal properties of sandstone and limestone rocks are presented in the analytical solution section. In addition, Table 4-5 shows the thermal properties of some metals used in the numerical model and verification work. Multiple sources are used to collect this data including CIBSE (2015), Pohanish (2016), KNOVEL (2008) and Prusa, Venkitachalam and Molian (1999).

Table 4-5: Thermal properties for some metals used in the models

| Substance | $c_p$ J/kg.K | $k$ W/m.K | $\rho$ kg/m³ | $T_m$ K | $L_f$ J/kg |
|---|---|---|---|---|---|
| Mild steel | 660 | 38 | 7,860 | 1,810 | 275,000 |
| Stainless steel | 460 | 17 | 7,900 | 1,672 | 270,000 |
| Aluminum | 900 | 237 | 2,702 | 933.5 | 399,334 |

## 4.3.2 The effect of boundary conditions

Boundary condition has a significant effect in heat transfer into surrounding and waste power during laser cutting accordingly. Figure 4-14 shows a comparison between cutting 50 mm thickness of stainless steel at 80 mm/min cutting speed (last time step). As shown, significantly higher heat transfer into surrounding is observed for line-source boundary condition compared to point-source because laser beam is always in contact with kerf wall all the time during laser cutting process. This can cause a significant increase in waste power compared to point-source.

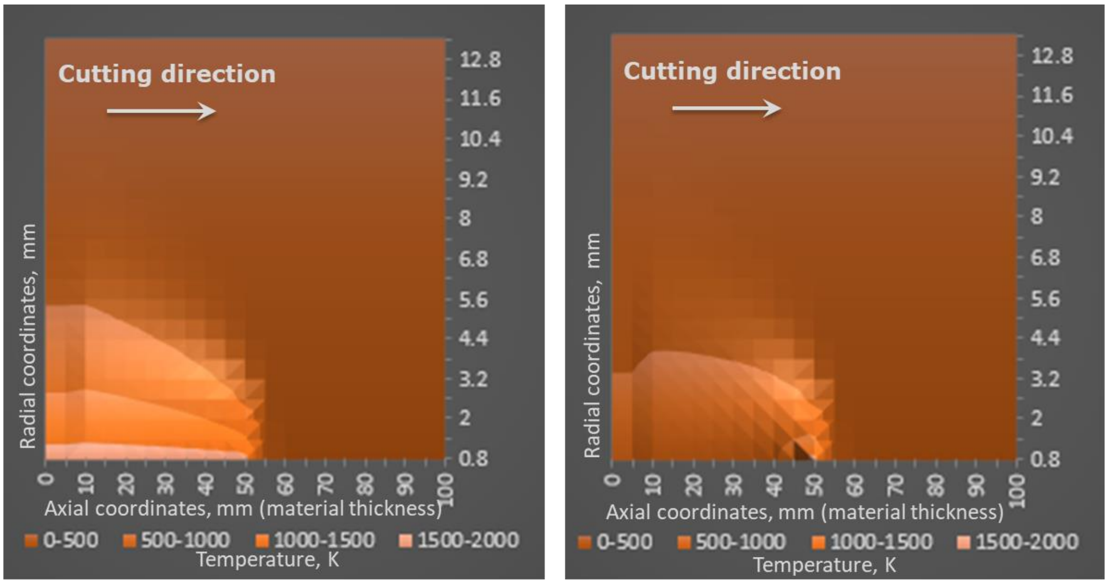


**Line-source boundary condition**
High heat transfer

**Point-source boundary condition**
Low heat transfer

Figure 4-14: Comparison between line-source and point-source boundary conditions

## 4.3.3 Comparison between numerical and analytical models

Figure 4-15 and Figure 4-16 show examples of cutting 0.5 m thickness of sandstone rock, 100% oil saturated, with various porosity (zero, 15% and 30%) for cutting by melting and cutting by vaporization respectively. Note that zero porosity has been considered in all sensitivity analyses because the model may also be used for non-porous materials.

Waste power is calculated using the three methods; analytical, numerical line-source and numerical point-source for comparison. Also sensitivity analysis for Peclet number (Pe) is considered to represent various laser cutting speeds.

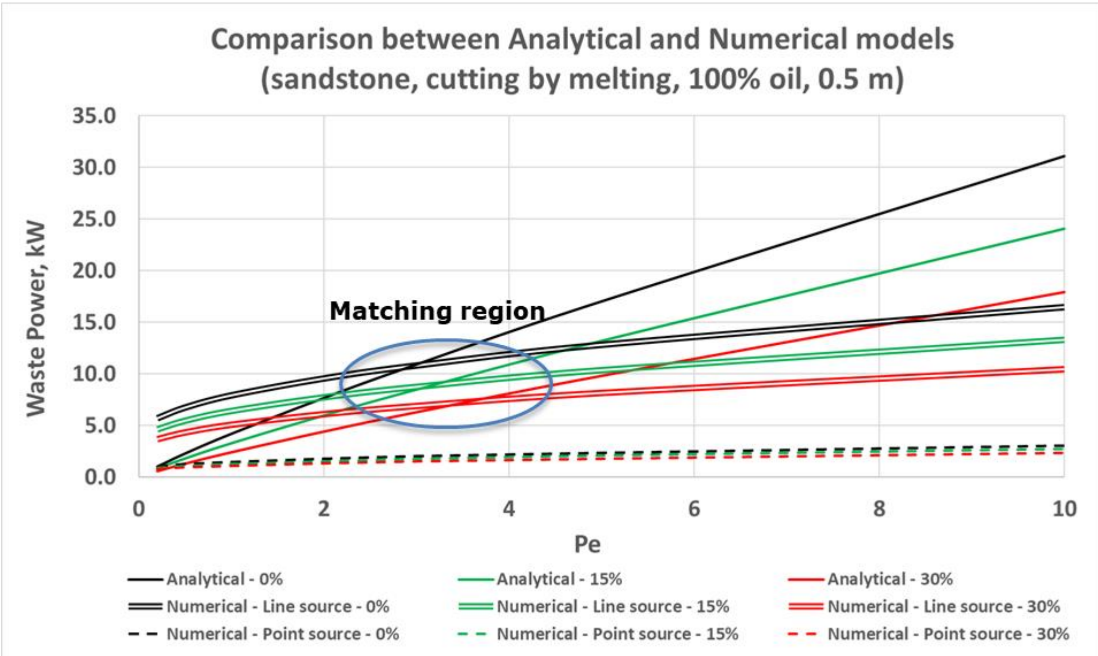


Figure 4-15: Comparison between numerical and analytical models (cutting by melting)

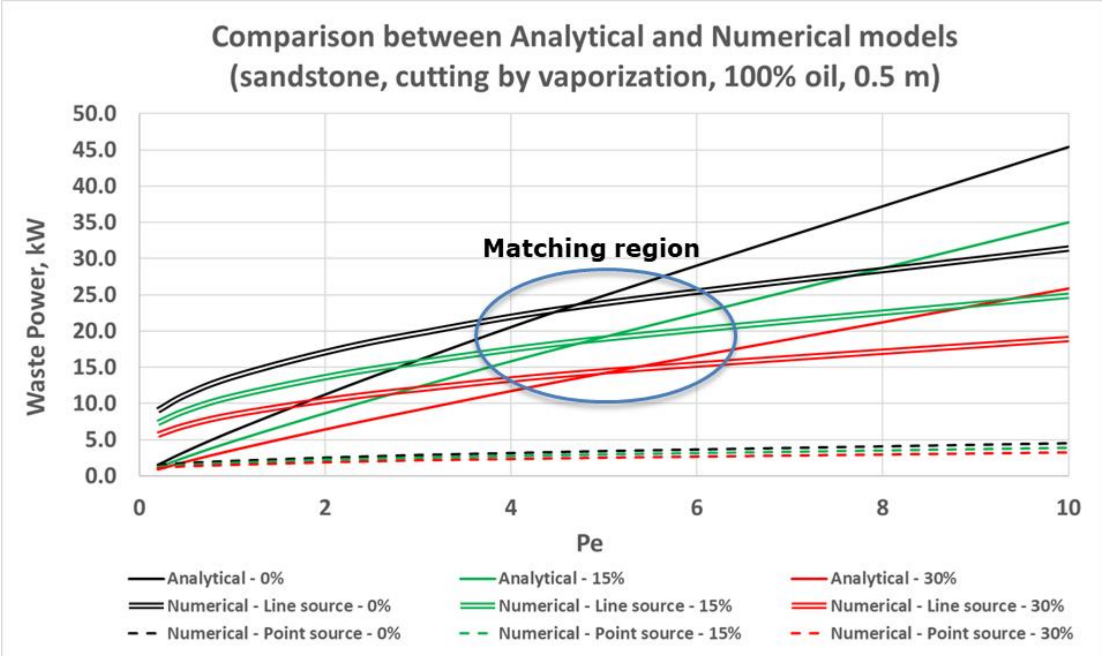


Figure 4-16: Comparison between numerical and analytical models (cutting by vaporization)

As shown, Numerical line-source model matches the analytical calculations at some regions (around 3.0 Pe for cutting by melting and around 5 Pe at cutting by vaporization) and numerical point-source matches the analytical calculations at very low Pe. However, the overall results show some spread and model verification with actual experimental data is essential to identify the most representative model.

## 4.4 Model's verifications

This section includes verifications for the numerical and analytical models, the results of both models are compared to the actual experimental data for cutting rock (sandstone and limestone) and metals (mild steel, stainless steel and Aluminium).

### 4.4.1 Verification-1 (pulsed Nd:YAG laser in carbonate rock)

The experimental tests conducted by Erfan et al. (2010) for Nd:YAG pulsed laser on carbonate rocks are used in verification-1. Table 4-6 shows the results of the tests including radiation time, material thickness and specific energy.

Table 4-6: Verification-1, experimental data (Erfan et al. 2010)

| | Saturation Type | Sample No. | Radiation Time (s) | Drilling Depth (mm) | SE (KJ/cc) | ROP (mm/s) |
|---|---|---|---|---|---|---|
| Carbonate Ahvaz-383-9 | Dry | 1 | 5 | 7.08 | 38.52 | 1.42 |
| | | 2 | 10 | 9.12 | 59.81 | 0.91 |
| | | 3 | 15 | 10.16 | 80.53 | 0.68 |
| | | 4 | 20 | 10.7 | 101.95 | 0.53 |
| | | 5 | 25 | 11.16 | 122.19 | 0.45 |
| | Water Satd | 1 | 5 | 6.01 | 45.38 | 1.2 |
| | | 2 | 10 | 8.23 | 66.28 | 0.82 |
| | | 3 | 15 | 9.2 | 88.94 | 0.61 |
| | | 4 | 20 | 9.73 | 112.12 | 0.49 |
| | | 5 | 25 | 9.92 | 137.47 | 0.4 |
| | Oil Satd | 1 | 5 | 6.61 | 41.26 | 1.32 |
| | | 2 | 10 | 8.7 | 62.7 | 0.87 |
| | | 3 | 15 | 9.82 | 83.32 | 0.65 |
| | | 4 | 20 | 10.2 | 106.96 | 0.51 |
| | | 5 | 25 | 10.51 | 129.75 | 0.42 |

This experiment represents cutting by melting technique also Nitrogen was used as purging gas.

Rock mineral composition is not reported and accordingly thermal properties of limestone (the common carbonate rock type) is assumed as well as fluid properties at room temperature (initial condition).

The reported rock porosity is within 5 – 15%. An average porosity of 10% is assumed in all calculations (numerical and analytical models).

Laser beam diameter is not reported. An average of 1 mm is assumed, however the comparisons are based on specific energy (per unit volume) rather than the actual power and accordingly this assumption can cause low and acceptable error.

Figure 4-17 shows the results of verification-1 including comparison between experimental data, numerical and analytical models. Similar results are observed for all other fluid saturations.

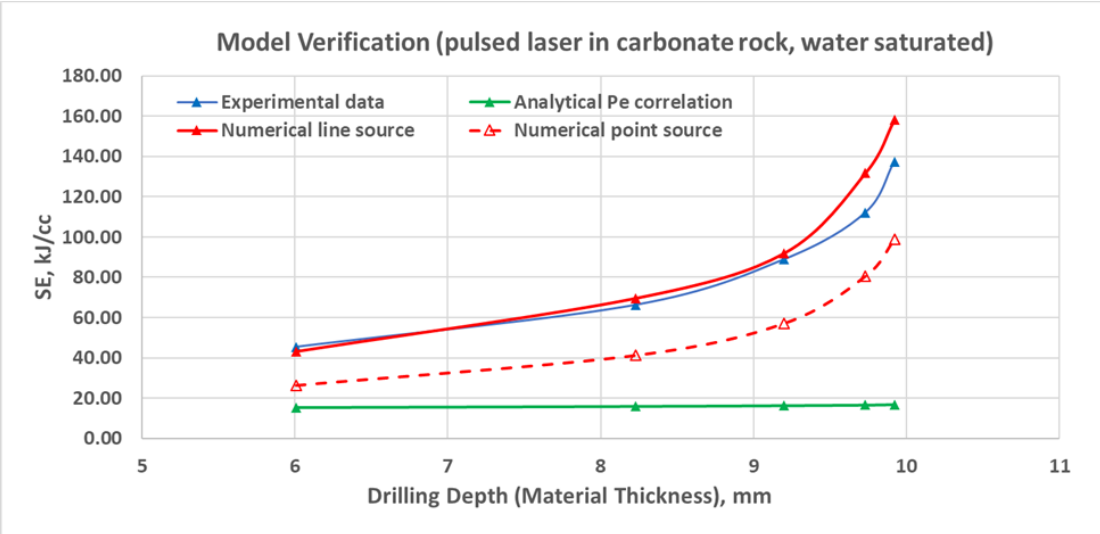


Figure 4-17: Verification-1 results (Nd:YAG pulsed laser on Carbonate rocks)

The results showed that line-source numerical model matches the experimental data with 5 – 15% deviation, while point-source numerical model underestimates the laser power requirements.

The analytical model showed very low specific energy, probably because Peclet number is lower than 0.2, the lower limit of using the waste power correlation proposed by Prusa, Venkitachalam and Molian (1999).

The results indicated that line-source could be the most suitable boundary condition for pulsed laser numerical modelling.

## 4.4.2 Verification-2 (CO2 laser cutting by vaporization in limestone)

This test was conducted by Carstens and Brown (1971) to study the feasibility of using laser to assist mechanical rock tunneling. Table 4-7 shows the results of laser cutting in limestone rock using CO2 laser power level of 3 – 4 kW.

Table 4-7: Verification-2, experimental data (Carstens and Brown 1971)

| Test number | Traverse speed, ipm | Kerf depth, inches |
|---|---|---|
| 14 | 13.2 | 0.661 |
| 15 | 10.4 | 0.859 |
| 16 | 7.9 | 1.19 |
| 17 | 5 | Penetrated |
| 18 | 7 | 1.45 |

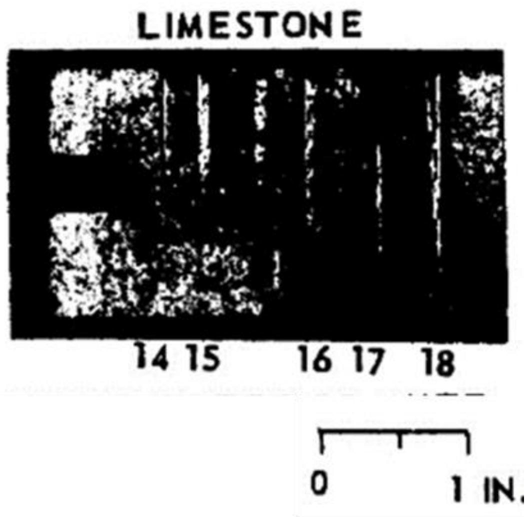


Dry sample with an average porosity of 10% is assumed, and also an average kerf width of 1 mm is assumed (from the rock sample's cross-section provided).

Clean cuts with almost no melt zone were created in this test without gas purging, which means rock vaporization temperature was reached and accordingly cutting by vaporization is considered in laser power modelling of this test. Figure 4-18 shows the results of verification-2 including comparison between experimental data, numerical and analytical models.

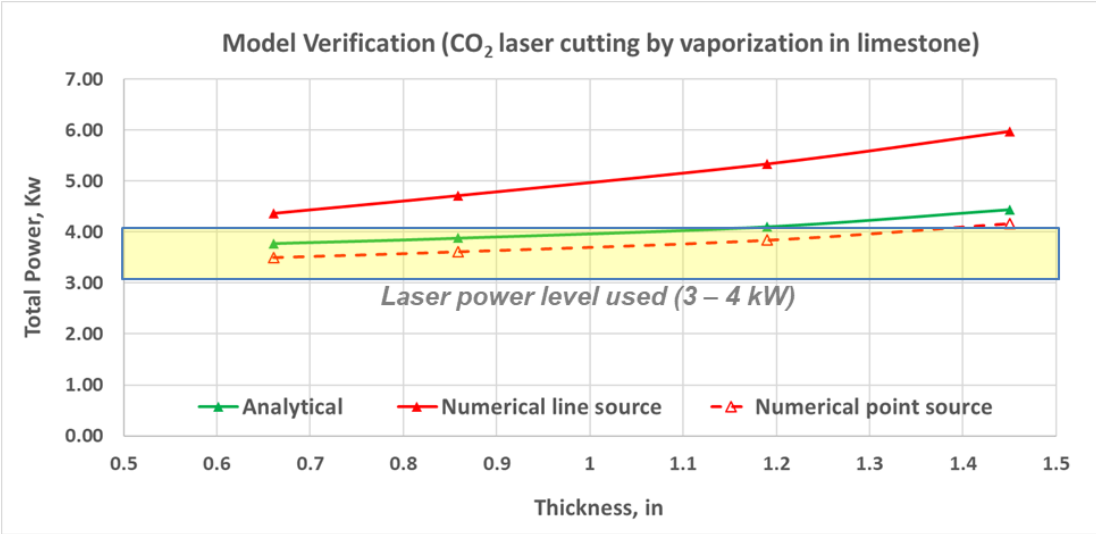


Figure 4-18: Verification-2 results (CO2 laser cutting by vaporization in limestone)

The results showed that numerical point-source and analytical models are very close to the laser power used in the test (good match), while numerical line-source is higher than experimental data.

Apparently point-source boundary condition is more relevant and better representing cutting by vaporization method. Probably once rock evaporates, laser beam will not be in contact with kerf wall.

Analytical model also matches experimental data because Peclet number is within the valid range of using the waste power correlation (0.2 – 10).

### 4.4.3 Verification-3 (cutting thick stainless-steel using fiber laser)

This test was conducted by Shin et al. (2019) for the purposes of dismantling nuclear facilities. Cutting 50 and 60 mm thick stainless-steel plates was conducted at surface (in air) and underwater using 6 kW fiber laser.

Table 4-8 shows the experimental results of cutting stainless steel by melting in air and underwater using compressed air as gas purging.

Table 4-8: Verification-3, experimental data (Shin et al. 2019)

| Condition | Thickness | Cutting speed | Kerf width | Power used in the experiment | Calculated Pe |
|---|---|---|---|---|---|
| | mm | mm/min | mm | kW | |
| In air | 50 | 140 | 1.1 | 6 | 0.27 |
| | 60 | 90 | 1.1 | 6 | 0.18 |
| Underwater | 50 | 100 | 1.4 | 6 | 0.25 |
| | 60 | 40 | 1.4 | 6 | 0.10 |
| | 50 | 80 | 1.6 | 6 | 0.23 |


Figure 4-19 shows verification-3 results including comparison between experimental data, numerical and analytical models.

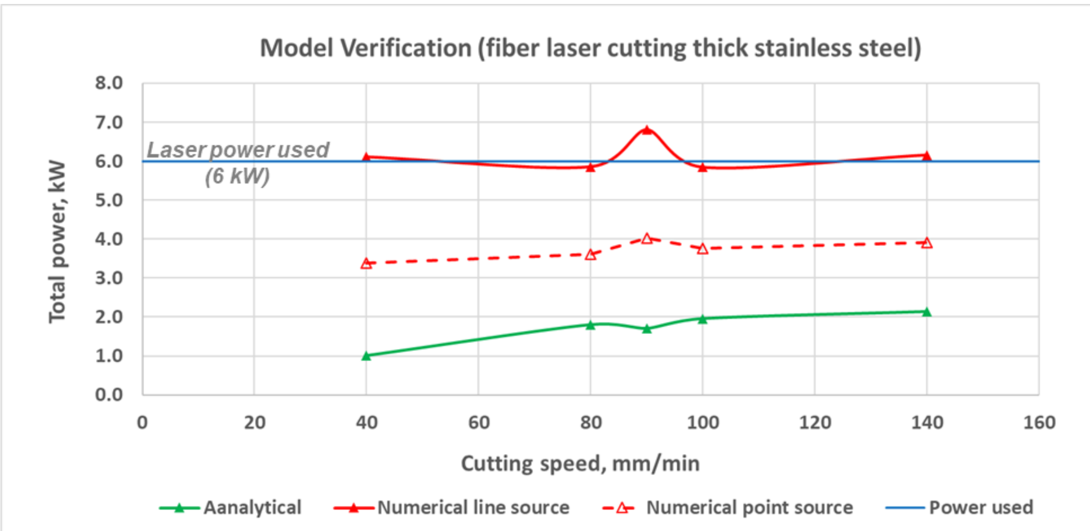


Figure 4-19: Verification-3 results (cutting thick stainless-steel using fiber laser)

The results showed that experimental data is perfectly matched with the numerical line-source model with only 2% deviation (except one point with

13% deviation) while numerical point-source and analytical models are lower than experimental data.

Analytical model doesn't match probably because Peclet numbers are lower than, or very close to, the lower limit of 0.2.

### 4.4.4 Verification-4 (cutting mild and stainless steel with CO2 laser and oxygen gas assist)

This experimental work was conducted by Powell et al. (1994) to measure the waste energy during laser cutting of mild and stainless steel.

50 mm diameter circle discs with various thicknesses were cut at maximum possible speed and the discs were placed in an insulated water bath immediately after cutting in order to measure the absorbed heat. Table 4-9 shows the results of Powell's experiment.

Table 4-9: Verification-4, experimental data (Powell et al. 1994)

| Sample | Material | Thickness (mm) | Cutting speed (m/min) | Kerf width (mm) |
|---|---|---|---|---|
| A | Mild steel | 1.55 | 6.4 | 0.30 |
| B | Mild steel | 2.9 | 3.15 | 0.30 |
| C | Mild steel | 4.8 | 1.8 | 0.35 |
| D | Mild steel | 8.0 | 0.8 | 0.40 |
| E | St. steel | 1.2 | 7.7 | 0.25 |
| F | St. steel | 1.9 | 4.08 | 0.30 |
| G | St. steel | 3.25 | 2.4 | 0.35 |
| H | St. steel | 5.0 | 1.53 | 0.35 |

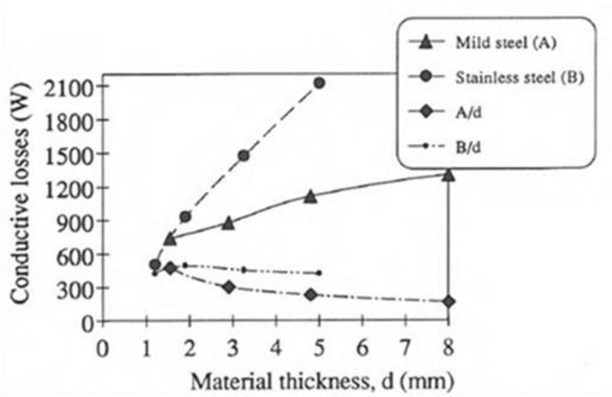


Figure 4-20 shows verification-4 results including comparison between experimental data, numerical and analytical models for mild steel.

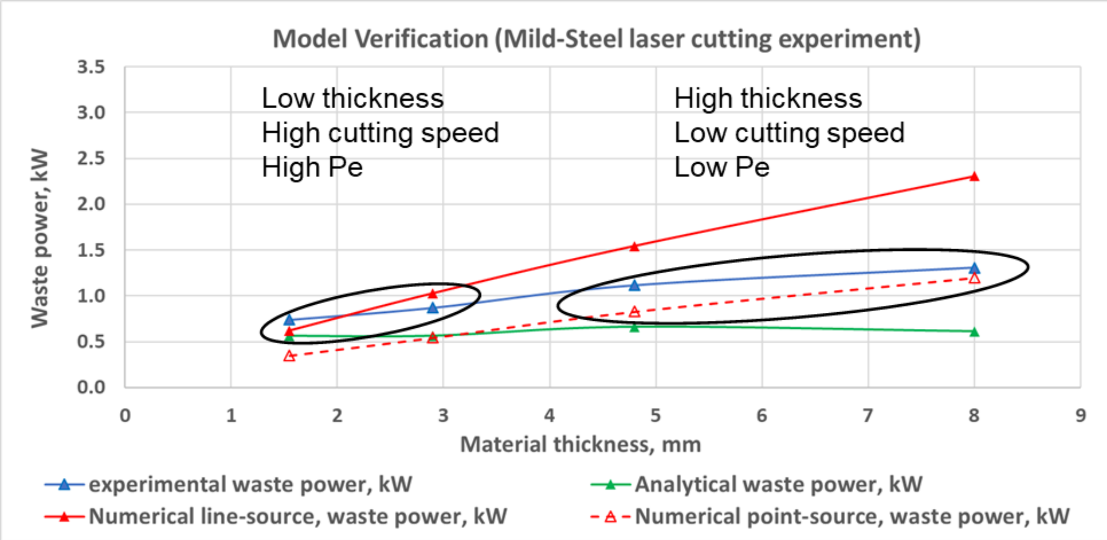


Figure 4-20: Verification-4 results (cutting mild steel with CO2 laser and oxygen gas assist)

The results showed that the experimental data of mild steel is matched with both numerical models as it is located between line-source and point-source models. Low thickness points (higher cutting speed and Pe) match the line-source model while high thickness points (lower cutting speed and Pe) match the point-source model.

Note that the experimental data for stainless-steel couldn't be matched (experimental waste power is approx. 3 times higher than all models).

There are many uncertainties in this experiment which could affect the accuracy of the results and mislead the interpretation, including the following:

1. Material was cut in polar (circular) coordinate while linear cutting coordinate is assumed in all the models.

2. The heat losses were measured in the cut disc then it was doubled assuming equal heat losses was occurred (transferred) into the other

side of the material, which is not necessarily correct. This assumptions (approximation) might significantly affect the comparison.

3. Thermal properties for the materials used in the experiment are not provided. For example, there is a wide range of stainless-steel grades with different thermal properties and this could be the reason that experimental data for stainless steel couldn't be matched.

4. The experiment showed that stainless steel losses is significantly higher than mild steel, while the opposite might be correct because thermal conductivity for mild steel is generally higher than stainless steel.

5. The experimental waste power exceeded the used laser power due to the heat generated by oxidation (oxygen gas assist was used), but this wouldn't affect the accuracy of the comparison because the comparison made between waste power rather than total laser power.

The overall finding from this experiment, after considering all the above uncertainties, is that experimental data is better matching the numerical model than analytical model.

### 4.4.5 Verification-5 (cutting stainless steel and aluminium with CO2 laser and nitrogen gas)

This experimental data presented by Webb and Jones (2004) is used. This data represents average (approximate) laser processing parameters required to cut various material thickness. Table 4-10 shows the experimental data used in verification-5 for stainless steel and aluminium.

Table 4-10: Verification-5, experimental data (Webb and Jones 2004)

| Approximate cutting speed for stainless steel | | | |
|---|---|---|---|
| Thickness | Approximate max cutting speed at 3.5 kW | Nitrogen pressure | Nozzle diameter |
| mm | m/min | bar | mm |
| 1 | 10 | 12 | 1.5 |
| 2 | 6.6 | 13 | 1.7 |
| 3 | 4.1 | 14 | 2 |
| 4 | 3 | 14 | 2 |
| 6 | 1.8 | 14 | 2.5 |
| 8 | 1.2 | 14 | 2.5 |
| 10 | 0.8 | 14 | 3 |
| 12 | 0.4 | 14 | 3 |

| Approximate cutting speed for aluminium alloys | | | |
|---|---|---|---|
| Thickness | Approximate max cutting speed at 3.5 kW | Nitrogen pressure | Nozzle diameter |
| mm | m/min | bar | mm |
| 1 | 10 | 10 | 1.5 |
| 2 | 7 | 10 | 1.7 |
| 3 | 4 | 10 | 2 |
| 4 | 3 | 10 | 2 |
| 5 | 2 | 10 | 2 |
| 6 | 1 | 10 | 2.5 |

Figure 4-21 shows the results of verification-5 including comparison between experimental data, numerical and analytical models for stainless steel and aluminium.

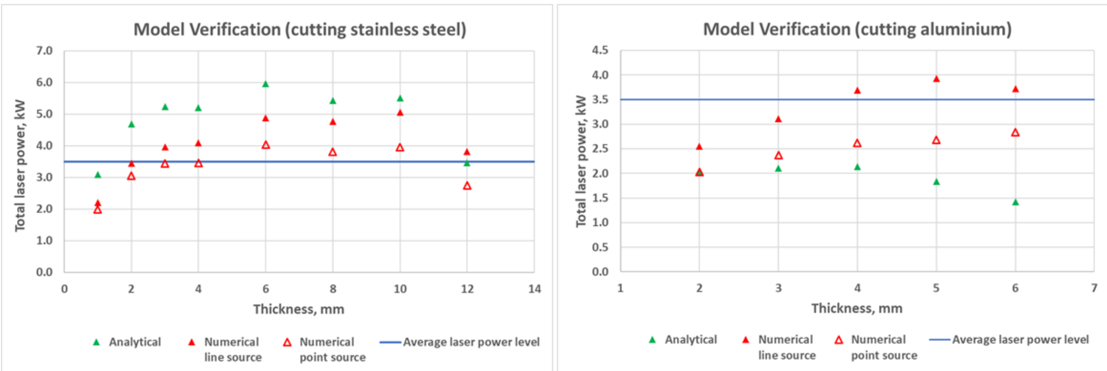


Figure 4-21: Verification-5 results (cutting stainless steel and aluminium)

Numerical point-source model showed better matching with stainless-steel experimental data, while line-source model showed better matching with aluminium data. (note the uncertainty in stainless steel thermal properties).

The following is a summary of the uncertainties and assumptions made in this verification which could affect the accuracy of the results:

1. The data presented by Webb and Jones represents average (approximate) laser processing parameters and should be used as guideline only. Perfect match with analytical and numerical models is not expected accordingly.

2. The reported nozzle diameters are assumed to be similar to kerf widths, which it is not necessarily correct.

3. Thermal properties of the material used in the experiments are not reported and this can affect the accuracy of the results. Note that there is a wide range of stainless-steel grades.

Although perfect match is not expected due to the above uncertainties, the overall results showed better matching with numerical model than analytical model.

## 4.5 New waste power correlations

Numerical line source model showed good matching with experimental data in all verification work for cutting by melting including metals (mild steel, stainless steel and aluminium) and non-metals (carbonate rocks).

In order to develop a simple and reliable correlation which can be used to analytically calculate laser waste power, the numerical line-source verification data is plotted against Peclet number as shown in Figure 4-22.

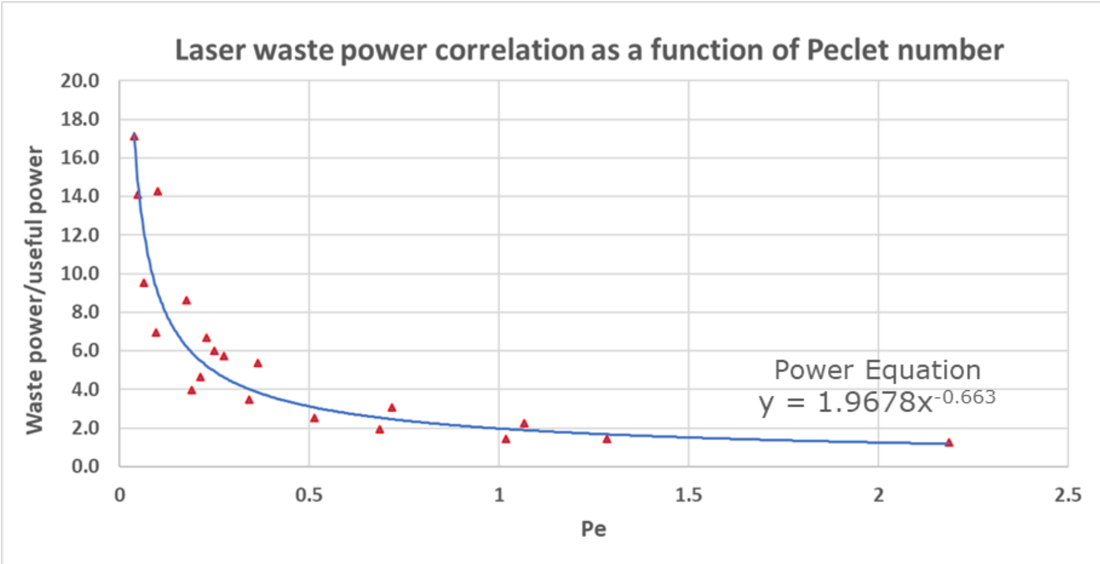


Figure 4-22: New waste power correlation as a function of Peclet number

Waste power for all the materials used in the verification work (metal and non-metal) can fit the following correlation as a function of useful power and Peclet number:

$$\frac{P_{waste}}{P_{useful}} = 1.9678 \ P_e{}^{-0.663} \text{ -----------------------------------------------(4.1)}$$

Where $P_{waste}$ and $P_{useful}$ are the waste and useful laser power respectively and $P_e$ is Peclet number (dimensionless).

Another correlation is developed by plotting the data against cutting speed as shown in Figure 4-23. The correlation can be written as following, note that the effect of thermal diffusivity is not considered in this correlation:

$$\frac{P_{waste}}{P_{useful}} = -1.341 \ ln\, v \ + 4.103 \text{ ----------------------------------------(4.2)}$$

Where $P_{waste}$ and $P_{useful}$ are the waste and useful laser power respectively and $v$ is laser cutting speed in meters/minute.

Note that if cutting speed data was converted to natural log before plotting, the data would be fitted with the linear equation y = -1.341x + 4.103 where x=ln(v), so the same correlation would be generated.

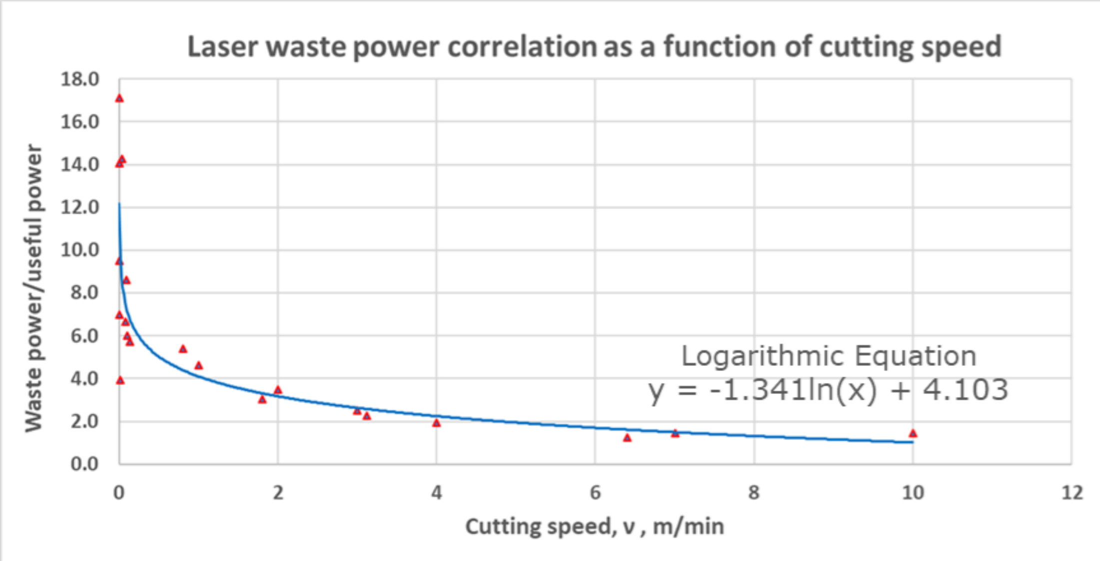


Figure 4-23: New waste power correlation as a function of cutting speed

Various material thickness are included in this data, however the maximum thickness used in the verification work is 60 mm. Further experimental tests are recommended to confirm the validity of using these correlations for very thick materials (in the magnitude of meters if possible).

## 4.6 Laser power calculations using the new correlations

Total laser power required to cut sandstone and limestone rocks is calculated for various material thickness and various porosity using the new suggested waste power correlation. Figure 4-24 shows the total laser power calculated for cutting by melting at 0.2 Peclet number and 100% water saturation. More details are provided in Appendix-2.

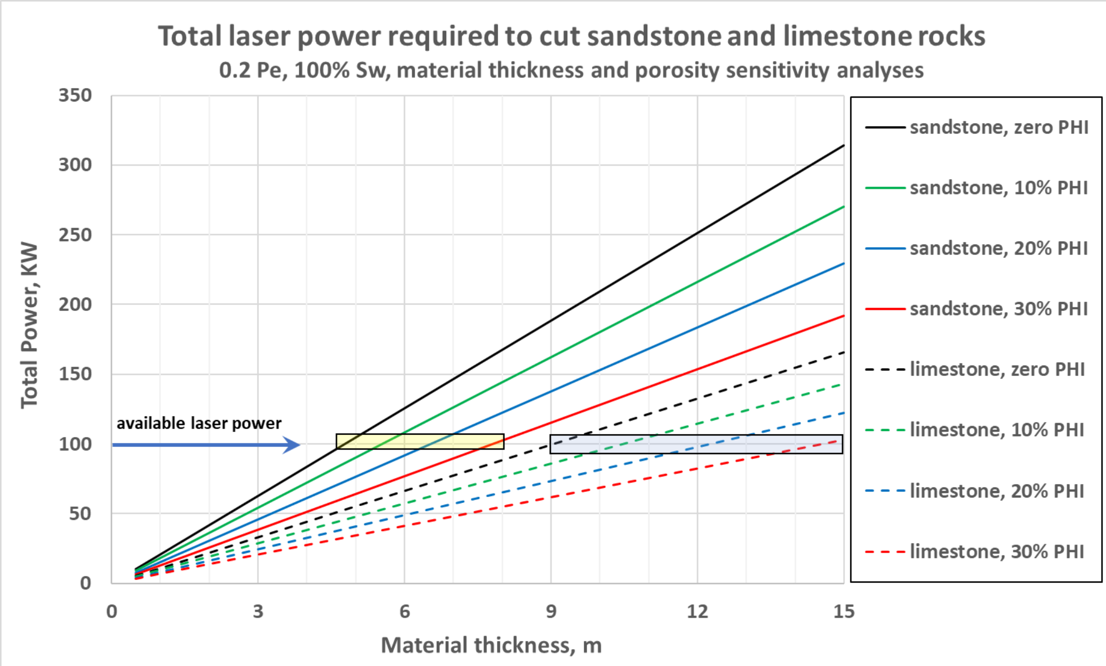


Figure 4-24: Laser power calculations using the new waste power correlation

The results showed that sandstone required higher laser power than limestone due to the higher thermal diffusivity and melting temperature of sandstone compared to limestone. Also laser power decreases with increasing porosity as described in the analytical solution section.

The results indicated that 100 kW laser power is capable to cut 5 – 8 m of sandstone and 9 – 15 m of limestone rock. The overall conclusion and finding from this analysis is that 100 kW laser power can cut a range of 5 – 15 m of porous material depending on porosity and thermal properties.

Figure 4-25 shows the waste power ratio to total power used for various Peclet numbers. Waste power ratio decreases with increasing Peclet number due to the significant increases of useful power with Peclet number and also the lower heat transfer into surrounding due to the high speed associated with high Peclet number as described in the analytical solution section.

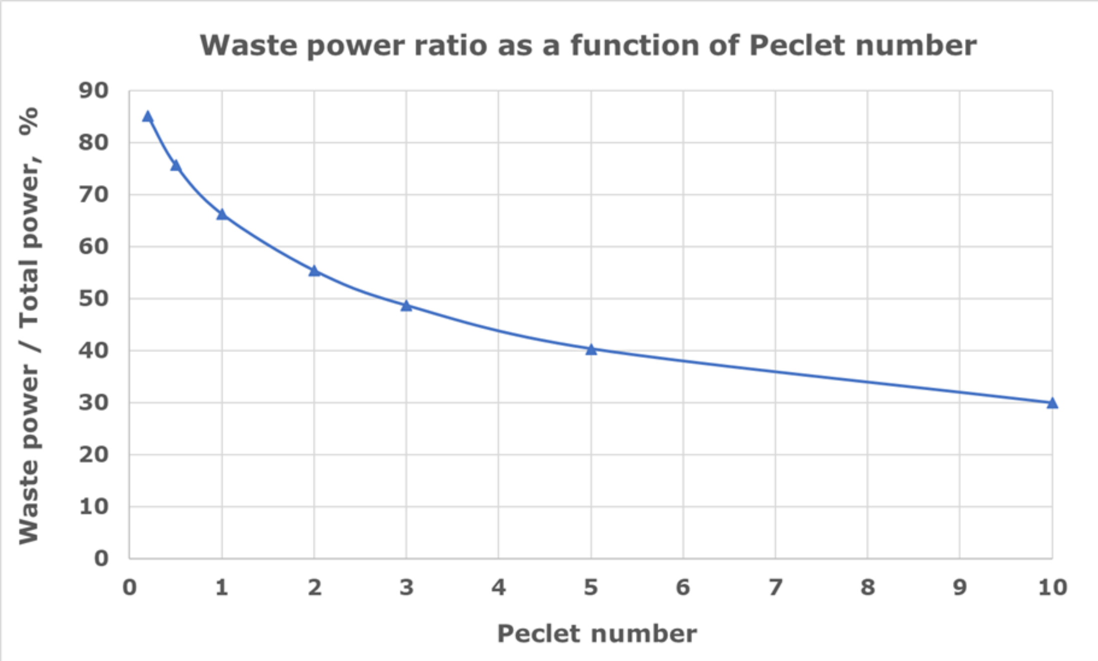


Figure 4-25: Waste power ratio as a function of Peclet number

It is observed that 85% of total power could be lost due to heat transfer into surrounding for cutting at low Peclet number (low cutting speed) and this losses decrease up to 30% for cutting at high Peclet number. However, significant laser power would be required to cut at high Peclet number. This waste power ratio is similar for various rock types, thickness and porosity.

## 4.7 Suggested methodology to calculate laser power

Based on the results, analyses and findings of the analytical and numerical work conducted in this research and presented in the previous sections, the following methodology is suggested to analytically calculate the total laser power required to cut a particular thickness of porous material by melting without the needs to build complex numerical models.

1. Identify rock type, porosity and fluid saturations exist in porous media including gas, oil and water.

2. Identify the physical and thermal properties of the rock including heat capacity, thermal conductivity, density and latent heat of melting.

3. Identify the physical and thermal properties of each fluid phase (gas, oil and water) exist in porous media under reservoir conditions (reservoir pressure and temperature) including heat capacity, thermal conductivity and density for each phase. Ideally laboratory work should be conducted to measure these properties, if not possible, approximations and assumptions can be made (thermal properties at standard conditions can be used).

4. Use phase diagrams for water and hydrocarbon oil in order to identify the temperature of vaporization for water and oil at reservoir pressure.

5. Calculate the latent heat of vaporizations for oil and water at the temperature of vaporization of each one using the following equation, or to be measured on the laboratory.

$$L_v = A \left( 1 - \frac{T}{T_c} \right)^n \text{------------------------------------------------}(4.3)$$

6. Calculate the effective thermal properties using volumetric average approach as following:

$$\overline{\rho c_p}_{eff} = \phi \left( \overline{\rho c_p}_w S_w + \overline{\rho c_p}_o S_o + \overline{\rho c_p}_g S_g \right) + (1 - \phi) \overline{\rho c_p}_{rock} \text{-----}(4.4)$$

$$\overline{\rho L_h}_{eff} = \phi \left( \overline{\rho L_v}_w S_w + \overline{\rho L_v}_o S_o \right) + (1 - \phi) \overline{\rho L_h}_{rock} \text{---------------}(4.5)$$

$$\alpha_{eff} = \phi \left( \alpha_w S_w + \alpha_o S_o + \alpha_g S_g \right) + (1 - \phi)\ \alpha_{rock} \text{------------}(4.6)$$

7. Identify the desired material thickness to be cut, kerf width and cutting speed. Note that cutting speed could be limited to the capacity of the available laser technology and it is also affected by material thickness.

8. Calculate Peclet number for the material to be cut using the following equation:

$$P_e = \frac{w\,v}{2\,\alpha_{eff}} \text{ ----------------------------------------------------------(4.7)}$$

Peclet number to be calculated for each stage separately as described in Table 4-11 (note that each stage has different effective thermal properties).

9. Calculate the total laser power required to cut the desired material thickness using the following equations. Note that the other way is also valid, where maximum thickness to be cut can be calculated from the maximum available laser power.

$$Total\ laser\ power\ =\ useful\ power\ +\ waste\ power \text{ --------------(4.8)}$$

$$useful\ power = v\ d\ w\ \left(\overline{\rho c_p}_{eff1}\Delta T_1 + \overline{\rho c_p}_{eff2}\Delta T_2 + \overline{\rho L_h}_{eff}\right) \text{ -------(4.9)}$$

$$\frac{waste\ power}{useful\ power} = 1.9678\ \ P_e^{\ -0.663} \text{ ------------------------------------(4.10)}$$

Laser power calculations will be conducted on stages as shown in Table 4-11. The effective thermal properties will be calculated for each stage separately according to the fluid types and saturations exist in porous media at each stage. Table 4-11 represents the case when water, oil and gas exist initially in the porous media and temperature of vaporization of oil is less than that of water. For simplicity, same thermal properties can be assumed for all gas states including water-vapor and oil-vapor.

Table 4-11: Laser power calculation's stages based on fluid phase changes in porous media during laser processing

| Stages | Temperature range | Fluid types exist in the porous media |
|---|---|---|
| Stage-1 | $\boldsymbol{T \leq T_{v_o}} \quad (\boldsymbol{T_i \overset{to}{\rightarrow} T_{v_o}})$<br>from initial temperature to the temperature of vaporization of oil | water, oil and gas |
| Stage-2 | $\boldsymbol{T_{v_o} \leq T \leq T_{v_w}} \quad (\boldsymbol{T_{v_o} \overset{to}{\rightarrow} T_{v_w}})$<br>between the temperature of vaporizations of oil and water respectively | Water, oil-vapor and gas |
| Stage-3 | $\boldsymbol{T \geq T_{v_w}} \quad (\boldsymbol{T_{v_w} \overset{to}{\rightarrow} T_{m_r}})$<br>between the temperature of vaporizations of water and the melting temperature of rock | Water-vapor, oil-vapor and gas |

## 4.8 Summary

The main findings of the analytical model can be summarized as following:

1. Total laser power, including useful and waste powers, decreases with increasing porosity for any Peclet number and any fluid saturation exists in the porous media.

2. Useful power decreases with increasing porosity due to the fact that the volume of rock to be melted decreases with increasing porosity

while waste power decreases with increasing porosity because the thermal conductivity of fluids is much lower than that of rock and accordingly the heat transfer into surrounding decreases with increasing porosity.

3. The waste power ratio (to total power) decreases with increasing Peclet number because higher Peclet number is associated with higher cutting speed and accordingly less heat transfer (waste energy) into surrounding and also due to the significant increase in useful power.

4. The effect of porosity in reducing laser power is significant compared to the effect of fluid type exist in porous media.

5. Water requires slightly more power compared to oil and gas and this is mainly due to the high latent heat of vaporization for water. The effect of other thermal properties including heat capacity, thermal conductivity and density of fluids are minimal in laser power requirement.

6. Cutting by vaporization requires significantly higher laser power compared to that required for cutting by melting mainly due to a significant increase in useful power.

7. Useful power for cutting by vaporization is approximately 5 times higher than that for cutting by melting due to the high energy required to heat the rock up to vaporization temperature in addition to the high latent heat of vaporization, while waste power is higher by only 1.5 times which represents the increasing in heat transfer

into surrounding associated with the incremental heat added to the rock in order to reach vaporization temperature. However, total laser power is higher by approximately 4 times in case of cutting by vaporization.

8. Limestone rock requires significantly lower power than sandstone rock. Useful power is lower due to the lower temperature of melting and vaporization and latent heats while waste power is lower due to the lower thermal diffusivity of limestone compared to sandstone.

9. The range of total laser power required to cut 10 – 20 m of rock by melting at 0.2 Pe is 50 – 100 kW and 25 – 50 kW (half power) for sandstone and limestone respectively.

The main findings of the numerical model and verification work can be summarized as following:

1. Numerical and analytical models have been verified by experimental data of laser cutting by melting and vaporization for metal and non-metal materials.

2. Numerical model, with both line-source and point-source boundary conditions, showed better matching with experimental data than analytical model.

3. Numerical line-source model showed better matching for cutting by melting method than other models.

4. Numerical Point-source model showed better matching for cutting by vaporization method than other models.

5. The analytical model, which includes the waste power correlation developed by Prusa, Venkitachalam and Molian (1999) underestimated the waste power compared to both numerical model and experimental data. The reason is probably the different coordinate system assumed by Prusa (2D polar and Cartesian coordinates), also Prusa's model was verified by CO2 laser cutting of mild-steel with oxygen gas assist which is different energy balance equation due to the heat added up to the system by oxidation. However, the 3D model in cylindrical and axial coordinate system developed in this research is better representing the actual physics during laser cutting.

6. A new correlation has been developed from the verified numerical line-source model which showed good matching for cutting by melting for metals and non-metals. The results of laser power modeling using the new developed correlation indicated that 100 kW laser power is capable to cut a range of 5 – 15 m of porous material depending on rock porosity and thermal properties. 100 kW is within the capacity of the available laser technology as described in the laser technology screening section.

7. A methodology to analytically calculate laser power without the needs of developing complex numerical models has been developed.

# Chapter 5: Reservoir simulation modeling

Conventional hydraulic fracturing technique is capable to create a single fracture perpendicular to the minimum stress direction so fracture is propagating into the direction of minimum resistance.

The proposed laser induced fracture technique can create multiple fractures (network) in all directions around wellbore because the applied laser energy is independent of formation stress's magnitudes and orientations in addition to the significant improvement in reservoir porosity and permeability due to the microfractures created in the Heat Affected Zone (HAZ). Heat affected zone is the area heated up due to laser interaction and its property is significantly changed even prior to reaching melting point.

Reservoir flow simulation model has been developed in this research in order to identify the potential improvement in well productivity due to laser induced fractures. Sensitivity analysis for the improvement areas around wellbore (material thickness) is also considered.

It is worth mentioning that laser does not have a direct effect in the production results shown in this chapter since the simulation results are merely based on the altered permeability around wellbore (representing HAZ) or effective wellbore radius (representing fracture half-length) as described later in this chapter.

## 5.1 The effect of heat in reservoir characteristics

As shown in the literature review section, the laboratory experiment tests conducted in the past showed a significant improvement in rock porosity and permanently due to laser interaction, in addition to the microfractures created in the heat affected zone due to quartz expansion, clay dehydration and limestone dissociation.

Also when water is heated up to high temperature, it will evaporate and causes increase in the volume and pressure of the porous media and fractures can be created when this high pressure gases try to expand and escape out into surrounding. Water exists in porous media in the form of connate water saturation (rock wetting phase) or in the form of minerals that contain an appreciated amount of water such as clays. However, when porous media filled by gas is heated up, gas pressure will also increase and expand, causing microfractures in the surrounding.

The results of laboratory tests have been used in the flow modelling in this research in order to identify the potential improvement in well productivity due to laser interaction.

## 5.2 Radial flow diffusivity equation

Radial flow is the appropriate coordinate system to describe flow around wellbore and compare various flow conditions prior and post laser interaction. Radial flow partial differential equation was described by Dake (1978) and Chen, Huan and Ma (2006) as following:

$$\frac{\partial P}{\partial t} = \frac{k}{\varphi \mu c_t}\left(\frac{\partial^2 P}{\partial r^2} + \frac{1}{r}\ \frac{\partial P}{\partial r}\right) \text{-------------------------------------------}(5.1)$$

Where;

$P$ = reservoir pressure

$t$ = time

$r$ = the radius around wellbore

$k$ = reservoir permeability

$\varphi$ = reservoir porosity

$\mu$ = fluid viscosity

$c_t$ = total compressibility

The assumptions of using this equation include homogenous and isotropic porous medium, single phase flow and laminar flow. In addition, the effect of gravity is ignored and it is assumed that fluid property is independent of pressure. gas pseudo-pressure m(p) approach and pressure-squared approximation is considered for gas flow.

This diffusivity equation has been used to build a reservoir flow model and compare flow rates under various improvement area around wellbore due to laser interaction.

## 5.3 Finite difference solution

Finite difference method has been used to solve the partial differential equation in radial coordinates. Figure 5-1 shows a schematic of the radial flow system from reservoir boundary to wellbore at time levels n and n+1.

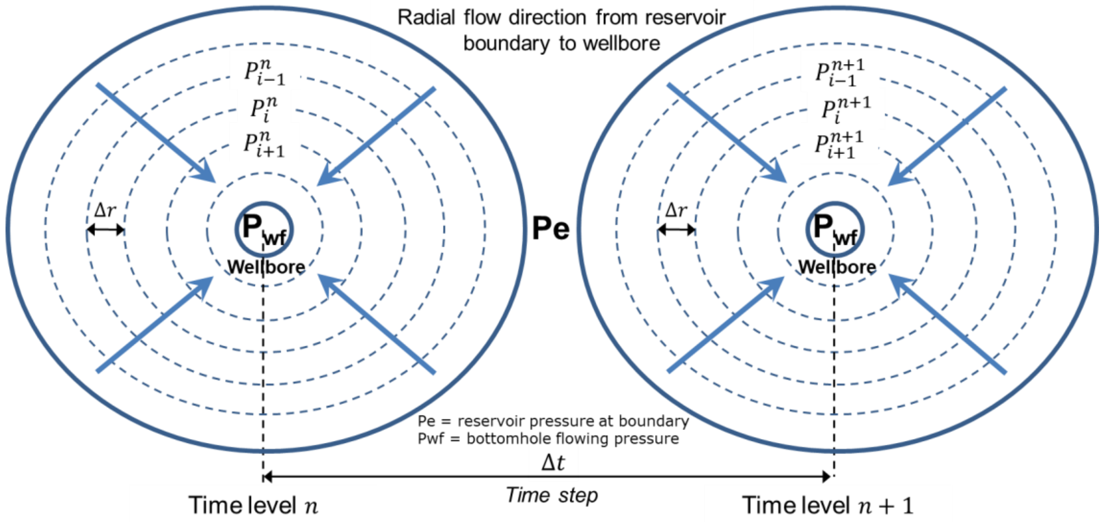


Figure 5-1: Radial flow schematic

The derivatives of partial differential equation can be solved using finite difference solution as following:

The 1st time derivative in radial coordinates:

$$\left[\frac{\partial P}{\partial t}\right]_i = \frac{P_i^{n+1} - P_i^n}{\Delta t} \text{ ------------------------------------------------------(5.2)}$$

The 2nd spatial derivative in radial coordinates:

$$\left[\frac{\partial^2 P}{\partial r^2}\right]_i = \frac{P_{i+1}^n + P_{i-1}^n - 2P_i^n}{\Delta r^2} \text{ ---------------------------------------------(5.3)}$$

The 1st spatial derivative in radial coordinates:

$$\left[\frac{\partial P}{\partial r}\right]_i = \frac{P_i^{n+1} - P_i^n}{\Delta r} \text{ ------------------------------------------------------(5.4)}$$

Substitute the derivatives in the partial differential equation:

$$\frac{P_i^{n+1} - P_i^n}{\Delta t} = \frac{k}{\varphi \mu c_t} \left[ \left( \frac{P_{i+1}^n + P_{i-1}^n - 2P_i^n}{\Delta r^2} \right) + \frac{1}{r} \left( \frac{P_i^{n+1} - P_i^n}{\Delta r} \right) \right] \text{--(5.5)}$$

Rearrange the equation and keep $P_i^{n+1}$ in one side, so the final equation can be written as following:

$$P_i^{n+1} = \frac{\frac{\Delta t}{\Delta r^2} \frac{k}{\varphi \mu c_t} \left[ P_{i+1}^n + P_{i-1}^n - P_i^n \left( 2 + \frac{\Delta r}{r} - \frac{\Delta r^2}{\Delta t} \frac{\varphi \mu c_t}{k} \right) \right]}{\left( 1 - \frac{\Delta t}{r \Delta r} \frac{k}{\varphi \mu c_t} \right)} \text{--------------(5.6)}$$

## 5.4 Wellbore-Reservoir coupling

Pressure diffusion (dissipation) from wellbore to reservoir boundary has been calculated numerically using the partial differential equation and finite difference solution showed in the previous section.

Darcy law has been used as a connection (coupling) between wellbore and reservoir in order to calculate the flow rate relative to pressure change at each time step. Reservoir simulation can be run under either bottomhole flowing pressure control or flow rate control using Well Index (WI), the ratio between flow rate and drawdown as shown in the following Darcy's law for steady-state radial flow condition (Fanchi 2018).

$$WI = \frac{Q_o}{\Delta P} = \frac{0.00708\, k\, h}{\mu_o\, \beta_o\, [ln(r_e/r_w) + S]} \text{------------------------------------(5.7)}$$

Where;

$WI$ = Well Index, bbl/day/psi

$Q_o$ = oil flow rate, bbl/day

$\Delta P$ = pressure change $(p_e - p_{wf})$, psi

$h$ = net reservoir thickness, ft

$\mu_o$ = oil viscosity, cp

$r_w$ = wellbore radius, ft

$k$ = effective reservoir permeability, mD $r_e$ = reservoir drainage radius, ft

$\beta_o$ = oil formation volume factor, RB/STB $S$ = skin factor

The following Darcy's equations are used for liquid and gas under unsteady state and pseudo steady state radial flow conditions (Ahmed 2010).

### 5.4.1 Darcy's law for slightly compressible fluids, liquid

Darcy's law for unsteady state radial flow condition:

$$p_i - p_{wf} = 162.6 \left(\frac{Q_o \beta_o \mu_o}{kh}\right)\left[log\frac{kt}{\varphi\mu c_t r_w^2} - 3.23 + 0.87S\right] \text{-----------(5.8)}$$

Darcy's law for pseudo steady state radial flow condition:

$$Q_o = \frac{0.00708\, kh(p_r - p_{wf})}{\mu_o\, \beta_o \left[ln\frac{r_e}{r_w} - 0.75 + S\right]} \text{-----------------------------------------(5.9)}$$

Where;

$p_i$ = initial reservoir pressure, psi $t$ = flowing time, hr

$p_{wf}$ = bottomhole flowing pressure, psi $\varphi$ = reservoir porosity

$Q_o$ = oil flow rate, bbl/day $c_t$ = total compressibility, psi$^{-1}$

$\beta_o$ = oil formation volume factor, RB/STB $r_w$ = wellbore radius, ft

$\mu_o$ = oil viscosity, cp $r_e$ = reservoir drainage radius, ft

$k$ = reservoir permeability, mD $p_r$ = average reservoir pressure, psi

$h$ = reservoir thickness, ft $S$ = skin factor

### 5.4.2 Darcy's law for compressible fluid, gas

Gas properties change significantly with pressure, Al-Hussainy linearized the flow equation by introducing the gas pseudo-pressure m(p) term, so the equation can be satisfied for gas flow (Ahmed 2010). This term can be solved by numerical integration of the area under the curve of gas pressure function $(2p/\mu_g z)$ at each pressure, where z is gas deviation factor.

Diffusivity equation for radial gas flow, after Al-Hussainy:

$$\frac{\partial m(p)}{\partial t} = \frac{k}{\varphi \mu c_t}\left(\frac{\partial^2 m(p)}{\partial r^2} + \frac{1}{r}\frac{\partial m(p)}{\partial r}\right) \text{------------------------------(5.10)}$$

where;

$$m(p) = \int_0^p \frac{2p}{\mu z} dp \text{------------------------------------------------------(5.11)}$$

There are three solutions to calculate gas flow rate depending on reservoir pressure; the exact m(p) solution, pressure-squared approximation and pressure approximation methods.

Pressure-squared approximation for unsteady state radial gas flow:

$$p_i^2 - p_{wf}^2 = 1637\left(\frac{Q_g T \bar{z}\bar{\mu}}{kh}\right)\left[log\frac{kt}{\varphi \mu_i c_{ti} r_w^2} - 3.23 + 0.87S\right] \text{---------(5.12)}$$

Pressure-squared approximation for pseudo steady state radial gas flow:

$$Q_g = \frac{kh\left(p_r^2 - p_{wf}^2\right)}{1422\, T\bar{\mu}\bar{z}\left[ln\frac{r_e}{r_w} - 0.75 + S\right]} \text{---------------------------------------(5.13)}$$

Where;

$\bar{z}\bar{\mu}$ = gas deviation factor and viscosity at average pressure $\bar{p}$ and;

$\bar{p} = \sqrt{\left(p_i^2 + p_{wf}^2\right)/2}$

$\mu_i c_{ti}$ = gas viscosity and total compressibility at initial reservoir pressure

$Q_g$ = gas flow rate, Mscf/day

$T$ = reservoir temperature, R

## 5.5 Modelling lased zone around wellbore

Laser interaction with formation can create multiple fractures around wellbore, in addition to the potential permeability and porosity improvement in the Heat Affected Zone (HAZ). The improvement in well productivity post laser-interaction could be related to one of the above reasons or a combination of both of them. However, due to the complexity of predicting the actual causes of improvement post laser-interaction, two scenarios have been considered in the reservoir simulation modelling as following:

1. Modelling the improvement in reservoir characteristics due to heat affected zone only using laboratory experimental data. This scenario ignore the actual cuts created in the rock (assuming they will be closed again after interaction) and focus only on the positive effect caused by heat such as dehydration or expansion of various minerals and creating microfractures.

   Table 5-1 shows the results of the experimental work conducted by Batarseh et al. (2012) where 6 kW laser power was applied for 8 seconds into various rock samples and permeability was measured before and after laser. This experimental data is used to model the HAZ in this scenario.

Table 5-1: Permeability improvement due to laser, experimental data (Batarseh et al. 2012)

| Sample | | Unlased | Lased | % of increasing |
|---|---|---|---|---|
| Berea sandstone | High | 7754 | 7914 | 2 |
| | Low | 554 | 674 | 22 |
| Shaly sandstone | Sst | 111 | 301 | 171 |
| Limestone | LS | 0.03 | 0.04 | 33 |
| Shale | SH | 0.43 | 0.55 | 28 |

Note that some of this experimental work was conducted to very high permeability rock samples which typically not good candidates for hydraulic fracturing. However, the ratios of improvement have been used in reservoir simulation rather than the actual values of rock permeability.

The altered area around wellbore (lased zone), is introduced into the simulation model in a form of skin factor. Hawkins equation (Stewart 2011) has been used to calculate the equivalent skin factors for various degree of improvement in reservoir properties and various radius of treatment around wellbore (sensitivity analysis). Skin factor for each laser interaction zone is incorporated into Darcy flow equation.

Hawkins equation is shown below:

$$S = \left( \frac{k}{k_a} - 1 \right) \ ln \ \frac{r_a}{r_w} \text{------------------------------------}(5.14)$$

Where;

$S$ = skin factor

$k$ = reservoir permeability

$k_a$ = altered permeability

$r_a$ = Radius of altered zone around wellbore

$r_w$ = wellbore radius

2. The effect of creating laser induced fractures (laser cutting of various rock thickness) on well productivity has been considered in this scenario. For simplicity, a single fracture, similar to conventional hydraulic fracture, is assumed. The effect of heat on mineralogy (HAZ), and rock types, is not considered in this scenario.

   Effective wellbore radius is used to represent various fracture half-length as following (Temizel et al. 2019):

$$r_{w_{eff}} = \frac{x_f}{2} \text{ -------------------------------------------------- } (5.15)$$

Where;

$r_{w_{eff}}$ = effective wellbore radius

$x_f$ = fracture half-length

## 5.6 Input data and assumptions

Table 5-2 shows the input data, assumptions and sensitivity analyses used in the reservoir simulation modelling.

Table 5-2: Input data and assumptions for reservoir simulation modelling

| Parameter | Symbol | Value | Unit | Remarks |
|---|---|---|---|---|
| Permeability | k | 1.0 | mD | Sensitivity analysis (0.01, 0.1, 1.0, 10.0 mD) |
| Porosity | φ | 10 | % | Sensitivity analysis (5, 10, 20, 30%) |
| viscosity | μ | 0.5 (oil), 0.2 (water), 0.02 (gas) | cp | Average at reservoir condition |
| Total compressibility | Ct | 14.6E-06 (oil), 9.0E-6 (water), 300E-06 (gas) | 1/psi | Average at reservoir condition |
| Drainage radius | re | 100 | m | Sensitivity analysis (100, 200, 250 m) |
| Reservoir drainage area | A | 8 | acres | Sensitivity analysis (8, 31, 49 acres) |
| Wellbore radius | rw | 4.25 | inch | |
| Initial reservoir pressure | Pe | 3000 | psi | Sensitivity analysis (1000, 2000, 3000 psi) |
| Bottomhole flowing pressure | Pwf | 500 | psi | Fixed flowing pressure at wellbore |
| Reservoir thickness (height) | h | 10 | m | Sensitivity analysis (1, 10, 50 m) |
| Oil FVF | ßo | 1.2 | Rb/STB | |
| Reservoir temperature | T | 610 | R | |
| gas deviation factor | z | 0.77 | | Average at reservoir condition |
| Skin (basecase) | S | 0 | | Equivalent skin for each lased zone is calculated and considered in the sensitivity analysis |
| Reservoir boundary condition | | | | Closed system, depletion reservoir, No-Flow boundary condition |

## 5.7 Reservoir simulation results

Reservoir simulation model has been developed and radial flow diffusivity equation is solved using finite difference method. Reservoir flow performance is modelled prior to laser interaction, to represent the base case production, and post laser interaction under various conditions in order to calculate the potential flow improvement for each scenario. Production and pressure performance are modelled under fixed bottomhole flowing pressure.

### 5.7.1 Production forecast prior to laser (basecase)

Figure 5-2 shows the basecase production and reservoir pressure depletion over time for limited reservoir area, 100 m radius, during transient and Pseudo steady state flow conditions.

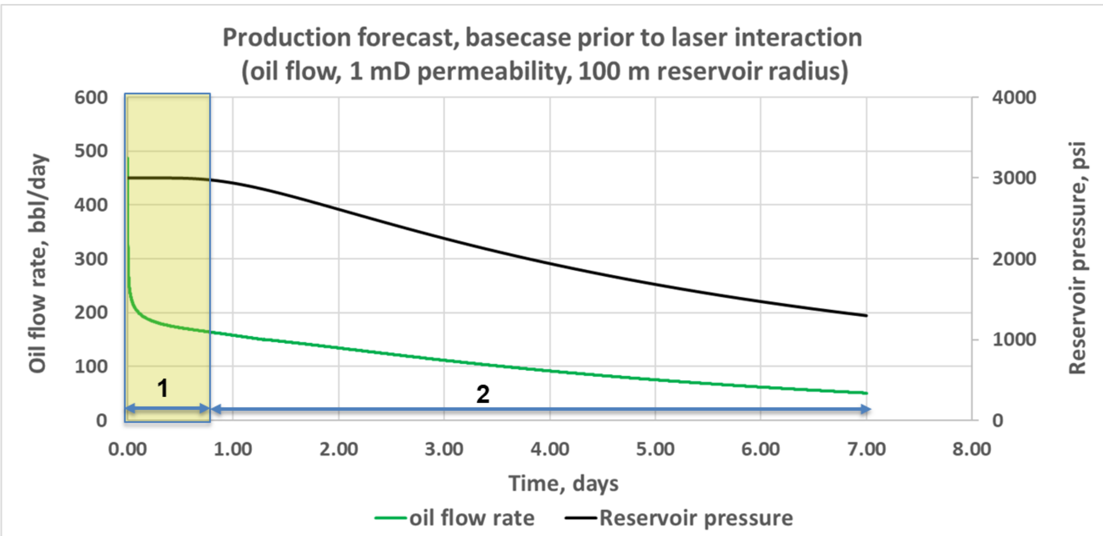


Figure 5-2: Basecase production prior to laser interaction (oil, 1 mD, 100 m reservoir radius)

Period-1 represents the transient (unsteady state) flow condition and period-2 represents the pseudo steady state flow condition when pressure depletion reach reservoir boundary in closed system (No-Flow reservoir boundary condition).

Figure 5-3 shows reservoir pressure distribution overtime from wellbore to reservoir boundary during transient and pseudo steady state flow conditions (basecase, oil, 1 mD reservoir permeability and 100 m reservoir radius). For this scenario, pseudo steady state flow started after approximately 1.0 day of production.

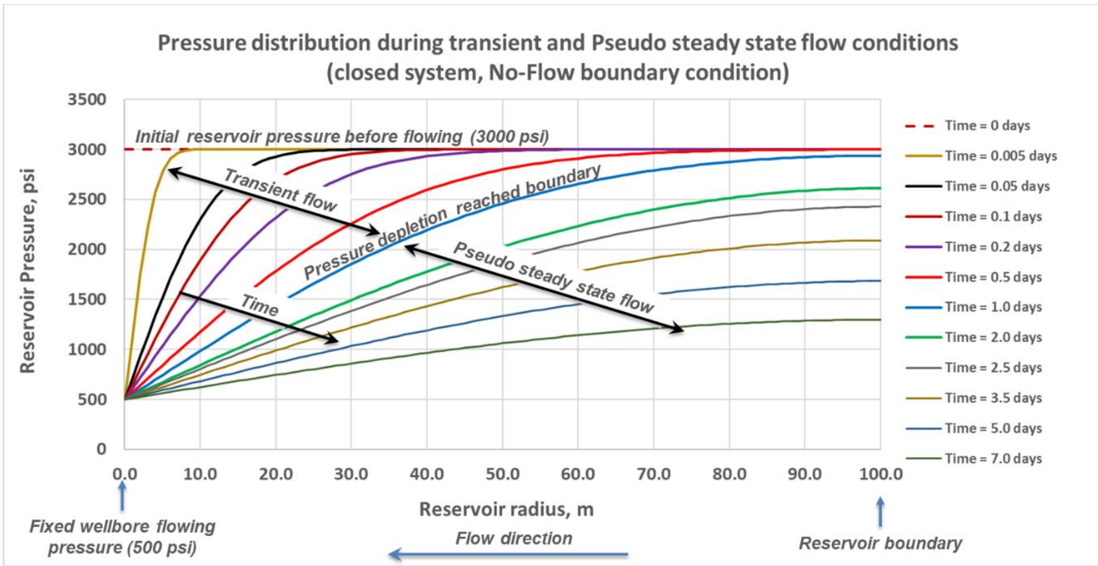


Figure 5-3: Reservoir pressure under transient and pseudo steady flow conditions (basecase, oil, 1 mD, 100 m reservoir radius)

### 5.7.2 Production forecast post laser (HAZ scenario)

This scenario focus on the flow improvement post laser interaction due to the increased permeability in the Heat Affected Zone (HAZ) using the experimental data shown in Table 5-1.

Figure 5-4 and Figure 5-5 show production forecast post laser interaction for sandstone (clean and shaly) and limestone respectively compared to the basecase production (unlased) for oil saturated reservoir, 1.0 mD permeability and 100 m reservoir radius. Sensitivity analysis for radius of laser interaction (area of improvement) around wellbore, 1 – 20 meters, is also considered.

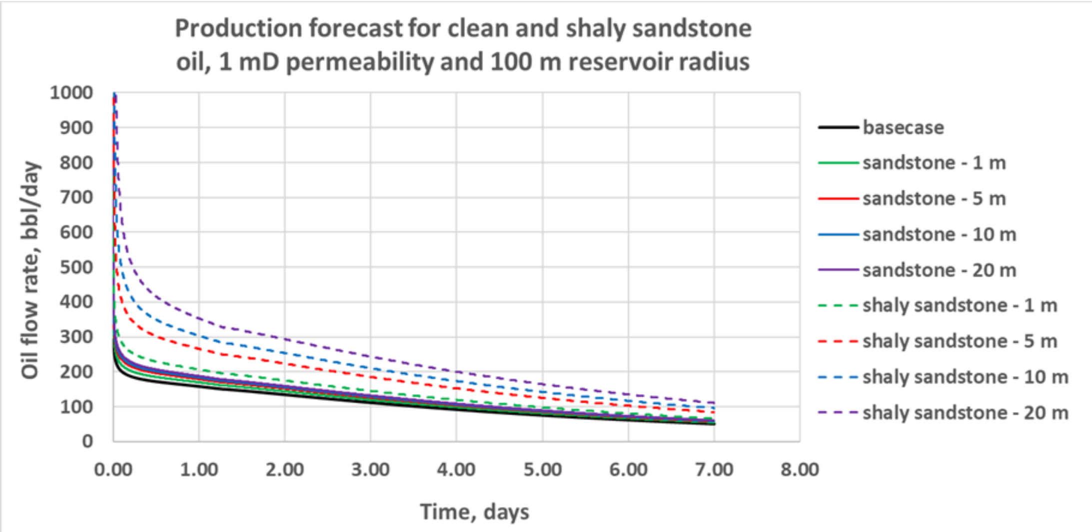


Figure 5-4: production forecast post laser interaction for clean and shaly sandstone (HAZ scenario)

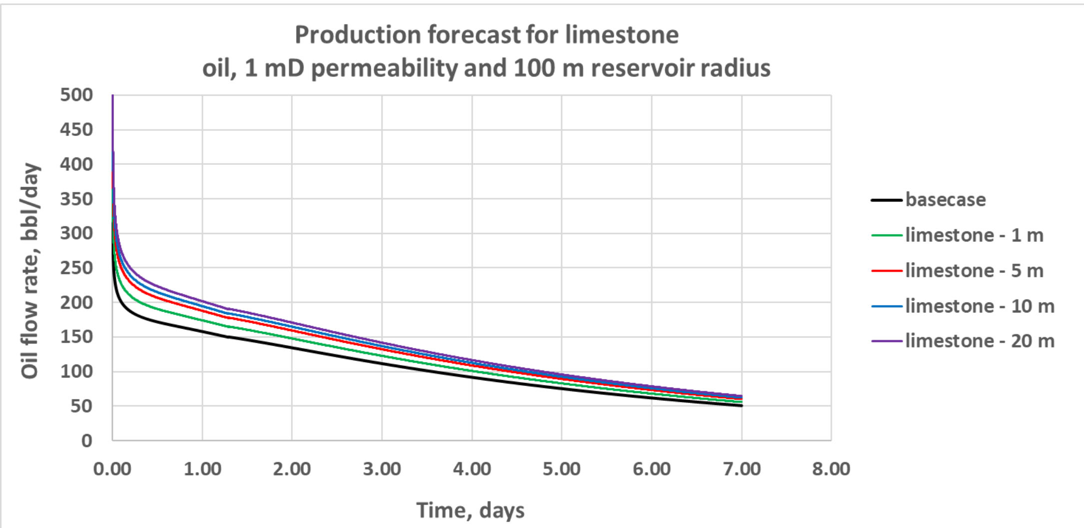


Figure 5-5: Production forecast post laser interaction for limestone (HAZ scenario)

Significant increase in production is observed initially post laser interaction, especially for shaly sandstone reservoir, then depleted overtime due to the limited reservoir volume. Production is sensitive to the area of laser interaction around wellbore.

### 5.7.3 Fold of Increase post laser (HAZ scenario)

Fold of Increase (FOI) is the ratio of improvement (production rate post laser interaction to basecase production prior to laser interaction). For example; FOI of 1.0 means no improvement (exactly the same production as the basecase), and FOI of 2.0 means double production.

Figure 5-6 and Figure 5-7 show the calculated FOI overtime during transient and pseudo steady state flow conditions for sandstone and limestone respectively (oil saturated reservoir, 1.0 mD permeability, 100 m reservoir radius and laser interaction radius sensitivity analysis).

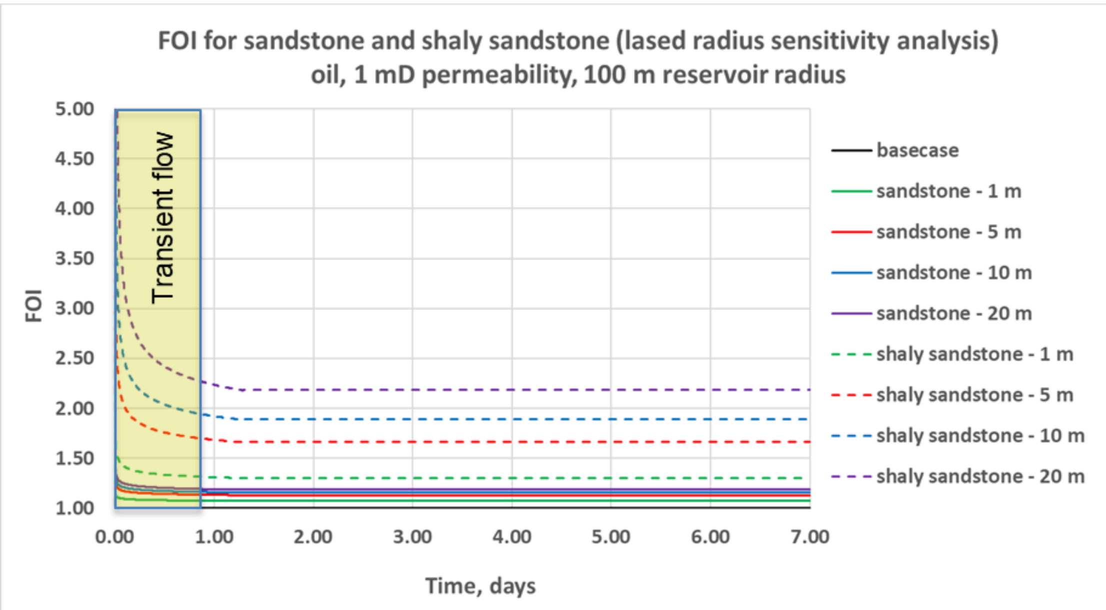


Figure 5-6: Fold of Increase overtime for clean and shaly sandstone (HAZ scenario)

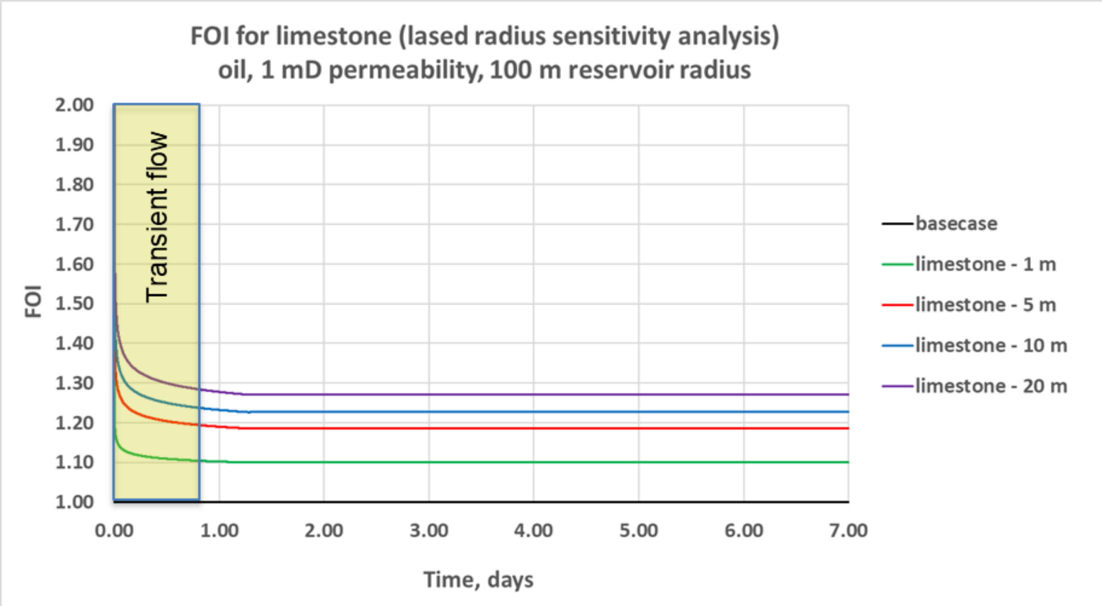


Figure 5-7: Fold of Increase overtime for limestone (HAZ scenario)

The results indicated a very high FOI during transient flow (over 5), then decreases overtime and stabilized at pseudo steady-state flow condition.

The results also indicated a significant flow improvement in shaly sandstone compared to clean sandstone and limestone formations, due to the significant improvement in permeability post laser interaction for shaly sandstone which shown in Table 5-1 and considered in this modelling scenario. This high FOI for shaly sandstone, as well as the high permeability post laser interaction showed in the experimental data, could be due to clay dehydration, water evaporation and microfractures.

Figure 5-8 shows the stabilized FOI at pseudo steady state flow condition for various rock types and various radius of laser interactions.

Shaly sandstone showed good improvement, approximately 2.2 FOI (over double production) under pseudo steady state flow condition for 20 m lased radius around wellbore. Sandstone and limestone showed limited improvement (1.2 - 1.3 FOI) compared to shaly sandstone under the same radius of laser interaction of 20 m. This results reflect the experimental data (Table 5-1) used in this modelling scenario, where significant improvement in permeability post laser interaction was indicated for shaly sandstone compared to clean sandstone and limestone rocks.

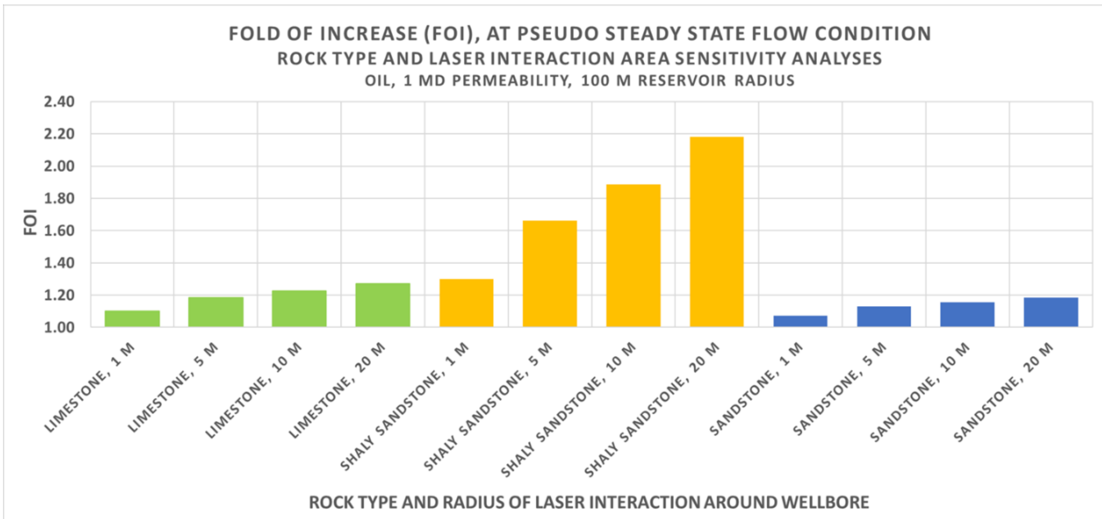


Figure 5-8: Fold of Increase at pseudo steady state flow condition (HAZ scenario)

### 5.7.4 Sensitivity analyses (HAZ scenario)

Sensitivity analyses for various reservoir properties have been conducted including reservoir size, permeability, porosity, pressure, thickness and fluid saturation.

Figure 5-9 shows reservoir size sensitivity analysis (100 - 250 m reservoir radius) at pseudo steady state flow condition for various rock types and various laser treatment areas around wellbore (oil saturated rock and 1 mD reservoir permeability).

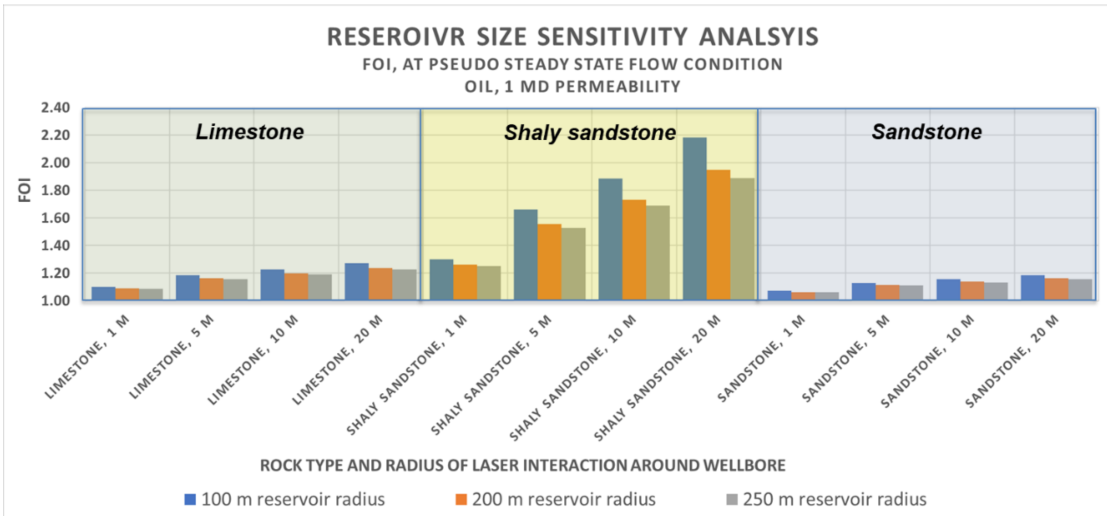


Figure 5-9: Reservoir size sensitivity analysis (HAZ scenario)

FOI decreases with increasing reservoir size at any particular laser treatment area around wellbore. Large reservoir size would require relatively large laser treatment area comparted to small reservoirs in order to achieve similar FOI. The effect of reservoir size is minor for sandstone and limestone rocks but relatively high for shaly sandstone.

Figure 5-10 shows reservoir permeability sensitivity analysis (0.01 – 10 mD) during transient and pseudo steady state flow conditions for shaly sandstone and 20 m lased zone radius around wellbore (oil saturated rock, 10% porosity and 100 m reservoir radius).

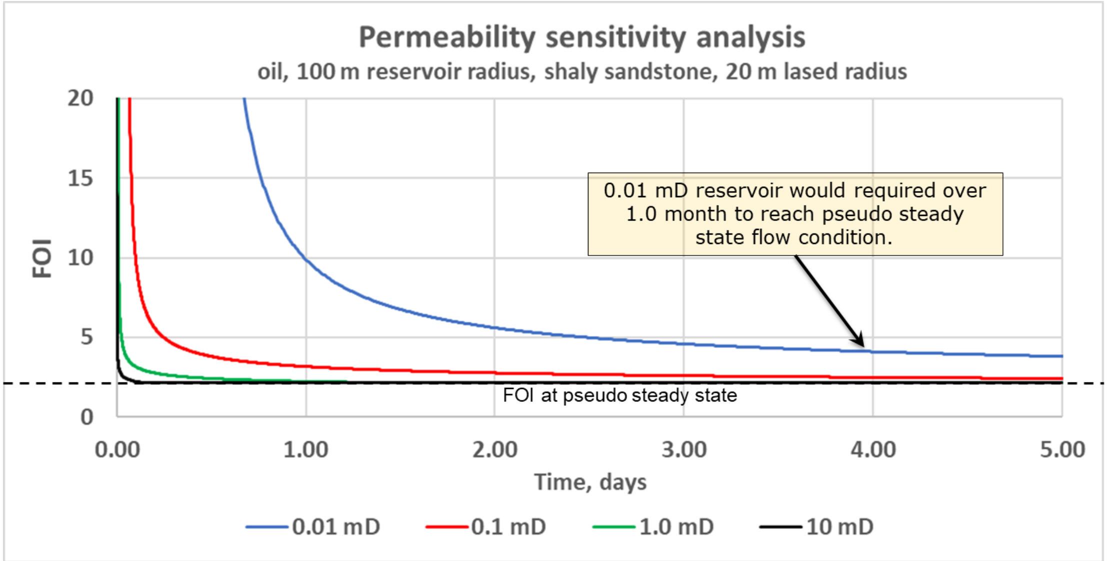


Figure 5-10: Reservoir permeability sensitivity analysis (HAZ scenario)

Significant FOI is observed during transient flow for low permeability reservoirs compared to higher permeability reservoirs. Once pseudo steady-state flow condition is reached, the effect of reservoir permeability diminished and similar FOI for all reservoir permeabilities established.

As shown in Figure 5-10, high permeability reservoirs reach pseudo steady state flow condition in short time compared to low permeability reservoirs. For this particular case, 0.01 mD reservoir would require more than 1.0 month to reach pseudo steady state flow condition.

Figure 5-11 shows reservoir porosity sensitivity analysis (5 – 30%) during transient and pseudo steady state flow conditions for shaly sandstone and 20 m lased zone radius around wellbore (oil saturated rock, 1.0 mD permeability and 100 m reservoir radius).

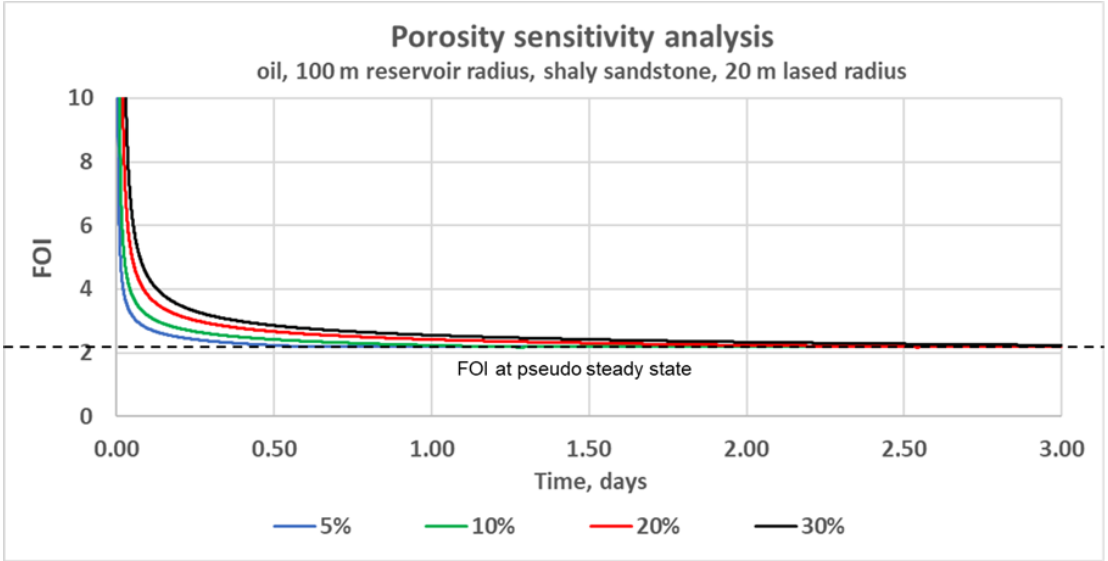


Figure 5-11: Reservoir porosity sensitivity analysis (HAZ scenario)

Low porosity reservoirs reach pseudo steady-state faster than high porosity reservoirs due to the limited porous volume and faster pressure depletion accordingly. Significant FOI is observed during transient flow for higher porosity reservoirs compared to lower porosity reservoirs. Once pseudo steady-state flow condition is reached, the effect of porosity diminished and similar FOI for all reservoir porosities established.

Figure 5-12 shows sensitivity analyses for reservoir pressure and thickness for shaly sandstone, oil saturated, 1.0 mD permeability, 10% porosity, 100 m reservoir radius and 20 m lased zone radius.

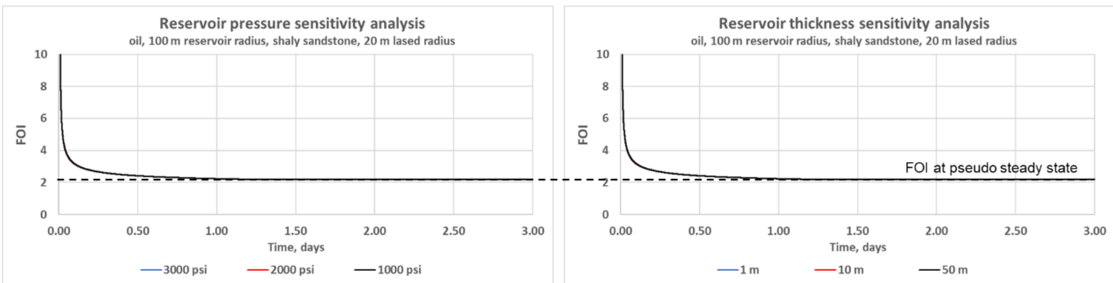


Figure 5-12: Reservoir pressure and thickness sensitivity analyses (HAZ scenario)

Higher reservoir pressure and thickness can definitely yield higher flow rate. However, the ratio of improvement post laser interaction (FOI) is identical for various reservoir pressures and various reservoir thicknesses during both transient and pseudo steady-state flow conditions.

Fluid saturation sensitivity analysis is conducted and the results showed similar Fold of Increase (FOI) for all fluid types exist in porous media including oil, gas and water. Figure 5-13 shows gas flow rate post laser interaction compared to the basecase gas rate prior to laser interaction (1.0 mD permeability and 100 m reservoir radius). Significant improvement in gas flow rate is observed for shaly sandstone compared to clean sandstone formation.

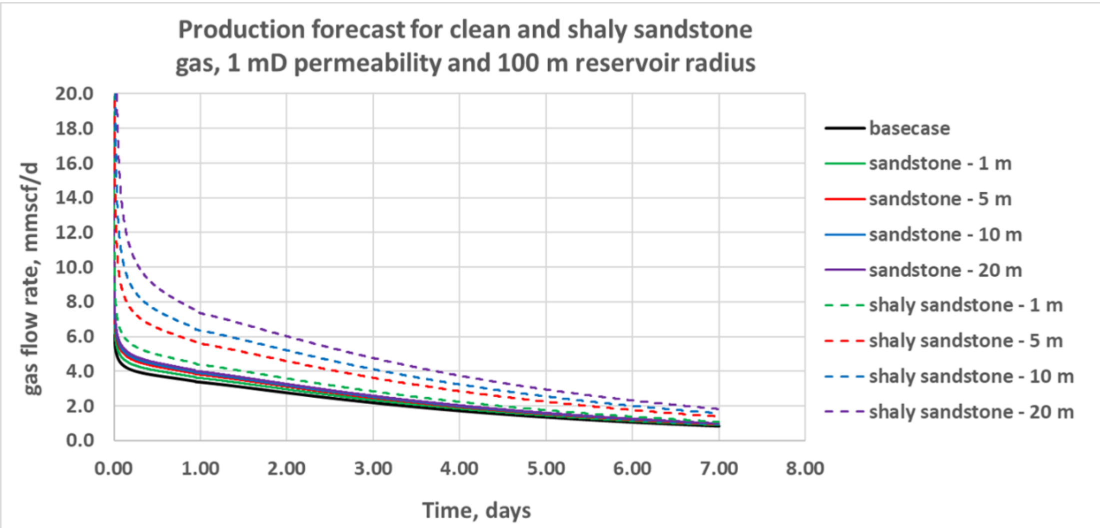


Figure 5-13: Fluid saturation sensitivity analysis (HAZ scenario)

### 5.7.5 Equivalent skin post laser (HAZ scenario)

Table 5-3 shows summary of the potential Fold of Increase (FOI) and equivalent skin factor could be achieved post laser interaction including rock type, reservoir size and radius of lased zone sensitivity analyses at pseudo steady state flow condition. Other reservoir characteristics including permeability, porosity, thickness, pressure and fluid saturation showed similar FOI at pseudo steady-state flow condition.

Equivalent skin factor post laser interaction for shaly sandstone reservoirs can exceed -3. This value is within the typical range of equivalent skin could be achieved post conventional matrix stimulation including acidizing and hydraulic fracturing techniques.

Table 5-3: Equivalent skin and FOI summary (HAZ modelling)

| Reservoir radius, m | Reservoir area, acre | Rock type | Limestone | | | | Shaly sandstone | | | | Sandstone | | | |
|---|---|---|---|---|---|---|---|---|---|---|---|---|---|---|
| | | Radius of lased zone, m | 1 | 5 | 10 | 20 | 1 | 5 | 10 | 20 | 1 | 5 | 10 | 20 |
| | | Equivalent skin factor | -0.55 | -0.95 | -1.12 | -1.30 | -1.40 | -2.42 | -2.86 | -3.29 | -0.40 | -0.69 | -0.82 | -0.94 |
| 100 | 8 | FOI | 1.10 | 1.19 | 1.23 | 1.27 | 1.30 | 1.66 | 1.89 | 2.18 | 1.07 | 1.13 | 1.16 | 1.18 |
| 200 | 31 | | 1.09 | 1.16 | 1.20 | 1.24 | 1.26 | 1.56 | 1.73 | 1.95 | 1.06 | 1.11 | 1.14 | 1.16 |
| 250 | 49 | | 1.09 | 1.16 | 1.19 | 1.23 | 1.25 | 1.53 | 1.69 | 1.89 | 1.06 | 1.11 | 1.13 | 1.16 |

### 5.7.6 Production forecast post laser (laser induced fractures scenario)

This scenario focus on modelling the created fractures only and ignores the effect of heat on rock characteristics around the fractures (HAZ), so this scenario is not sensitive to rock type. For simplicity a single fracture (two cuts in opposite directions around wellbore) is considered.

Figure 5-14 shows production forecast post laser interaction compared to basecase production (unlased) for oil saturated reservoir, 1.0 mD permeability and 100 m reservoir radius. Sensitivity analysis for laser induced fracture half-length, 1 – 20 meters, is also considered.

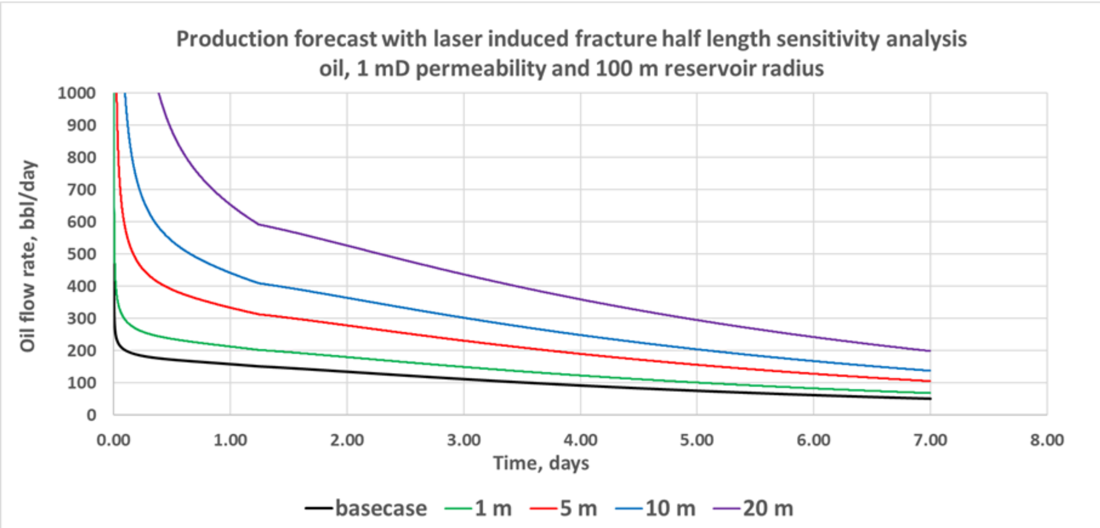


Figure 5-14: Production forecast post laser interaction (laser induced fractures scenario)

Significant increase in production is observed post laser interaction during both transient and pseudo steady state flow conditions. Production enhancement is sensitive to the created fracture half-length.

### 5.7.7 Fold of Increase post laser (laser induced fractures scenario)

Figure 5-15 shows the calculated Fold of Increase (FOI) overtime during transient and pseudo steady state flow conditions (oil saturated reservoir, 1.0 mD permeability, 100 m reservoir radius and fracture half-length sensitivity analysis).

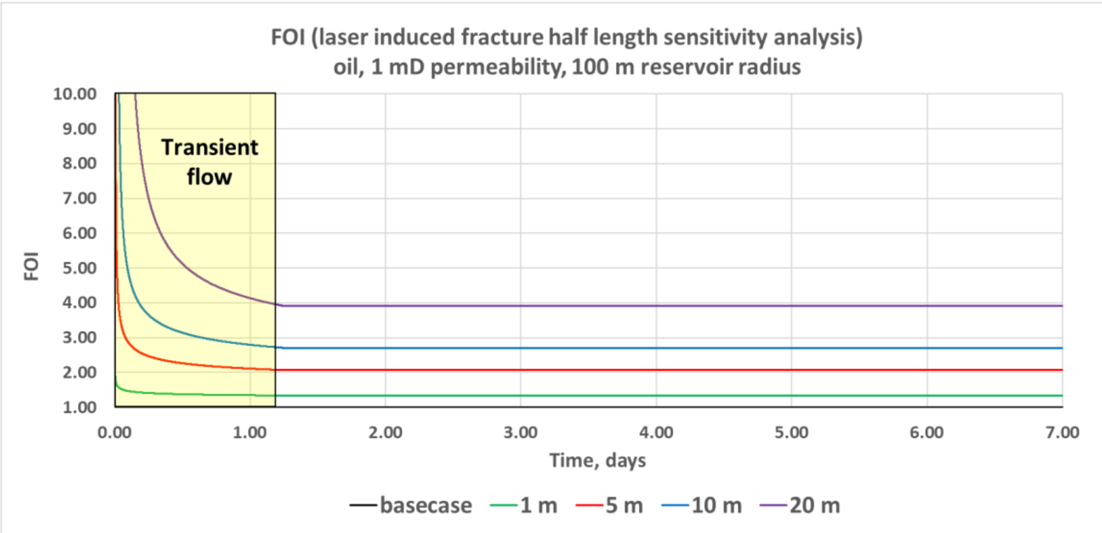


Figure 5-15: Fold of Increase overtime (laser induced fractures scenario)

The results showed a very high FOI during transient flow (over 10), then decreases overtime and stabilized at pseudo steady-state flow condition.

Figure 5-16 shows the stabilized FOIs at pseudo steady state flow condition for various laser induced fracture half-length. Approximately 4.0 FOI could be achieved with 20 m fracture half-length under pseudo steady state flow condition.

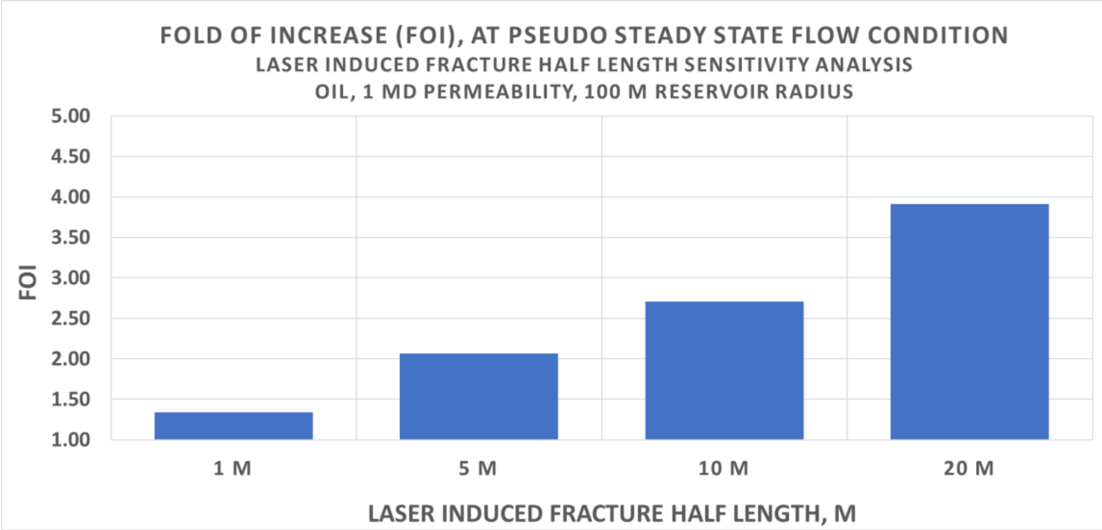


Figure 5-16: Fold of Increase at pseudo steady state flow condition (laser induced fractures scenario)

### 5.7.8 Sensitivity analyses (laser induced fractures scenario)

Sensitivity analyses have been conducted to all reservoir characteristics, similar to the sensitivity analyses conducted and presented in the HAZ scenario, including permeability, porosity, pressure, thickness, reservoir size and fluid saturation.

The same findings observed and presented in the HAZ scenario are also observed in the laser induced fractures scenario. In order to avoid repetition, only permeability sensitivity analysis is presented in this section as shown in Figure 5-17.

Low permeability reservoirs can yield much higher fold of increase compared to high permeability reservoirs during transient flow condition. Once pseudo steady state flow condition is reached, the effect of reservoir permeability diminished and same FOI for all reservoir permeabilities established. Note that low permeability reservoirs can be produced under transient flow condition for long period of time (months or years) and accordingly an appreciated volume of oil and gas could be achieved.

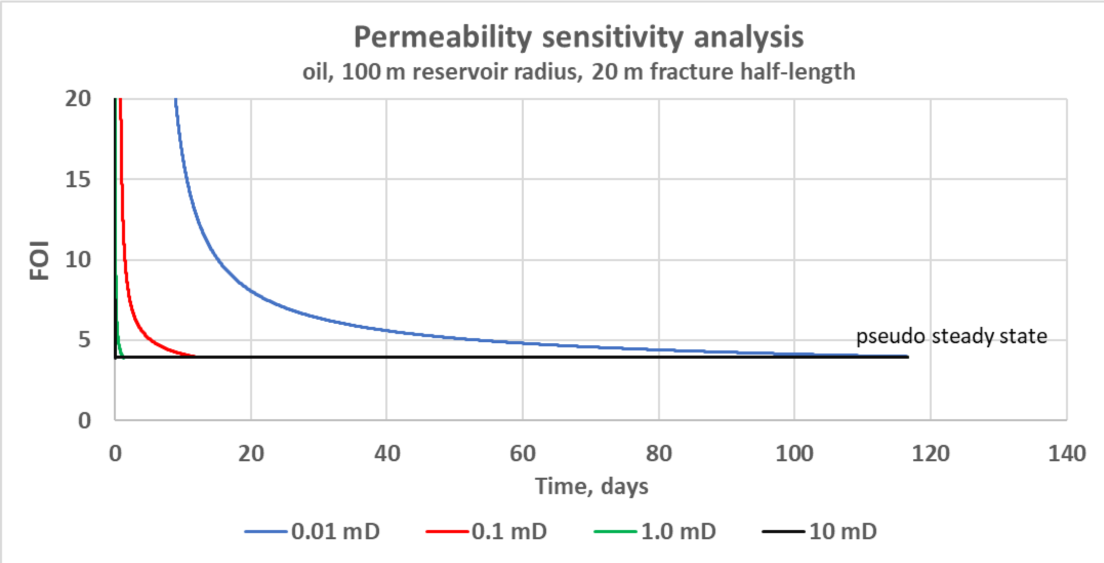


Figure 5-17: Reservoir permeability sensitivity analysis (laser induced fractures scenario)

### 5.7.9 Comparison between HAZ and laser induced fractures scenarios

The same findings are observed in the sensitivity analyses of both scenarios as shown in the previous sections. The only difference is that laser induced fractures can yield much higher Fold of Increase (FOI) during both transient and pseudo steady state flow conditions compared to Heat Affect Zone (HAZ) scenario.

Table 5-4 shows a comparison between the potential FOI could be achieved at pseudo steady state flow condition for HAZ and laser induced fractures scenarios with various depth of laser treatment around wellbore (100 m reservoir radius).

Table 5-4: Comparison between HAZ and laser induced fractures scenarios

| depth of laser treatment around wellbore, (radius of HAZ or fracture half-length) | | 1 m | 5 m | 10 m | 20 m |
|---|---|---|---|---|---|
| FOI related to HAZ | Shaly sandstone | 1.3 | 1.66 | 1.89 | 2.18 |
| | Limestone | 1.1 | 1.19 | 1.23 | 1.27 |
| | Sandstone | 1.07 | 1.13 | 1.16 | 1.18 |
| FOI related to laser induced fractures | Any rock type | 1.34 | 2.07 | 2.71 | 3.91 |

As shown, approximately 4.0 FOI can be achieved with single laser induced fracture of 20 m (on each side of the wellbore) compared to 2.2 FOI for HAZ scenario. Much higher FOIs are observed during transient flow specially for low permeability reservoirs (can exceed 20 FOI). Note that significantly higher FOI can be achieved if multiple laser induced fractures (network) are successfully created around wellbore.

## 5.8 Laser induced fractures and power requirements

Laser powers required to create various fracture half-lengths are calculated using the analytical model and methodology suggested in this research. The equivalent Fold of Increases (FOIs) post laser interaction are also calculated using reservoir simulation laser induced fractures scenario.

Figure 5-18 shows the FOIs could be achieved under pseudo steady state flow condition by creating single fracture (1 – 20 m on each side of the wellbore) and the laser power required to create each fracture length for sandstone and limestone rocks assuming cutting by melting, 0.2 Peclet number (1 mm kerf width, 1.45 and 0.73 m/hr cutting speed for sandstone and limestone respectively), 15% porosity, oil saturated rock and 100 m reservoir radius.

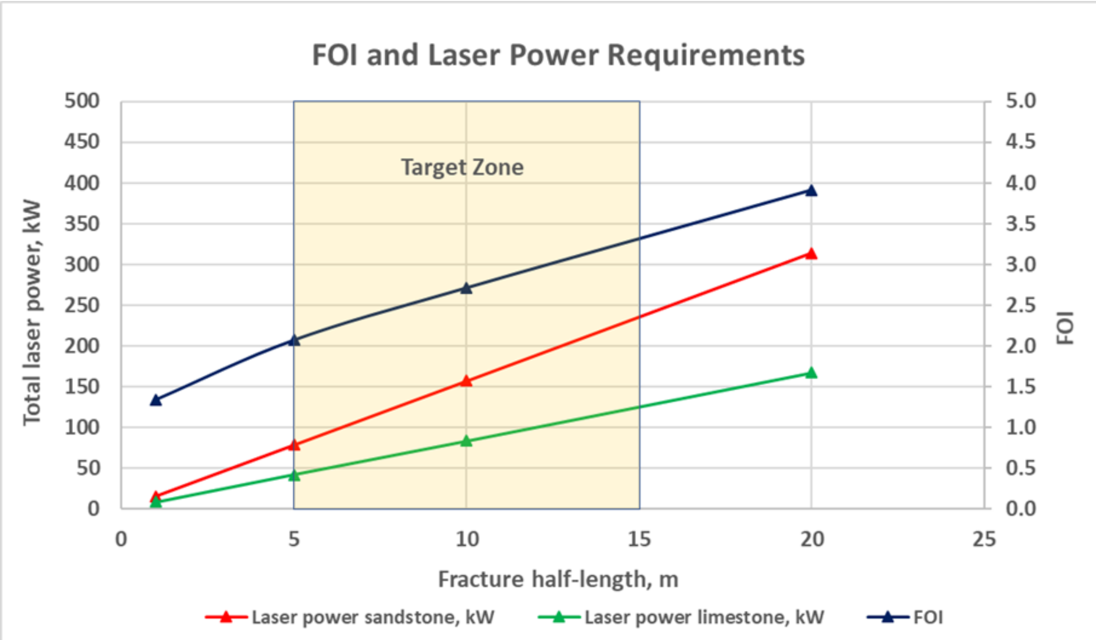


Figure 5-18: FOI and laser power requirements

An average of 10 m (target zone 5 – 15 m) fracture half-length could be achieved with 100 kW (range of 50 – 100 kW) average laser power depending on rock type, mineralogy and porosity. This power is within the available capacity of laser technology, and approximately 2 – 3 FOI in well productivity could be achieved.

## 5.9 Summary and limitations of reservoir simulation modelling

This section includes a summary of the main findings and also discussion about model limitations and the results presented in this chapter.

The main findings of the reservoir simulation model can be summarized as following:

1. The aim of reservoir simulation model is to calculate the potential Fold of Increase (FOI), ratio of flow improvement, due to laser interaction with porous media around wellbore under various reservoir conditions and various radius of laser interaction.

2. Reservoir simulation model has been developed using radial flow partial differential equation (diffusivity equation). The equation is solved numerically using finite difference solution.

3. Sensitivity analyses have been conducted to rock type, fluid saturation, reservoir permeability, porosity, pressure, thickness, drainage area (reservoir size), as well as the radius of laser interaction around wellbore.

4. Two approaches are considered in modelling the lased zone around wellbore including Heat Affected Zone (HAZ) and laser induced fractures.

5. The results of reservoir simulation model showed significant improvement in well productivity for shaly sandstone compared to clean sandstone and limestone reservoirs. This high FOI could be due to clay dehydration, water evaporation and microfractures created in the HAZ.

6. Significant Fold of Increase (FOI) is observed during transient flow, then FOI decreases overtime and stabilized at pseudo steady-state flow condition.

7. Very high FOI is observed during transient flow for low permeability and high porosity reservoirs. However, once pseudo steady-state flow condition is reached, the effect of reservoir permeability and porosity diminished and FOI stabilized.

8. Similar FOI is observed for various fluid saturations, reservoir pressures and thicknesses. However, FOI is sensitive to reservoir size where relatively large lased zone would be required to achieve high FOI in large reservoirs.

9. The range of FOIs and equivalent skin observed during transient and pseudo steady state post laser treatment is similar to the potential improvement could be achieved by conventional matrix stimulation including acidizing and hydraulic fracturing techniques.

10. An average of 10 m fracture half-length could be achieved with 100 kW average laser power depending on rock type, mineralogy and porosity and this can yield approximately 2 – 3 FOI in well productivity. This power requirements are within the available capacity of laser power technology as shown in the literature review section.

The following is a discussion about the limitations of the reservoir simulation model developed in this research and the results presented in this chapter:

1. The reservoir simulation model developed in this research is a simple radial flow model assuming homogenous and isotropic porous medium, single phase, laminar flow, no gravity effect and fluid property is independent of pressure. This model might not be suitable

for complex structures and flow conditions such as multiphase flow in multilayer reservoir system. However, the model is sufficient for the purpose of this research to determine the ratio of improvement (FOI) by comparing flow rates pre and post treatment under various conditions.

2. Laser does not have a direct effect in the production results since the simulation results are merely based on the altered permeability around wellbore (representing HAZ) or effective wellbore radius (representing fracture half-length).

3. For simplicity, single fracture was assumed to model the laser induced fractures scenario. However, fracture network can be created around wellbore by applying the laser induced fracture technique proposed in this research and accordingly the results presented in this chapter regarding the potential Fold of Increase post laser might be underestimated.

4. Zero skin was assumed as initial condition (basecase) prior to laser treatment. If positive skin due to formation damage during drilling and completion exist, laser treatment would yield significantly higher FOIs compared to the results shown in this chapter.

# Chapter 6: Conclusions and recommendations

This chapter provides a brief summary of the work done and the main findings in this research including literature review, laser cutting and reservoir simulation modeling. Also contribution to knowledge and recommended future work are concluded.

## 6.1 Summary

### 6.1.1 Literature review

The researches and studies conducted in the past regarding the using of laser in oil industry are limited to perforation and drilling applications. They are still under researching phase and have not been implemented in oil industry. The existing laser applications in oil industry is limited to fiber-optic downhole temperature sensing (monitoring).

Numerous numerical models were developed in the past to simulate temperature distribution during laser material processing. The majority of them focused on metals (non-porous material) and therefore there is a lack of literature regarding the modelling of laser material processing in porous media. A simulation model which is more relevant to the proposed application has been developed and discussed in this research.

Many laboratory experiment work was conducted to various rock types and significant improvement in rock porosity and permeability due to laser interaction was observed. Microfractures were also observed in the heat affected zone due to quartz expansion, clay dehydration and limestone dissociation. These results has been considered in the reservoir simulation modelling in this research.

Laser technology screening was conducted in this research and indicated that CO2 gas laser could be the most suitable laser type for the proposed laser induced fracture application. It can provide a continuous wave power greater than 100 KW.

### 6.1.2 Laser power modelling

Laser power modelling has been developed in this research using analytical and numerical solutions. Based on the results of those models and the verification work conducted with experimental data, a methodology has been developed and proposed to simply calculate laser power using the new waste power correlation developed in this research without the needs to develop complex numerical models.

The following is a brief summary of the analytical model findings:

Energy balance equation (Powell et al. 1994) and waste power correlation (Prusa, Venkitachalam and Molian 1999) are used to develop an analytical model for laser power calculations. Porosity and fluid saturation exist in porous media are incorporated into the analytical model using effective thermal property concept.

A methodology to model fluid phase changing during laser interaction including temperature and latent heat of vaporization for fluids exist in porous media under downhole condition using phase diagrams is developed.

Cutting by vaporization is suggested in this research in order to avoid the complex kerf cleaning operation under downhole condition. However, it may require significantly higher laser power compared to cutting by melting technique (approximately 4 times).

Laser power is sensitive to rock type and porosity more than the fluids exist in porous media. Laser power significantly decreases with increasing porosity and limestone rock requires significantly lower power than sandstone. The effect of fluids in porous media is minimal, however, water requires slightly more power compared to oil and gas.

The following is a brief summary of the numerical model findings:

Partial differential equation for transient heat transfer in cylindrical and axial coordinates is used to numerically calculate the waste energy during laser cutting and the equation is solved using finite difference solution. Porosity and fluid saturations are incorporated into the model using effective thermal properties (volumetric average).

Melting fraction concept is considered to represent the melting progression of the rock during heat transfer and in similar manner, vaporization fraction is considered to represent the vaporization progression of the liquids exist in porous media during heat transfer.

Two scenarios for the dynamic heat source boundary conditions including line-source and point-source are suggested and considered in modeling heat transfer into surrounding in this research in order to identify the optimum scenario for various laser processing including cutting by melting and vaporization techniques.

Models are verified by experimental data and numerical model showed better matching with experimental data than analytical model. Numerical line-source model showed better matching for cutting by melting while point-source model showed better matching for cutting by vaporization.

A new and simple correlation is developed and suggested in this research in order to analytically calculate laser waste power as a function of useful power and Peclet number without the need to build complex numerical models. This correlation is developed from the verified numerical line-source model which showed good matching for cutting by melting for metals and non-metals.

The results of laser power modeling indicated that 100 kW laser power is capable to cut a range of 5 – 15 m (average of 10 m) of porous material depending on rock porosity and thermal properties.

### 6.1.3 Reservoir simulation modelling

Reservoir simulation model is developed using radial flow partial differential equation (diffusivity equation) and the equation is solved numerically using finite difference solution. Sensitivity analyses are conducted to rock type, fluid saturation, reservoir permeability, porosity, pressure, thickness, reservoir size and the radius of laser interaction around wellbore.

Two approaches are considered in modelling the lased zone around wellbore including Heat Affected Zone (HAZ) and laser induced fractures. Significant

Fold of Increase (FOI) is observed during transient flow, then FOI decreases overtime and stabilized at pseudo steady-state flow condition.

Significant improvement in well productivity is observed for shaly sandstone compared to clean sandstone and limestone reservoirs. Also very high FOI is observed during transient flow for low permeability and high porosity reservoirs.

The range of FOIs and equivalent skin observed during transient and pseudo steady state post laser treatment is similar to the potential improvement could be achieved by conventional matrix stimulation including acidizing and hydraulic fracturing techniques.

An average of 10 m fracture half-length could be achieved with 100 kW average laser power depending on rock type, mineralogy and porosity and this can yield approximately 2 – 3 FOI in well productivity. This power requirements are within the available capacity of laser technology.

## 6.2 Contributions to knowledge

This research contributes to the existing knowledge of laser material processing as following:

1. The appropriate and more relevant analytical and numerical models which represent the actual physics of laser cutting process of thick and porous material have been developed. The existing laser material processing focus on modelling laser cutting of very thin metals.

2. Modification to heat balance equation is considered by incorporating melting and vaporization fraction concept into the partial differential equation to model phase changing progression during laser cutting.

3. Latent heat was not considered (or not clearly presented) in many of the numerical models developed in the past to simulate temperature distribution during laser processing. However, latent heat of fusion and vaporizations has been incorporated into the analytical and numerical models and clearly presented in this research.

4. New waste power's correlation and methodology have been developed and suggested in this research to analytically calculate laser power requirements without the needs of developing complex numerical models.

5. Two boundary conditions including line-source and point-source are suggested and considered in this research in order to represent the actual physics of the dynamic heat source during laser cutting. The suitable application of each boundary condition is identified.

6. Cutting by vaporization is suggested and considered in this research. The existing laser cutting applications focus on cutting by melting.

7. Although the objectives of this research is to use laser induced fracture as an alternative fracturing technique in oil industry, the methodology and results of this research can also be used in other industries and applications including medical and material processing.

## 6.3 Recommendations for future work

1. The experimental work conducted to porous media in the past was limited to creating very short cuts or measuring the effect of heat in changing mineralogy. It is recommended to conduct intensive experimental work for creating deep fractures in porous media using high laser power.

2. The challenges and operational concerns of using laser technology under downhole condition including footprint, cooling, cleaning, etc. are not considered in this research. It is recommended to conduct more investigation about the suitable laser technology could be used for the proposed application and any potential modifications to laser equipment could be considered to achieve the target.

3. Two boundary conditions for laser dynamic heat source were considered in this research including line-source and point-source models. The suitability of each model with various cutting conditions was verified with experimental data. However, The maximum material thickness used in the verification work was 60 mm. More investigation is recommended to verify the boundary conditions for very thick material, assuming high laser power technology will allow experimental tests for cutting very thick material in future.

4. In order to establish a strong link between laser and flow simulation modelling, it is recommended to model the thermal induced stresses in the rock caused by heat transfer into surrounding during laser cutting (temperature distribution), then develop a correlation

between the thermal stresses, micro-fractures density and flow enhancement.

5. Clean cuts (fractures) post laser cutting are assumed in the reservoir flow simulation in this research which is a valid assumption in case of proper and efficient cleaning during cutting by melting. However, for cutting by vaporization, there is a risk of material solidification inside porous media which may cause blocking or restriction to flow. More investigation and modelling is recommended regarding the negative effect on flow performance due to the potential material solidification could be formed inside porous media during cutting by vaporization.

6. Rock properties including Young's Modulus, Shear Modulus and Bulk Modulus could be significantly reduced after laser interaction as shown in the experimental work presented in the literature review section. It is recommended to study the effect of laser in reducing rock strength and the potential risk of induced sand production accordingly.

# References


AHMED, T., 2010. *Reservoir engineering handbook.* 4th ed. Elsevier.

ARNOLD, K. and STEWART, M., 2008. *Surface production operations - design of oil handling systems and facilities, volume 1.* 3rd ed. Elsevier.

ASHRAE, 2017. *2017 ASHRAE handbook - fundamentals.* SI ed. American Society of Heating, Refrigerating and Air-Conditioning Engineers, Inc. (ASHRAE).

BATARSEH, S. et al., 2003. Well perforation using high-power lasers. *SPE Annual Technical Conference and Exhibition*, pp.10

BATARSEH, S.I. et al., 2012. High power laser application in openhole multiple fracturing with an overview of laser research; past, present and future. *SPE Saudi Arabia Section Technical Symposium and Exhibition*, pp.10

BATARSEH, S.I., GAHAN, B.C. and SHARMA, B., 2005. Innovation in wellbore perforation using high-power laser*. International Petroleum Technology Conference*, pp.7

BAZARGAN, M. et al., 2012. Using the laser irradiation to improve the rate of production of Iran south west formation*. SPE Kuwait International Petroleum Conference and Exhibition*, pp.7

BENNETT, C.O. and MYERS, J.E., 1983. *Momentum, heat and mass transfer.* 3rd ed. McGraw-Hill, Chemical engineering series.

BRITISH BROADCASTING CORPORATION (BBC), *Fracking halted after government pulls support, 2nd November 2019.* [online] Available from: https://www.bbc.co.uk/news/business-50267454 2019

CARSTENS, J.P. and BROWN, C.O., 1971. Rock cutting by laser*. Fall Meeting of the Society of Petroleum Engineers of AIME*, pp.11

CHEN, Z., HUAN, G. and MA, Y., 2006. *Computational methods for multiphase flows in porous media.* Society for Industrial and Applied Mathematics.

CIBSE, 2015. *Environmental design - CIBSE guide A.* 8th ed. CIBSE.

COKER, A.K., 2007. *Ludwig's applied process design for chemical and petrochemical plants, volume 1.* 4th ed. Elsevier.

DA SILVA, M.G. et al., 2017. Application of lasers for perforation of petroleum wells*. OTC Brasil*, pp. 16

DAKE, L.P., 1978. *Fundamentals of reservoir engineering.* Elsevier.

ERFAN, M.R. et al., 2010. Drilling of Middle-Eastern reservoir carbonate rocks by high power ND:YAG laser*. IADC/SPE Asia Pacific Drilling Technology Conference and Exhibition*, pp.9

FANCHI, J.R., 2018. *Principles of applied reservoir simulation.* 4th ed. Elsevier.

FU, C.H., GUO, Y.B. and SEALY, M.P., 2014. A predictive model and validation of laser cutting of nitinol with a novel moving volumetric pulsed heat flux*. Journal of Materials Processing Technology*, 214(12), pp. 2926-2934

FUCHS, H.U., 1996. *The dynamic of heat.* Springer.

GAHAN, B.C. et al., 2001. Laser drilling: determination of energy required to remove rock*. SPE Annual Technical Conference and Exhibition*, pp.11

GAHAN, B.C. et al., 2005. Effect of downhole pressure conditions on high-power laser perforation*. SPE Annual Technical Conference and Exhibition*, pp.7

GAHAN, B.C. et al., 2004. Analysis of efficient high-power fiber lasers for well perforation*. SPE Annual Technical Conference and Exhibition*, pp.9

GRAVES, R.M. and BAILO, E.T., 2004. Porosity and permeability changes in lased rocks calculated using fractal fragmentation theory*. Canadian International Petroleum Conference*, pp.8

GRAVES, R.M. and O'BRIEN, D.G., 1998. StarWars laser technology applied to drilling and completing gas wells*. SPE Annual Technical Conference and Exhibition*, pp.10

GRAVES, R.M. et al., 2002a. Comparison of specific energy between drilling with high power lasers and other drilling methods*. SPE Annual Technical Conference and Exhibition*, pp.8

GRAVES, R.M. et al., 2002b. Temperatures induced by high power lasers: effects on reservoir rock strength and mechanical properties*. SPE/ISRM Rock Mechanics Conference*, pp.7

HOSSAIN, M., ACAR, M. and MALALASEKERA, W., 2005. A mathematical model for airflow and heat transfer through fibrous webs. *Proceedings of* *the Institution of Mechanical Engineers, Part E: Journal of Process Mechanical Engineering,* 219(4), pp. 357-366

JAHN, F., COOK, M. and GRAHAM, M., 1998. *Hydrocarbon exploration and production.* Elsevier.

JAMALI, S. et al., 2019. Application of high powered laser technology to alter hard rock properties towards lower strength materials for more efficient drilling, mining, and geothermal energy production. *Geomechanics for Energy and the Environment*, 20, pp. 100112

KESHAVARZI, R., 2011. Laser perforation for hydraulic fracturing in oil and gas wells*. 45th U.S. Rock Mechanics / Geomechanics Symposium*, pp.5

KESHAVARZI, R. et al., 2010. A neural network approach for predicting the penetration depth during laser perforation in limestone*. 44th U.S. Rock Mechanics Symposium and 5th U.S. Canada Rock Mechanics Symposium*, pp.6

KHAN, M.I. and ISLAM, M.R., 2007. *The petroleum engineering handbook - sustainable operations.* Gulf Publishing Company.

KNOVEL, 2008. *Knovel Critical Tables.* 2nd ed. Knovel.

KOBAYASHI, T. et al., 2008. Underwater laser drilling: drilling underwater granite by CO2 laser. *SPE Indian Oil and Gas Technical Conference and Exhibition*, pp.12

KUNDAKCIOGLU, E., LAZOGLU, I. and RAWAL, S., 2016. Transient thermal modeling of laser-based additive manufacturing for 3D freeform structures. *International Journal of Advanced Manufacturing Technology*, 85(1-4), pp. 493-501

LI, M. et al., 2019. Investigation on rock breaking for sandstone with high power density laser beam. *Optik*, 180, pp. 635-647

LI, M. et al., 2018. Numerical simulation and experimental investigation on fracture mechanism of granite by laser irradiation. *Optics & Laser Technology*, 106, pp. 52-60

MODEST, M.F., 1996. Three-dimensional, transient model for laser machining of ablating/decomposing materials. *International Journal of Heat and Mass Transfer,* 39(2), pp. 221-234

MONTGOMERY, C.T. and SMITH, M.B., 2010. Hydraulic fracturing: history of an enduring technology. *Journal of Petroleum Technology,* 62(12), pp. 26-40

O'BRIEN, D.G., GRAVES, R.M. and O'BRIEN, E.A., 1999. StarWars laser technology for gas drilling and completions in the 21st century. *SPE Annual Technical Conference and Exhibition*, pp.10

OTTO, A., KOCH, H. and VAZQUEZ, R.G., 2012. Multiphysical simulation of laser material processing. *Physics Procedia,* 39, pp. 843-852

PEI, W. et al., 2017. Numerical simulation and parametric analysis of selective laser melting process of AlSi10Mg powder. *Applied Physics A: Materials Science and Processing,* 123(8),

POHANISH, R.P., 2016. *Machinery's handbook pocket companion.* Revised 1st ed. Industrial Press.

POWELL, J. et al., 1994. Energy redistribution in laser cutting. *Welding Research Abroad,* 40(2), pp. 31-37

PRUSA, J.M., VENKITACHALAM, G. and MOLIAN, P.A., 1999. Estimation of heat conduction losses in laser cutting. *International Journal of Machine Tools and Manufacture,* 39(3), pp. 431-458

REZAEE, R., 2015. *Fundamentals of gas shale reservoirs.* John Wiley & Sons.

SHENG, P.S. and JOSHI, V.S., 1995. Analysis of heat-affected zone formation for laser cutting of stainless steel. *Journal of Materials Processing Technology,* 53(3), pp. 879-892

SHIN, J.S. et al., 2019. Underwater cutting of 50 and 60 mm thick stainless steel plates using a 6-kW fiber laser for dismantling nuclear facilities. *Optics & Laser Technology,* 115, pp. 1-8

SILFVAST, W.T., 2004. *Laser fundamentals.* 2nd ed. Cambridge

SINHA, P. and GOUR, A., 2006. Laser drilling research and application: an update. *SPE/IADC Indian Drilling Technology Conference and Exhibition*, pp.5

SPEIGHT, J.G., 2016. *Handbook of hydraulic fracturing.* John Wiley & Sons.

STEWART, G., 2011. *Well test design & analysis.* PennWell.

TEMIZEL, C. et al., 2019. *Formulas and calculations for petroleum engineering.* Elsevier.

U.S. ENERGY INFORMATION ADMINISTRATION (EIA), *Natural gas production.* [online] Available from: https://www.eia.gov/ 2017

VERHOEVEN, J.C.J. et al., 2003. Modelling laser induced melting. *Mathematical and Computer Modelling,* 37(3), pp. 419-437

WEBB, C. and JONES, J., 2004. *Handbook of laser technology and applications.*

WORCH, E., 2015. *Hydrochemistry - Basic concept and exercises.* De Gruyter.

YILBAS, B.S., SHAUKAT, M.M. and ASHRAF, F., 2017. Laser cutting of various materials: Kerf width size analysis and life cycle assessment of cutting process. *Optics & Laser Technology,* 93, pp. 67-73

# Appendix-1: The effect of temperature on thermal properties

Experimental correlations were developed to calculate the change in thermal properties as a function of temperature (Coker 2007).

1. Thermal conductivity of gas

$$k_g = A + BT + CT^2$$

Where;

$k_g$ = thermal conductivity of gas, W/m K

$A, B\ and\ C$ = Regression coefficients

$T$ = Temperature, K

Regression coefficients for thermal conductivity of some light hydrocarbon compounds in gaseous state and water vapor

| Substance | Formula | A | B | C | $T_{min}$, K | $T_{max}$, K |
|---|---|---|---|---|---|---|
| Methane | ($C_1$) $CH_4$ | -0.00935 | 1.4028E-04 | 3.3180E-08 | 97 | 1400 |
| Ethane | ($C_2$) $C_2H_6$ | -0.01936 | 1.2547E-04 | 3.8298E-08 | 225 | 825 |
| Propane | ($C_3$) $C_3H_8$ | -0.00869 | 6.6409E-05 | 7.8760E-08 | 233 | 773 |
| Water vapor | $H_2O$ | 0.00053 | 4.7093E-05 | 4.9551E-08 | 275 | 1073 |

## 2. Thermal conductivity of inorganic liquid (and solids)

$$k = A + BT + CT^2$$

Where;

$k$ = Thermal conductivity of liquid or solid, W/m K

$A, B\ and\ C$ = Regression coefficients

$T$ = Temperature, K

Regression coefficients for thermal conductivity of water

| Substance | Formula | A | B | C | $T_{min}$, K | $T_{max}$, K |
|---|---|---|---|---|---|---|
| Water liquid | H2O | -0.2758 | 4.6120E-03 | -5.5391E-06 | 273 | 633 |

## 3. Thermal conductivity of organic liquid

$$\log_{10} k_{liq} = A + B\left(1 - \frac{T}{C}\right)^{2/7}$$

Where;

$k_{liq}$ = Thermal conductivity of liquid, W/m K

$A, B\ and\ C$ = Regression coefficients

$T$ = Temperature, K

Regression coefficients for thermal conductivity of some relatively heaver hydrocarbon compounds in liquid states

| Substance | Formula | A | B | C | $T_{min}$, K | $T_{max}$, K |
|---|---|---|---|---|---|---|
| n-Pentane | ($C_5$) C5H12 | -1.2287 | 0.5822 | 469.65 | 143 | 446 |
| n-Heptane | ($C_7$) C7H16 | -1.8482 | 1.1843 | 540.26 | 183 | 513 |
| n-Decane | ($C_{10}$) C10H22 | -1.7768 | 1.0839 | 618.45 | 243 | 588 |

## 4. Heat capacity of ideal gas

$$c_{p_g} = A + BT + CT^2 + DT^3 + ET^4$$

Where;

$c_{p_g}$ = Heat capacity of ideal gas, J/mol K

$A, B, C, D\ and\ E$ = Regression coefficients

$T$ = Temperature, K

Regression coefficients for heat capacity of some light hydrocarbon compounds in gaseous states and water vapor

| Substance | Formula | A | B | C | D | E | $T_{min}$, K | $T_{max}$, K |
|---|---|---|---|---|---|---|---|---|
| Methane | ($C_1$) CH4 | 34.942 | -3.9957E-02 | 1.9184E-04 | -1.5303E-07 | 3.9321E-11 | 50 | 1500 |
| Ethane | ($C_2$) C2H6 | 28.146 | 4.3447E-02 | 1.8946E-04 | -1.9082E-07 | 5.3349E-11 | 100 | 1500 |
| Water vapor | H2O | 33.933 | -8.4186E-03 | 2.9906E-05 | -1.7825E-08 | 3.6934E-12 | 100 | 1500 |

## 5. Heat capacity of liquid

$$c_{p_l} = A + BT + CT^2 + DT^3$$

Where;

$c_{p_l}$ = Heat capacity of liquid, J/mol K

$A, B, C\ and\ D$ = Regression coefficients

$T$ = Temperature, K

Regression coefficients for heat capacity of some relatively heavier hydrocarbon compounds in liquid states and water

| Substance | Formula | A | B | C | D | $T_{min}$, K | $T_{max}$, K |
|---|---|---|---|---|---|---|---|
| n-Pentane | ($C_5$) C5H12 | 80.641 | 6.2195E-01 | -2.2682E-03 | 3.7423E-06 | 144 | 423 |
| n-Heptane | ($C_7$) C7H16 | 101.121 | 9.7739E-01 | -3.0712E-03 | 4.1844E-06 | 184 | 486 |
| n-Decane | ($C_{10}$) C10H22 | 79.741 | 1.6926 | -4.5287E-03 | 4.9769E-06 | 244 | 557 |
| Water liquid | H2O | 92.053 | -3.9953E-02 | -2.1103E-04 | 5.3469E-07 | 273 | 615 |

# Appendix-2: Laser power calculations using the new correlation

Laser power calculations for cutting oil saturated porous media by melting, using the new waste power correlation developed in this research, including sensitivity analyses for rock type, material thickness, Peclet numbers and porosity are presented in this section.

Sandstone, 10% porosity

| Material thickness, m | Laser power, kW | | | | | |
|---|---|---|---|---|---|---|
| | Useful | Waste | Total | Useful | Waste | Total |
| | 0.2 Pe | | | 0.5 Pe | | |
| 0.5 | 1.3 | 7.4 | 8.7 | 3.2 | 10.1 | 13.3 |
| 1 | 2.6 | 14.8 | 17.4 | 6.5 | 20.1 | 26.6 |
| 5 | 12.9 | 73.9 | 86.8 | 32.3 | 100.6 | 132.9 |
| 10 | 25.8 | 147.8 | 173.7 | 64.6 | 201.3 | 265.9 |
| 15 | 38.8 | 221.7 | 260.5 | 96.9 | 301.9 | 398.8 |
| 20 | 51.7 | 295.6 | 347.3 | 129.2 | 402.6 | 531.8 |
| 30 | 77.5 | 443.4 | 521.0 | 193.8 | 603.9 | 797.7 |
| 50 | 129.2 | 739.1 | 868.3 | 323.0 | 1006.4 | 1329.4 |
| | 1.0 Pe | | | 2.0 Pe | | |
| 0.5 | 6.5 | 12.7 | 19.2 | 12.9 | 16.1 | 29.0 |
| 1 | 12.9 | 25.4 | 38.3 | 25.8 | 32.1 | 58.0 |
| 5 | 64.6 | 127.1 | 191.7 | 129.2 | 160.6 | 289.8 |
| 10 | 129.2 | 254.2 | 383.5 | 258.4 | 321.1 | 579.6 |
| 15 | 193.8 | 381.4 | 575.2 | 387.6 | 481.7 | 869.3 |
| 20 | 258.4 | 508.5 | 766.9 | 516.8 | 642.3 | 1159.1 |
| 30 | 387.6 | 762.7 | 1150.4 | 775.2 | 963.4 | 1738.7 |
| 50 | 646.0 | 1271.2 | 1917.3 | 1292.0 | 1605.7 | 2897.8 |
| | 3.0 Pe | | | 5.0 Pe | | |
| 0.5 | 19.4 | 18.4 | 37.8 | 32.3 | 21.9 | 54.2 |
| 1 | 38.8 | 36.8 | 75.6 | 64.6 | 43.7 | 108.3 |
| 5 | 193.8 | 184.1 | 377.9 | 323.0 | 218.7 | 541.7 |
| 10 | 387.6 | 368.2 | 755.8 | 646.0 | 437.3 | 1083.4 |
| 15 | 581.4 | 552.3 | 1133.7 | 969.0 | 656.0 | 1625.0 |
| 20 | 775.2 | 736.3 | 1511.6 | 1292.0 | 874.7 | 2166.7 |
| 30 | 1162.8 | 1104.5 | 2267.4 | 1938.1 | 1312.0 | 3250.1 |
| 50 | 1938.1 | 1840.9 | 3778.9 | 3230.1 | 2186.7 | 5416.8 |
| | 10.0 Pe | | | | | |
| 0.5 | 64.6 | 27.6 | 92.2 | | | |
| 1 | 129.2 | 55.2 | 184.4 | | | |
| 5 | 646.0 | 276.2 | 922.2 | | | |
| 10 | 1292.0 | 552.4 | 1844.5 | | | |
| 15 | 1938.1 | 828.6 | 2766.7 | | | |
| 20 | 2584.1 | 1104.8 | 3688.9 | | | |
| 30 | 3876.1 | 1657.2 | 5533.4 | | | |
| 50 | 6460.2 | 2762.0 | 9222.3 | | | |

## Sandstone, 20% porosity

| Material thickness, m | Laser power, kW | | | | | |
|---|---|---|---|---|---|---|
| | Useful | Waste | Total | Useful | Waste | Total |
| | 0.2 Pe | | | 0.5 Pe | | |
| 0.5 | 1.1 | 6.0 | 7.1 | 2.6 | 8.2 | 10.8 |
| 1 | 2.1 | 12.0 | 14.1 | 5.3 | 16.4 | 21.6 |
| 5 | 10.5 | 60.1 | 70.6 | 26.3 | 81.9 | 108.1 |
| 10 | 21.0 | 120.2 | 141.2 | 52.5 | 163.7 | 216.3 |
| 15 | 31.5 | 180.3 | 211.9 | 78.8 | 245.6 | 324.4 |
| 20 | 42.0 | 240.4 | 282.5 | 105.1 | 327.4 | 432.5 |
| 30 | 63.1 | 360.7 | 423.7 | 157.6 | 491.2 | 648.8 |
| 50 | 105.1 | 601.1 | 706.2 | 262.7 | 818.6 | 1081.3 |
| | 1.0 Pe | | | 2.0 Pe | | |
| 0.5 | 5.3 | 10.3 | 15.6 | 10.5 | 13.1 | 23.6 |
| 1 | 10.5 | 20.7 | 31.2 | 21.0 | 26.1 | 47.1 |
| 5 | 52.5 | 103.4 | 155.9 | 105.1 | 130.6 | 235.7 |
| 10 | 105.1 | 206.8 | 311.9 | 210.2 | 261.2 | 471.4 |
| 15 | 157.6 | 310.2 | 467.8 | 315.3 | 391.8 | 707.1 |
| 20 | 210.2 | 413.6 | 623.8 | 420.4 | 522.4 | 942.8 |
| 30 | 315.3 | 620.4 | 935.7 | 630.5 | 783.6 | 1414.2 |
| 50 | 525.5 | 1034.0 | 1559.4 | 1050.9 | 1306.1 | 2357.0 |
| | 3.0 Pe | | | 5.0 Pe | | |
| 0.5 | 15.8 | 15.0 | 30.7 | 26.3 | 17.8 | 44.1 |
| 1 | 31.5 | 29.9 | 61.5 | 52.5 | 35.6 | 88.1 |
| 5 | 157.6 | 149.7 | 307.4 | 262.7 | 177.9 | 440.6 |
| 10 | 315.3 | 299.5 | 614.7 | 525.5 | 355.7 | 881.2 |
| 15 | 472.9 | 449.2 | 922.1 | 788.2 | 533.6 | 1321.8 |
| 20 | 630.5 | 598.9 | 1229.5 | 1050.9 | 711.4 | 1762.3 |
| 30 | 945.8 | 898.4 | 1844.2 | 1576.4 | 1067.1 | 2643.5 |
| 50 | 1576.4 | 1497.3 | 3073.7 | 2627.3 | 1778.6 | 4405.8 |
| | 10.0 Pe | | | | | |
| 0.5 | 52.5 | 22.5 | 75.0 | | | |
| 1 | 105.1 | 44.9 | 150.0 | | | |
| 5 | 525.5 | 224.7 | 750.1 | | | |
| 10 | 1050.9 | 449.3 | 1500.2 | | | |
| 15 | 1576.4 | 674.0 | 2250.3 | | | |
| 20 | 2101.8 | 898.6 | 3000.4 | | | |
| 30 | 3152.7 | 1347.9 | 4500.7 | | | |
| 50 | 5254.5 | 2246.6 | 7501.1 | | | |

## Sandstone, 30% porosity

| Material thickness, m | Laser power, kW | | | | | |
|---|---|---|---|---|---|---|
| | Useful | Waste | Total | Useful | Waste | Total |
| | 0.2 Pe | | | 0.5 Pe | | |
| 0.5 | 0.8 | 4.8 | 5.6 | 2.1 | 6.5 | 8.6 |
| 1 | 1.7 | 9.5 | 11.2 | 4.2 | 13.0 | 17.2 |
| 5 | 8.3 | 47.7 | 56.1 | 20.9 | 65.0 | 85.9 |
| 10 | 16.7 | 95.5 | 112.2 | 41.7 | 130.0 | 171.8 |
| 15 | 25.0 | 143.2 | 168.3 | 62.6 | 195.0 | 257.6 |
| 20 | 33.4 | 191.0 | 224.3 | 83.5 | 260.0 | 343.5 |
| 30 | 50.1 | 286.4 | 336.5 | 125.2 | 390.1 | 515.3 |
| 50 | 83.5 | 477.4 | 560.9 | 208.7 | 650.1 | 858.8 |
| | 1.0 Pe | | | 2.0 Pe | | |
| 0.5 | 4.2 | 8.2 | 12.4 | 8.3 | 10.4 | 18.7 |
| 1 | 8.3 | 16.4 | 24.8 | 16.7 | 20.7 | 37.4 |
| 5 | 41.7 | 82.1 | 123.8 | 83.5 | 103.7 | 187.2 |
| 10 | 83.5 | 164.2 | 247.7 | 166.9 | 207.5 | 374.4 |
| 15 | 125.2 | 246.4 | 371.5 | 250.4 | 311.2 | 561.6 |
| 20 | 166.9 | 328.5 | 495.4 | 333.8 | 414.9 | 748.7 |
| 30 | 250.4 | 492.7 | 743.1 | 500.8 | 622.4 | 1123.1 |
| 50 | 417.3 | 821.2 | 1238.5 | 834.6 | 1037.3 | 1871.9 |
| | 3.0 Pe | | | 5.0 Pe | | |
| 0.5 | 12.5 | 11.9 | 24.4 | 20.9 | 14.1 | 35.0 |
| 1 | 25.0 | 23.8 | 48.8 | 41.7 | 28.3 | 70.0 |
| 5 | 125.2 | 118.9 | 244.1 | 208.7 | 141.3 | 349.9 |
| 10 | 250.4 | 237.8 | 488.2 | 417.3 | 282.5 | 699.8 |
| 15 | 375.6 | 356.7 | 732.3 | 626.0 | 423.8 | 1049.7 |
| 20 | 500.8 | 475.7 | 976.4 | 834.6 | 565.0 | 1399.6 |
| 30 | 751.2 | 713.5 | 1464.6 | 1251.9 | 847.5 | 2099.4 |
| 50 | 1251.9 | 1189.1 | 2441.0 | 2086.5 | 1412.5 | 3499.0 |
| | 10.0 Pe | | | | | |
| 0.5 | 41.7 | 17.8 | 59.6 | | | |
| 1 | 83.5 | 35.7 | 119.1 | | | |
| 5 | 417.3 | 178.4 | 595.7 | | | |
| 10 | 834.6 | 356.8 | 1191.5 | | | |
| 15 | 1251.9 | 535.3 | 1787.2 | | | |
| 20 | 1669.2 | 713.7 | 2382.9 | | | |
| 30 | 2503.8 | 1070.5 | 3574.4 | | | |
| 50 | 4173.1 | 1784.2 | 5957.3 | | | |

# Limestone, 10% porosity

| Material thickness, m | Laser power, kW | | | | | |
|---|---|---|---|---|---|---|
| | Useful | Waste | Total | Useful | Waste | Total |
| | 0.2 Pe | | | 0.5 Pe | | |
| 0.5 | 0.7 | 3.9 | 4.6 | 1.7 | 5.3 | 7.1 |
| 1 | 1.4 | 7.8 | 9.2 | 3.4 | 10.7 | 14.1 |
| 5 | 6.9 | 39.2 | 46.1 | 17.1 | 53.4 | 70.5 |
| 10 | 13.7 | 78.4 | 92.1 | 34.3 | 106.8 | 141.1 |
| 15 | 20.6 | 117.6 | 138.2 | 51.4 | 160.2 | 211.6 |
| 20 | 27.4 | 156.9 | 184.3 | 68.6 | 213.6 | 282.2 |
| 30 | 41.1 | 235.3 | 276.4 | 102.8 | 320.4 | 423.2 |
| 50 | 68.6 | 392.1 | 460.7 | 171.4 | 534.0 | 705.4 |
| | 1.0 Pe | | | 2.0 Pe | | |
| 0.5 | 3.4 | 6.7 | 10.2 | 6.9 | 8.5 | 15.4 |
| 1 | 6.9 | 13.5 | 20.3 | 13.7 | 17.0 | 30.8 |
| 5 | 34.3 | 67.5 | 101.7 | 68.6 | 85.2 | 153.8 |
| 10 | 68.6 | 134.9 | 203.5 | 137.1 | 170.4 | 307.5 |
| 15 | 102.8 | 202.4 | 305.2 | 205.7 | 255.6 | 461.3 |
| 20 | 137.1 | 269.8 | 406.9 | 274.2 | 340.8 | 615.0 |
| 30 | 205.7 | 404.7 | 610.4 | 411.3 | 511.2 | 922.5 |
| 50 | 342.8 | 674.5 | 1017.3 | 685.5 | 852.0 | 1537.5 |
| | 3.0 Pe | | | 5.0 Pe | | |
| 0.5 | 10.3 | 9.8 | 20.1 | 17.1 | 11.6 | 28.7 |
| 1 | 20.6 | 19.5 | 40.1 | 34.3 | 23.2 | 57.5 |
| 5 | 102.8 | 97.7 | 200.5 | 171.4 | 116.0 | 287.4 |
| 10 | 205.7 | 195.3 | 401.0 | 342.8 | 232.0 | 574.8 |
| 15 | 308.5 | 293.0 | 601.5 | 514.2 | 348.1 | 862.2 |
| 20 | 411.3 | 390.7 | 802.0 | 685.5 | 464.1 | 1149.6 |
| 30 | 617.0 | 586.0 | 1203.0 | 1028.3 | 696.1 | 1724.4 |
| 50 | 1028.3 | 976.7 | 2005.0 | 1713.9 | 1160.2 | 2874.1 |
| | 10.0 Pe | | | | | |
| 0.5 | 34.3 | 14.7 | 48.9 | | | |
| 1 | 68.6 | 29.3 | 97.9 | | | |
| 5 | 342.8 | 146.5 | 489.3 | | | |
| 10 | 685.5 | 293.1 | 978.6 | | | |
| 15 | 1028.3 | 439.6 | 1468.0 | | | |
| 20 | 1371.1 | 586.2 | 1957.3 | | | |
| 30 | 2056.6 | 879.3 | 2935.9 | | | |
| 50 | 3427.7 | 1465.5 | 4893.2 | | | |

# Limestone, 20% porosity

| Material thickness, m | Laser power, kW | | | | | |
|---|---|---|---|---|---|---|
| | Useful | Waste | Total | Useful | Waste | Total |
| | 0.2 Pe | | | 0.5 Pe | | |
| 0.5 | 0.6 | 3.2 | 3.8 | 1.4 | 4.4 | 5.8 |
| 1 | 1.1 | 6.4 | 7.6 | 2.8 | 8.8 | 11.6 |
| 5 | 5.6 | 32.1 | 37.8 | 14.0 | 43.8 | 57.8 |
| 10 | 11.2 | 64.3 | 75.5 | 28.1 | 87.5 | 115.6 |
| 15 | 16.9 | 96.4 | 113.3 | 42.1 | 131.3 | 173.4 |
| 20 | 22.5 | 128.5 | 151.0 | 56.2 | 175.0 | 231.2 |
| 30 | 33.7 | 192.8 | 226.5 | 84.3 | 262.6 | 346.8 |
| 50 | 56.2 | 321.3 | 377.5 | 140.4 | 437.6 | 578.0 |
| | 1.0 Pe | | | 2.0 Pe | | |
| 0.5 | 2.8 | 5.5 | 8.3 | 5.6 | 7.0 | 12.6 |
| 1 | 5.6 | 11.1 | 16.7 | 11.2 | 14.0 | 25.2 |
| 5 | 28.1 | 55.3 | 83.4 | 56.2 | 69.8 | 126.0 |
| 10 | 56.2 | 110.5 | 166.7 | 112.4 | 139.6 | 252.0 |
| 15 | 84.3 | 165.8 | 250.1 | 168.5 | 209.5 | 378.0 |
| 20 | 112.4 | 221.1 | 333.5 | 224.7 | 279.3 | 504.0 |
| 30 | 168.5 | 331.6 | 500.2 | 337.1 | 418.9 | 756.0 |
| 50 | 280.9 | 552.7 | 833.6 | 561.8 | 698.2 | 1260.0 |
| | 3.0 Pe | | | 5.0 Pe | | |
| 0.5 | 8.4 | 8.0 | 16.4 | 14.0 | 9.5 | 23.6 |
| 1 | 16.9 | 16.0 | 32.9 | 28.1 | 19.0 | 47.1 |
| 5 | 84.3 | 80.0 | 164.3 | 140.4 | 95.1 | 235.5 |
| 10 | 168.5 | 160.1 | 328.6 | 280.9 | 190.2 | 471.0 |
| 15 | 252.8 | 240.1 | 492.9 | 421.3 | 285.2 | 706.6 |
| 20 | 337.1 | 320.2 | 657.2 | 561.8 | 380.3 | 942.1 |
| 30 | 505.6 | 480.2 | 985.9 | 842.7 | 570.5 | 1413.1 |
| 50 | 842.7 | 800.4 | 1643.1 | 1404.5 | 950.8 | 2355.2 |
| | 10.0 Pe | | | | | |
| 0.5 | 28.1 | 12.0 | 40.1 | | | |
| 1 | 56.2 | 24.0 | 80.2 | | | |
| 5 | 280.9 | 120.1 | 401.0 | | | |
| 10 | 561.8 | 240.2 | 802.0 | | | |
| 15 | 842.7 | 360.3 | 1203.0 | | | |
| 20 | 1123.6 | 480.4 | 1603.9 | | | |
| 30 | 1685.4 | 720.6 | 2405.9 | | | |
| 50 | 2808.9 | 1200.9 | 4009.9 | | | |

# Limestone, 30% porosity

| Material thickness, m | Laser power, kW | | | | | |
|---|---|---|---|---|---|---|
| | Useful | Waste | Total | Useful | Waste | Total |
| | 0.2 Pe | | | 0.5 Pe | | |
| 0.5 | 0.5 | 2.6 | 3.0 | 1.1 | 3.5 | 4.6 |
| 1 | 0.9 | 5.2 | 6.1 | 2.3 | 7.0 | 9.3 |
| 5 | 4.5 | 25.8 | 30.3 | 11.3 | 35.1 | 46.3 |
| 10 | 9.0 | 51.5 | 60.5 | 22.5 | 70.2 | 92.7 |
| 15 | 13.5 | 77.3 | 90.8 | 33.8 | 105.2 | 139.0 |
| 20 | 18.0 | 103.0 | 121.0 | 45.0 | 140.3 | 185.3 |
| 30 | 27.0 | 154.6 | 181.6 | 67.5 | 210.5 | 278.0 |
| 50 | 45.0 | 257.6 | 302.6 | 112.6 | 350.8 | 463.4 |
| | 1.0 Pe | | | 2.0 Pe | | |
| 0.5 | 2.3 | 4.4 | 6.7 | 4.5 | 5.6 | 10.1 |
| 1 | 4.5 | 8.9 | 13.4 | 9.0 | 11.2 | 20.2 |
| 5 | 22.5 | 44.3 | 66.8 | 45.0 | 56.0 | 101.0 |
| 10 | 45.0 | 88.6 | 133.6 | 90.1 | 111.9 | 202.0 |
| 15 | 67.5 | 132.9 | 200.5 | 135.1 | 167.9 | 303.0 |
| 20 | 90.1 | 177.2 | 267.3 | 180.1 | 223.9 | 404.0 |
| 30 | 135.1 | 265.8 | 400.9 | 270.2 | 335.8 | 606.0 |
| 50 | 225.2 | 443.1 | 668.2 | 450.3 | 559.7 | 1010.0 |
| | 3.0 Pe | | | 5.0 Pe | | |
| 0.5 | 6.8 | 6.4 | 13.2 | 11.3 | 7.6 | 18.9 |
| 1 | 13.5 | 12.8 | 26.3 | 22.5 | 15.2 | 37.8 |
| 5 | 67.5 | 64.2 | 131.7 | 112.6 | 76.2 | 188.8 |
| 10 | 135.1 | 128.3 | 263.4 | 225.2 | 152.4 | 377.6 |
| 15 | 202.6 | 192.5 | 395.1 | 337.7 | 228.6 | 566.4 |
| 20 | 270.2 | 256.6 | 526.8 | 450.3 | 304.9 | 755.2 |
| 30 | 405.3 | 385.0 | 790.3 | 675.5 | 457.3 | 1132.8 |
| 50 | 675.5 | 641.6 | 1317.1 | 1125.8 | 762.1 | 1888.0 |
| | 10.0 Pe | | | | | |
| 0.5 | 22.5 | 9.6 | 32.1 | | | |
| 1 | 45.0 | 19.3 | 64.3 | | | |
| 5 | 225.2 | 96.3 | 321.4 | | | |
| 10 | 450.3 | 192.5 | 642.9 | | | |
| 15 | 675.5 | 288.8 | 964.3 | | | |
| 20 | 900.7 | 385.1 | 1285.7 | | | |
| 30 | 1351.0 | 577.6 | 1928.6 | | | |
| 50 | 2251.7 | 962.7 | 3214.3 | | | |